Submitted to Physical Review C

LBL-1951
Preprint c. 2

CORE POLARIZATION IN INELASTIC SCATTERING

F. Petrovich, H. McManus, J. Borysowicz, and
G. R. Hammerstein

RECEIVED
LAWRENCE
RADIATION LABORATORY

JAN 27 1977

LIBRARY AND
DOCUMENTS SECTION

May 1976

Prepared for the U. S. Energy Research and
Development Administration under Contract W-7405-ENG-48

TWO-WEEK LOAN COPY

This is a Library Circulating Copy
which may be borrowed for two weeks.
For a personal retention copy, call
Tech. Info. Division, Ext. 5716

LAWRENCE BERKELEY LABORATORY
UNIVERSITY OF CALIFORNIA
BERKELEY

LBL-1951
c. 2

DISCLAIMER

This document was prepared as an account of work sponsored by the United States Government. While this document is believed to contain correct information, neither the United States Government nor any agency thereof, nor the Regents of the University of California, nor any of their employees, makes any warranty, express or implied, or assumes any legal responsibility for the accuracy, completeness, or usefulness of any information, apparatus, product, or process disclosed, or represents that its use would not infringe privately owned rights. Reference herein to any specific commercial product, process, or service by its trade name, trademark, manufacturer, or otherwise, does not necessarily constitute or imply its endorsement, recommendation, or favoring by the United States Government or any agency thereof, or the Regents of the University of California. The views and opinions of authors expressed herein do not necessarily state or reflect those of the United States Government or any agency thereof or the Regents of the University of California.

CORE POLARIZATION IN INELASTIC SCATTERING*

F. Petrovich†

Lawrence Berkeley Laboratory
University of California
Berkeley, California 94720

and

H. McManus, J. Borysowicz, and G. R. Hammerstein

Cyclotron Laboratory and Physics Department
Michigan State University
East Lansing, Michigan 48823

ABSTRACT

Inelastic scattering is a source of much useful information about core polarization effects in nuclei near closed shells. Although there have been many theoretical treatments of core polarization effects reported in the literature, the results of these calculations have rarely been applied to the interpretation of inelastic scattering data. In the present paper we review the microscopic models for the treatment of inelastic proton and electron scattering and the microscopic models for the treatment of core polarization. Estimates are made of core excited admixtures in the wave functions for low-lying states in ^{42}Ca, ^{50}Ti, ^{89}Y, ^{90}Zr, ^{207}Pb, and ^{209}Bi. The resulting wave functions are used to calculate theoretical (p,p') cross sections and (e,e') form factors for comparison with available experimental data. "Realistic" G matrix interactions are used as the starting point in both the structure and the (p,p') calculations. In the structure calculations the interaction is modified by means of a "bootstrap" prescription to account for important long-range core correlations and in the (p,p') calculations it is modified by the addition of an imaginary component. It is concluded that the overall features of the experimental data can be understood from these calculations.

*Work supported in part by the U. S. Energy Research and Development Administration and the N.S.F.

†Present address: Department of Physics and Astronomy, The Florida State University, Tallahassee, Florida 32306.

I. INTRODUCTION

The concept of core polarization is quite well known in the shell model interpretation of nuclei in the vicinity of closed shells. In the shell model a nuclear state is described in a restricted configuration space which presumably contains the bulk of its wave function, but not all its significant components. This restricted configuration space, commonly called the model space, usually consists of a few valence particles (holes) distributed among a small number of shell model orbitals outside (inside) an inert closed shell core. The term core polarization is generally associated with effects which are due to wave function admixtures not in the model space. The name arises because these admixtures most often will consist of core-excited configurations. Core polarization can be taken into account by defining effective operators in the model space which may be calculated by means of perturbation theory.

These ideas first appeared in the literature about twenty years ago[1,2] when it was first noted that there were discrepancies between the predictions of the simple shell model and the experimental values for nuclear magnetic moments, quadrupole moments, γ-transition rates, etc. Two different models were proposed at this time. One is a hybrid model in which the core is treated as a liquid drop which can be set into oscillation by interaction with the extra-core nucleons.[1] The other is a completely microscopic model[2] in which the core is considered to be an assemblage of nucleons - any of which might be raised to higher, unoccupied levels as a result of the two body forces which couple them to the valence nucleons.

In recent times this microscopic model has been pursued in considerably greater depth. The major impetus here has been the work of Brown and collaborators[3-8] whose purpose was to gain an understanding of the properties of finite

nuclei using "realistic" forces, i.e. interactions which can be derived directly from the free two-nucleon potential. As the nucleon-nucleon interaction is strong and singular, the first step in this approach is to truncate to a large shell model basis by applying Brueckner Hartree-Fock theory to get rid of the short range two-nucleon correlations and replace the singular interaction by a smooth well-behaved one, namely the bare G matrix. The second step is to truncate to the model space and to renormalize the bare G matrix to account for core polarization as described in the first paragraph above. The renormalized G matrix is the shell model effective interaction.

Kuo and Brown[4,8] have made a systematic study of nuclei with ^{16}O, ^{40}Ca, ^{48}Ca, ^{56}Ni, ^{88}Sr, and ^{208}Pb cores using second order perturbation theory in renormalizing the bare G matrix. They find that core polarization gives rise to a strong pairing effect which is the major feature of the observed spectra. Although the results of these calculations are quite impressive, attempts[9] to extend the perturbative treatment to higher orders have not met with the same success and the final status of core polarization and the effective interaction is still an open question. A similar situation prevails in regard to associated efforts[10] to calculate nuclear magnetic moments, quadrupole moments, and quadrupole transition rates. Lowest order perturbation theory provides a reasonable qualitative estimate of these effects, but there are still many ambiguities in the interpretation of the results of calculations which include higher order contributions. Much of this work has been reviewed recently by Barrett and Kirson.[11]

The purpose of the present paper is to present the results of calculations, similar to those of Ref. 10, but applied to the problem of inelastic scattering. In particular, we consider inelastic electron scattering and inelastic

proton scattering. Inelastic proton scattering at energies below 100 MeV is interesting, because the interaction between the incident proton and the bound nucleons is quite similar to the interaction between bound nucleons, i.e. the bare G matrix.[12,13] Electron scattering is primarily sensitive to proton excitations in the target nucleus while proton scattering is most sensitive to neutron excitations.[14] By comparing results for these two reactions a measure of both the proton and neutron components of the nuclear wave functions is obtained. In addition, inelastic scattering provides information about core polarization effects in transitions requiring large angular momentum transfer. Cross sections have been measured for transitions where there are up to 11 units of angular momentum transferred. This is to be contrasted with low momentum electromagnetic data which is essentially restricted to dipole, quadrupole, and some octupole phenomena.

The first attempt at treating core polarization in inelastic proton scattering was made by Love and Satchler.[15] They assume a hydrodynamical description of the core and showed that core polarization can give a large, even dominant, contribution to the cross section. The main purpose of the present paper is to show that the major features of inelastic scattering from nuclei near closed shells can be qualitatively understood in completely microscopic calculations based on "realistic" interactions. In the calculations, core excited admixtures in the nuclear wave functions are estimated using lowest order perturbation theory and a "bootstrap" prescription which accounts for long range core correlations. Agassi and Schaeffer[16] have previously made a similar, but considerably more limited study of these same effects. We also note that some results obtained with wave functions from the present paper have previously been reported elsewhere.[17,18]

In the next section of this paper we give a brief description of the

theoretical treatment of inelastic proton and inelastic electron scattering. We review the theory of effective operators and describe our calculations in Section III. The results of the calculations are discussed in Section IV and Section V contains the conclusions.

II. INELASTIC SCATTERING

A. Inelastic Proton Scattering

1. The Microscopic Model

In the microscopic model proton-nucleus scattering is described in terms of a projectile-target interaction which has the form

$$V = \sum_i t_{ip} \quad , \tag{1}$$

where t_{ip} is a two-body force acting between the projectile and the ith target nucleon. The two-body force t_{ip} has both real and imaginary parts, because, even in the most elaborate of reaction calculations, only a few of the allowed channels are treated explicitly. In principle, t_{ip} can be derived directly from the free two-nucleon potential. Such a calculation is not easy; however, as it requires the treatment of the repulsive hard cores which appear in the free two-nucleon potential combined with an explicit treatment of the excluded reaction channels.

Although a program of this type has not been carried out in detail, a reasonable prescription for t_{ip}, applicable in the energy region below 100 MeV, has been developed in recent years.[12,13] It is based on the assumptions that the real part of t_{ip} is not too different from the bound state G matrix and that the effects of the excluded reaction channels can be estimated perturbatively or treated phenomenologically. The first assumption has been tested in several calculations.[12-14] Attempts to estimate the effect of the excluded reaction channels have, so far, been restricted to the case of elastic scattering.[12,19] Satchler has proposed a method[20] whereby the imaginary part

of t_{ip} for inelastic scattering calculations can be inferred from the imaginary part of the phenomenological optical potential for elastic scattering. This method has proved to be useful in several calculations.[13,18,20,21] Additional comments concerning this prescription for t_{ip} may be found in Ref. 13.

Another problem which is encountered in any attempt to treat proton-nucleus scattering in a microscopic model is the indistinguishability of the incident proton and the target nucleons. In this situation the Pauli principle requires that the wave function for the projectile-target system be completely antisymmetrized - which in turn gives rise to "knock-on" exchange amplitudes in the transition matrix elements. These are non-local in the projectile coordinate and they are quite important, particularly in the case of inelastic transitions.[22,23,12,13] Computer codes are available which allow the inclusion of these exchange amplitudes and their properties have been studied in some detail.[13,22,23] In this work we include these terms with a zero-range approximation developed previously.[12,24]

2. The Interaction

In the present calculations we assume t_{ip} to be given by

$$t_{ip} = t_{ip}^{R} + it_{ip}^{I} \quad , \tag{2}$$

where R and I denote real and imaginary, respectively.

We take t_{ip}^{R} to be the long range part of the Hamada-Johnston (HJ) potential[25,4,5,12,13] with the closure approximation to the second order tensor contribution. We assume a 1.05 F separation distance and a closure energy denominator of 220 MeV. This is a local, even state central interaction which

can be written

$$t^R_{ip} = g_{ip} = g^0_{pq}\ (r_{ip}) + g^1_{pq}\ (r_{ip})\ \bar{\sigma}_i \cdot \bar{\sigma}_p \tag{3}$$

with q = p or n as i is a proton or neutron. The expression for the radial functions appearing in Eq. (3) have been given elsewhere[4,5,12,13] and will not be repeated here. For orientation we note that

$$g^0_{pn} \approx 3g^0_{pp} \approx 9g^1_{pn} \approx -3g^1_{pp} \tag{4}$$

with all components but g^1_{pp} being attractive.

We neglect the central interaction in odd states. This has been included in some calculations by fitting a regular functional form to the low energy nucleon-nucleon P-wave phase shifts[12,13] and its effect is not large. We do not include possible spin-orbit and tensor components in t^R_{ip}. The properties of these non-central interaction components have been discussed in detail elsewhere[26,27] and are only of secondary importance for most of the transitions considered in this paper.

For t^I_{ip} we follow Ref. 20 and argue that the imaginary part of the optical potential for elastic scattering is given by

$$U_I(r_p) = \langle\ g.s. |\ \sum_i\ t^I_{ip} | g.s.\ \rangle + \text{exchange terms.} \tag{5}$$

With the assumption that

$$t^I_{ip} = A_{pq}(r_i)\ \ \delta(\bar{r}_i - \bar{r}_p) \qquad (q = p,n) \tag{6}$$

the two terms on the right of Eq. (5) are equal and

$$U_I(r_p) = 2A_{pp}(r_p)\ \rho_p(r_p) + 2A_{pn}(r_p)\ \rho_n(r_p) \quad , \tag{7}$$

where ρ_p and ρ_n are the ground state proton and neutron density functions. With the additional assumption that

$$\rho_n = (N/Z)\ \rho_p \quad , \tag{8}$$

we obtain

$$\begin{aligned} U_I(r_p) &= A(r_p)\ \rho_p(r_p) \\ A &= 2\ [A_{pp} + (N/Z)A_{pn}] \quad . \end{aligned} \tag{9}$$

A can be determined by comparing directly U_I and ρ_p which are available from phenomenological analyses of elastic proton and electron scattering data. As A_{pp} and A_{pn} can not be determined separately from the data, we make the <u>ansatz</u> that A_{pp} and A_{pn} have the same radial shape and that their strengths are in the same ratio as the volume integrals of the corresponding components of t^R_{ip}, i.e.

$$A_{pn} = \alpha\ A_{pp} \quad . \tag{10}$$

For the long range part of the HJ potential $\alpha = 2.58$.[12]

In the above paragraph it has been assumed that the imaginary part of the projectile-target interaction for inelastic scattering is proportional to that for elastic scattering. It has been argued[28] that the various excluded channels contribute coherently to the imaginary part of the optical potential for elastic scattering, but that the separate contributions interfere to some

degree in the case of an inelastic excitation. This means that t_{ip}^{I} for elastic scattering should be greater than t_{ip}^{I} for inelastic scattering. With this argument in mind we simply point out that the prescription outlined above gives, in all probability, an upper limit on t_{ip}^{I} for inelastic transitions. We also mention that the assumption that $\alpha = 2.58$ in Eq. (10) is tantamount to assuming that excluded channels which favor neutron excitation, e.g. (p,p') and (p,d), are more important than those which favor proton excitation, e.g. (p,2p). Although this does not seem unreasonable, this point has not been investigated in detail and could, in fact, be wrong. Fortunately, the results to be presented are not critically dependent on this assumption.

3. The Distorted Wave Approximation

The differential cross section for inelastic proton scattering can be written as follows

$$\frac{d\sigma}{d\Omega} = \left(\frac{\mu}{2\pi\hbar^2}\right)^2 \frac{k_f}{k_i} \frac{1}{2(2J_i + 1)} \sum |T_{fi}|^2 \quad , \tag{11}$$

where μ is the reduced mass of the projectile-target system, k_f and k_i are the final and initial relative wave numbers, J_i is the initial spin of the target, T_{fi} is the transition amplitude, and the sum is over the initial and final projections of the projectile and target. In the distorted wave approximation the transition amplitude is given by

$$T_{fi} = \int \chi_f^{(-)*}(\bar{r}_p) \langle f|V|i \rangle \chi_i^{(+)}(\bar{r}_p) d^3r_p + \text{exchange terms}, \tag{12}$$

where the χ's are distorted waves and $|i\rangle$ and $|f\rangle$ are the initial and final states of the target. The first term in this equation is the direct amplitude

and the second is the "knock-on" exchange amplitude. With the approximation of Ref. 12 and 24, the exchange terms can be included by replacing V in the first term of Eq. (12) by

$$\bar{V} = \sum_i v_{ip} \quad , \tag{13}$$

where

$$v_{ip} = t^R_{ip} + 2\, i\, t^I_{ip} + t^R_{ip}\,(k_L{}^2)\;\; \delta(\bar{r}_i - \bar{r}_p) \quad . \tag{14}$$

For the imaginary component of V the direct and exchange amplitudes are equal because t^I_{ip}, as defined in Eq. (6), is assumed to be a zero-range interaction. This accounts for the factor of 2 multiplying t^I_{ip} in Eq. (14). The exchange amplitude corresponding to the real part of V is given by the last term in Eq. (14) where $t^R_{ip}\,(k_L{}^2)$ is the Fourier transform of t^R_{ip} evaluated at the wave number associated with the laboratory energy of the incident proton.

To understand this approximation it is sufficient to consider the scattering of a free nucleon from another nucleon bound in a fixed potential well. On the average the bound nucleon is at rest with respect to the incident nucleon. In order for the incident nucleon to knock out the bound nucleon and be captured in the potential well it necessary that it impart all its momentum to the bound nucleon. This is a very high energy argument in that we ignore the spread of momentum components in the wave function for the bound nucleon as well as the effect of the binding potential; however, in practice it is found to work quite well[12] even for energies below 100 MeV.

Noting that t^R_{ip} and $t^R_{ip}(k_L^2)$ have essentially the same sign, we see that the direct and exchange contributions in Eq. (14) are in phase. This is a direct consequence of the fact that the interaction being considered has only even state components. Exchange amplitudes for odd state interactions are out of phase with the direct amplitudes.[12,13,22,23] This is a contributing factor in allowing us to neglect the odd state components of the projectile-target interaction.

The essential point of the preceding development is that inelastic proton scattering cross sections can be understood reasonably well in local distorted wave calculations, that is

$$T_{fi} = \int \chi_f^{(-)*}(\bar{r}_p) \langle f|\bar{V}|i\rangle \chi_i^{(+)}(\bar{r}_p)\, d^3r_p \quad , \qquad (15)$$

where $\bar{V}$ is a pseudo-potential, derived from a "realistic" interaction, which incorporates the major features of "knock-on" exchange. The relative strengths of the components of $\bar{V}$ are very nearly the same as the relative strengths of the components of the real part of V which have been given in Eq. (4). As we are interested in treating nuclear wave functions which contain many components, the reduction of the calculations to the form of Eq. (15) is important. In this situation an exact treatment of Eq. (12) can be very expensive or, in some cases, impossible to carry out.

The evaluation of the integral in Eq. (15) is straightforward.[29] The procedure is to expand $\bar{V}$ in multipoles which correspond to definite orbital, spin, and total angular momentum transfer (LSJ). This expansion is given by

$$\bar{V} = \sum_{\substack{i \\ LSJ \\ M_J}} v^S_{pqL}(r_p;r_i)\,(-1)^{J+S+M_J}\, T^{LSJ}_{-M_J}(p)\, T^{LSJ}_{M_J}(i) \qquad (q = p,n) \qquad (16)$$

where $v^S_{pqL}(r_p;r_i)$ is the Lth multipole coefficient in the Legendre expansion of $v^S_{pq}(r_{ip})$ and $T^{LSJ}_{M_J}$ is the "spin-angle" tensor

$$T^{LSJ}_{M_J} = \sum_{M\lambda} \langle LSM\lambda | JM_J \rangle \, i^L \, Y_{LM} \, \sigma^S_\lambda \quad . \tag{17}$$

Inserting Eq. (16) into Eq. (15), performing the integration over the target coordinates and projectile spin coordinates, and carrying out the summations in Eq. (11), we obtain immediately the final expression for the differential cross section.

$$\frac{d\sigma}{d\Omega} = \left(\frac{\mu}{2\pi\hbar^2}\right)^2 \frac{k_f}{k_i} \frac{2J_f + 1}{2J_i + 1} \sum_{\substack{LSJ \\ M}} |\beta^{LM}_{SJ}|^2$$

$$\beta^{LM}_{SJ} = \frac{i^{-L}}{\hat{L}} \int \chi^{(-)*}_f(\bar{r}_p) \, \bar{F}^{LSJ}(r_p) \, Y^*_{LM}(\hat{r}_p) \, \chi^{(+)}_i(\bar{r}_p) d^3r_p \tag{18}$$

$$\hat{L} = [2L + 1]^{1/2}$$

We have ignored the effect of spin-orbit coupling in the optical potential in writing Eq. (18) although we do include it in the calculations. It gives rise to interference between amplitudes of the same J with different L and S.[29] In practice this interference is found to be weak.

All information pertaining to the projectile-target interaction and the details of nuclear structure are contained in the radial form factors, $\bar{F}^{LSJ}(r_p)$, which appear in Eq. (18). The nuclear structure information is confined to the radial nuclear transition densities which are defined by

$$F^{LSJ}_q(r) = \langle f \| \sum_i \frac{\delta(r-r_i)}{r_i^2} \, T^{LSJ}(i) \| i \rangle \qquad (q = p,n) \quad , \tag{19}$$

where $\langle \| \| \rangle$ is a reduced matrix element[30] and the sum on i runs over target protons or neutrons as q = p or n. The radial form factors are obtained by averaging $\bar{V}$ over the transition densities, i.e.

$$\bar{F}^{LSJ}(r_p) = \sum_{q=p,n} \int_0^\infty v^S_{pqL}(r_p;r)\, F_q^{LSJ}(r)\, r^2 dr \quad . \tag{20}$$

With the approximations employed here, inelastic proton scattering is simply a one-body operator with respect to the target. This is quite evident from Eq. (18) - (20). The selection rules for the reaction are contained in Eq. (19). These are:

$$J = \Delta(J_f J_i J) \qquad S = \Delta(\tfrac{1}{2}\,\tfrac{1}{2}\,S) \qquad L = \Delta(JSL) \tag{21}$$

$$\Delta\pi = (-1)^L \quad . \tag{22}$$

There is some violation of the parity selection rule, Eq. (22), when exchange is treated exactly.[13,22,23] Although it is possible to include the amplitudes which violate Eq. (22) in an approximate way,[24] we ignore them here as they contribute little to the differential cross sections.

We distinguish between normal parity ($\Delta\pi = (-1)^J$) and abnormal parity amplitudes ($\Delta\pi = (-1)^{J+1}$). In the former case the allowed values of LSJ are J0J and J1J and the reaction can proceed through the strong spin independent components of the projectile-target interaction. Neutron excitations will be most important here as $v^0_{pn} \approx 3v^0_{pp}$. In the latter case the allowed values of LSJ are J ± 11J and the reaction can proceed only through the weaker spin dependent parts of the projectile-target interaction. We will see in Section III that the effect of core polarization is to enhance the

S = 0 transition densities while retarding the S = 1 transition densities. For most of the transitions which will be considered in Section IV, a single S = 0 amplitude will make the dominant contribution to the cross section.

B. Inelastic Electron Scattering

The differential cross section for inelastic electron scattering is given by[31]

$$\frac{d\sigma}{d\Omega} = \frac{Z^2\sigma_M}{\eta} \left\{ |F_L(q)|^2 + 1/2\ (1 + 2\tan^2\frac{\theta}{2})\ |F_T(q)|^2 \right\} , \qquad (23)$$

where $Z^2\sigma_M$ is the Mott cross section which describes the scattering of a high energy electron by a point charge Z, η is a recoil factor, θ is the scattering angle, and q is the magnitude of the momentum transfer. $F_L(q)$ and $F_T(q)$ are the longitudinal and transverse form factors, respectively. As a result of the difference in the angular dependence of the two terms in Eq. (23), it is possible to determine both $F_L(q)$ and $F_T(q)$ from the experimental data. Since we will consider only cases where $F_L(q)$ is dominant or where $F_L(q)$ has been separated from $F_T(q)$, the following discussion will be confined to the longitudinal form factor. Details concerning the transverse form factor may be found in Ref. 31.

We assume here a Born approximation treatment with a local wave number correction to account for Coulomb distortion.[31] This approach has been shown to be adequate, even for heavy nuclei, provided we don't require information inside the nuclear surface.[14] With these assumptions the longitudinal form factor is given by

$$|F_L(q)|^2 = \frac{4\pi}{Z^2}\ \frac{2J_f+1}{2J_i+1} \sum_J \left| \int_0^\infty j_J(\kappa qr)\ \rho^J_{ch}\ (r)\ r^2 dr \right|^2 . \qquad (24)$$

In this equation $j_J(\kappa qr)$ is a spherical Bessel function and the factor κ appearing in its argument defines the local wave number. It is given by[31,14]

$$\kappa = 1 - V_c(0)/E \quad , \tag{25}$$

where $V_c(0)$ is the Coulomb potential at the center of the target and E is the energy of the incident electron. In addition $\rho^J_{ch}(r)$ is the radial charge transition density which is obtained by averaging the proton charge distribution[32] over the nuclear proton transition density defined in Eq. (19). The averaging integral is

$$\rho^J_{ch}(r) = \int_0^\infty \rho_P^J(r;r')\, F_p^{J0J}(r')\, r'^2 dr' \quad , \tag{26}$$

where $\rho_P^J(r;r')$ is the Jth multipole coefficient in the Legendre expansion of the proton charge distribution. The longitudinal form factor determined by inelastic electron scattering provides a measure of the S = 0 proton transition density, in contrast to inelastic proton scattering which, when a normal parity amplitude is dominant, is more sensitive to the S = 0 neutron transition density.

In closing this section we note that the longitudinal electron scattering form factor, in the region of small q, is simply related to the reduced transition probabilities determined in γ-decay measurements. To see this we replace the spherical Bessel function in Eq. (24) by the leading term in its power series which is valid for small argument and note that the averaging integral Eq. (26) conserves the Jth moment of $F_p^{J0J}(r)$,[33] i.e.

$$\int \rho^J_{ch}(r)\, r^{J+2}\, dr = \int F_p^{J0J}(r)\, r^{J+2} dr \quad . \tag{27}$$

We obtain

$$|F_L(q)|^2 \underset{q\to 0}{=} \frac{4\pi}{Z^2} \sum_J \frac{(\kappa q)^{2J}}{[(2J+1)!!]^2} \; B(EJ\uparrow) \quad , \tag{28}$$

where $B(EJ\uparrow)$ is the reduced transition probability

$$B(EJ\uparrow) = \frac{2J_f+1}{2J_i+1} \left| \int_0^\infty F_p^{J0J}(r)\; r^{J+2} dr \right|^2 \quad . \tag{29}$$

III. THEORY OF EFFECTIVE OPERATORS

The theory of effective operators is quite well known and has been discussed in many places.[5-7,11,34] We briefly review it here, following closely a discussion due to M. Harvey,[34] in order to provide background for the calculations to be presented.

A. Formal Theory

1. The Effective Hamiltonian

The nuclear Hamiltonian is generally written

$$H = H_0 + G \quad , \tag{30}$$

where H_0 is an independent particle Hamiltonian

$$H_0 = \sum_i T_i + \sum_i U_i \tag{31}$$

which has both kinetic and potential energy parts and

$$G = \sum_{i<j} g_{ij} \tag{32}$$

is the residual interaction. We assume that the difficulties associated with the hard core in the free two-nucleon potential have already been dealt with, so that g_{ij} is the bare G matrix interaction. It is usual to express the eigenfunction of H in terms of the complete set of states belonging to H_0.

$$H|\psi\rangle = E|\psi\rangle \tag{33}$$

$$|\psi\rangle = \sum_i \alpha_i |\phi_i\rangle \qquad\qquad H_0|\phi_i\rangle = \varepsilon_i|\phi_i\rangle \tag{34}$$

Since the set of basis states $\{|\phi\rangle\}$ is in general infinite in dimension, it is necessary to truncate to a finite basis in order to perform a practical calculation.

To affect this truncation the projection operators

$$P = \sum_{i\varepsilon d} |\phi_i\rangle \langle\phi_i|$$
$$Q = \sum_{i\varepsilon d} |\phi_i\rangle \langle\phi_i| \quad , \tag{35}$$

are introduced. In the above equation, d denotes the model space and the remaining space is referred to as the excluded space. Introducing the notation

$$|\psi_P\rangle = P|\psi\rangle \qquad |\psi_Q\rangle = Q|\psi \tag{36}$$

and noting that

$$P^2 = P \qquad Q^2 = Q \qquad QP = PQ = 0 \qquad P + Q = 1$$
$$PH_0Q = QH_0P = 0 \quad , \tag{37}$$

it is straightforward to show that

$$\bar{H}|\psi_P\rangle = [H_0 + \bar{G}]\ |\psi_P\rangle = E|\psi_P\rangle \tag{38}$$

$$\bar{G} = G + G\,\frac{Q}{E - H_0}\,\bar{G} \tag{39}$$

$$|\psi_P\rangle = \frac{Q}{E - H_0}\,\bar{G}\ |\psi_P\rangle \quad , \tag{40}$$

where the problem of diagonalizing H in an infinite basis has been replaced by the problem of diagonalizing an effective Hamiltonian $\bar{H}$ in a finite basis. $\bar{G}$ is the shell model effective interaction.

Equations (38) - (40) are completely equivalent to Eqs. (33) - (34) for those eigenstates of H which have some overlap with the model space. Eq. (38) gives the exact eigenvalues as well as the exact model space projection of the wave functions for these states. The components of the wave functions in the excluded space are given by Eq. (40). The claim made in the first of the two preceding sentences may seem surprising, since the number of eigenstates of H which have nonvanishing overlap with the model space surely exceeds the dimensionality of the model space. The solution to this problem comes in noting that $\bar{G}$ (hence $\bar{H}$) depends upon the exact eigenvalue, so that Eq. (38) is not the usual eigenvalue problem. In practical calculations the energy denominator appearing in the expression for $\bar{G}$ is fixed in some average way. This limits the approach to the treatment of a few eigenstates of H which presumably have a large overlap with the model space.

2. Normalization of Eigenfunctions

The normalization of $|\psi_P\rangle$ and $|\psi\rangle$ has not yet been specified. In accord with convention we normalize $|\psi_P\rangle$ to unity so that

$$\langle\psi_P|\bar{H}|\psi_P\rangle = E \quad . \tag{41}$$

The norm of $|\psi\rangle$ is then given by

$$n^2 = \langle \psi | \psi \rangle = \langle \psi_P | \psi_P \rangle + \langle \psi_Q | \psi_Q \rangle \quad . \tag{42}$$

Using Eq. (40) it immediately follows that

$$n^2 = \langle \psi_P | N^2 | \psi_P \rangle = \langle \psi_P | 1 + \bar{G} \frac{Q}{(E - H_0)^2} \bar{G} | \psi_P \rangle \quad . \tag{43}$$

With this normalization convention the admixtures of the true wave function in the model space and excluded space are

$$A_P^2 = \frac{1}{n^2} \qquad \text{and} \qquad A_Q^2 = \frac{n^2 - 1}{n^2} \quad , \tag{44}$$

respectively. If we write

$$|\psi_P \rangle = \sum_{i \varepsilon d} \alpha_i | \phi_i \rangle \quad , \tag{45}$$

then the amplitude of $|\phi_j \rangle$ $(j \varepsilon d)$ in the true wave function is

$$A_j = \alpha_j / n \qquad (j \varepsilon d) \quad . \tag{46}$$

In addition we find that the admixture of $|\phi_j \rangle$ $(j \not\varepsilon d)$ in the true wave function is

$$A_j = \sum_{i \varepsilon d} A_i \, a_{ji} \qquad (j \not\varepsilon d) \quad , \tag{47}$$

where

$$a_{ji} = \langle \phi_j | \frac{Q}{E - H_0} \bar{G} | \phi_i \rangle \qquad \begin{pmatrix} i \varepsilon d \\ j \not\varepsilon d \end{pmatrix} \tag{48}$$

is the amplitude of the excluded space configuration $|\phi_j \rangle$ in the model space configuration $|\phi_i \rangle$.

3. Effective Transition Operators

The transition matrix element of a one-body operator, $T = \sum_i t_i$, taken between two eigenstates of H, $|\psi^i\rangle$ and $|\psi^f\rangle$, is given by

$$\langle T\rangle_{fi} = n_i^{-1}\, n_f^{-1}\, \langle \psi^f | T | \psi^i \rangle \quad . \tag{49}$$

The factor $(n_i n_f)^{-1}$ is necessary because the wave functions of H have not been normalized to unity. Just as it is possible to replace the eigenvalue problem for H in an infinite basis by an eigenvalue problem for an effective Hamiltonian in a finite model space, $\langle T\rangle_{fi}$ can be expressed in terms of the matrix element of an effective, $\bar{T}$, taken between model space wave functions. The proof is short and serves to define the effective transition operator. We write

$$\langle T\rangle_{fi} = n_i^{-1}\, n_f^{-1}\, \langle \psi^f | \, (P + Q)\, T\, (P + Q)\, | \psi^i \rangle \quad . \tag{50}$$

Then we replace $|\psi_Q\rangle$ on the right by its expression in terms of $|\psi_P\rangle$, Eq. (40), to obtain

$$\langle T\rangle_{fi} = n_i^{-1}\, n_f^{-1}\, \langle \psi_P{}^f | \bar{T} | \psi_P{}^i \rangle \quad , \tag{51}$$

where

$$\bar{T} = T + T \frac{Q}{E - H_0} \bar{G} + \bar{G} \frac{Q}{E - H_0} \bar{T} + \bar{G} \frac{Q}{E - H_0} T \frac{Q}{E - H_0} \bar{G} \quad . \tag{52}$$

We also note that Eq. (51) can be rewritten as

$$\langle T\rangle_{fi} = \sum_{i,j\varepsilon d} A_i^f\, A_j^i\, \langle \phi_i | \bar{T} | \phi_j \rangle \quad . \tag{53}$$

B. Schematic Model and Discussion

It is clear from the above development that a complete discussion of the nuclear problem requires only a knowledge of the matrix elements $\langle \phi_i | \bar{G} | \phi_j \rangle$, $\langle \phi_i | N^2 | \phi_i \rangle$ and $\langle \phi_i | \bar{T} | \phi_j \rangle$ with $(i,j \varepsilon d)$. Actual calculation of these matrix elements is not a trivial matter, unfortunately, and even though this problem has received a great deal of attention it has yet to be completely solved.[11] Two estimates of the matrix elements of $\bar{T}$ are made in this work.

For the first estimate we use lowest order perturbation theory. In lowest order $\bar{G}$, N^2, and $\bar{T}$ are approximated by

$$G \approx G + G \frac{Q}{(\varepsilon_i + \varepsilon_j)/2 - H_0} G \tag{54}$$

$$N^2 \approx 1 \tag{55}$$

$$\bar{T} = T + T \frac{Q}{\varepsilon_j - H_0} G + G \frac{Q}{\varepsilon_i - H_0} T \quad , \tag{56}$$

where E has been suitably defined in terms of the eigenvalues of H_0. This approximation gives a coupling between the model space and the excluded space, but neglects entirely any configuration interaction in the excluded space. The latter is evident from the free propagators which appear in Eq. (54) and Eq. (56).

The low lying spectra of nuclei which are 2 particles (2p) or 2 holes (2h) away from closed shells are reproduced quite well in calculations employing Eq. (54).[4-8] The matrix elements of $\delta G = \bar{G} - G$ are strong and attractive in cases of the interaction energy of two identical nucleons coupled to zero total angular momentum with the main contribution coming from 3p - 1h or 3h - 1p states of energy $2\hbar\omega$. This is the pairing effect mentioned in the introduction of this paper. Calculations which use Eq. (55) and Eq. (56)[10] provide at best a qualitative estimate of transition matrix elements in nuclei np or nh away from closed shells. The main contribution to $\delta T = \bar{T} - T$ comes from (n+1)p-1h or (n+1)h-1p intermediate states of energy $2\hbar\omega$ and $1\hbar\omega$ for positive and negative parity transitions, respectively. Matrix elements of δT generally have the right sign and are of the correct order of magnitude, although they are typically underestimated. A specific difficulty occurs in effective charge calculations where it is found that polarization charges for valence protons are smaller than for valence neutrons which is in contradiction to experiment.

Lowest order perturbation theory implies a rather direct relationship between the renormalization of G and T in the case of states arising from two like nucleons in a (j^2) configuration, i.e. (2j+1)/2 states with $J^\pi = 0^+, 2^+, \ldots (2j-1)^+$. Specifically, pairing occurs as a result of coherent contributions from the coupling between the valence nucleons and core excitations of different multipolarity. On the other hand, transitions starting from the 0^+ state and ending on one of the higher spin states J_f^+ depend only on the coupling between the valence nucleons and core excitations of multipolarity J_f. Inelastic scattering affords an excellent opportunity to study the above relation, since it is the only source of experimental data which gives information on the

direct excitation of the higher spin states of these configurations.

To see the above schematically, we make use of the hydrodynamical description of the core and closure which allows us to write analytic expressions for the effective operators in the model space. Considering only coupling between the valence nucleons and normal parity core excitations we find[1,35]

$$\delta G = -\sum_{\substack{i<j \\ LM}} \theta_L \, k_v(r_i) \, k_v(r_j) \, Y^*_{LM}(\hat{r}_i) \, Y_{LM}(\hat{r}_j)$$

$$k_v(r) = -R_v \frac{dU(r - R_v)}{dR_v} \quad , \tag{57}$$

where the sum on i and j runs only over the valence nucleons, U_v is the potential which binds the valence nucleon to the core, R_v is the radius parameter in this potential, and

$$\theta_L = \frac{1}{C_L} \tag{58}$$

gives the effective strength of the coupling to 2^L-pole core excitations. C_L is the effective core stiffness parameter for 2^L-pole excitations. In a physical nucleus, there are, of course, more than one core excitation of each multipolarity. The reduction of the effect of these core excitations to a single coupling constant is where closure enters this model. In a similar manner, we find the core polarization correction to the projectile target interaction for the (p,p') reaction to be given by[15,35]

$$\delta\bar{V} = -\sum_{\substack{i \\ LM}} \theta_L k(r_p) k_v(r_i) Y^*_{LM}(\hat{r}_p) Y_{LM}(\hat{r}_i) \quad , \tag{59}$$

where $k(r_p)$ is defined in the same way as k_v except that the optical potential U replaces the bound state potential U_v.

Strictly Eq. (57) and Eq. (59) for δG and $\delta\bar{V}$ should contain some spin dependence. This comes from coupling between the valence nucleons and abnormal parity core excitations[35] and has been neglected primarily as a matter of convenience. It turns out that these spin dependent terms do not contribute to transitions between states of a (j^2) configuration as is shown in the Appendix. They do make a small contribution to the pairing energy, but we intend to compare Eq. (57) with appropriate two-body matrix elements rather than the experimental two-body spectra so their neglect causes no problem.

As examples, we consider the nuclei ^{50}Ti and ^{90}Zr both of which have two valence protons. The results of lowest order microscopic calculations[8,36] for the low lying spectra of these nuclei are compared with experiment in Fig. 1. Results obtained with $(G + \delta G)$ and without (G) the inclusion of core polarization are both shown. In the calculation for ^{50}Ti a full f-p shell model space has been assumed for the two valence protons.[8] The resulting wave functions for the lowest 0^+, 2^+, 4^+, and 6^+ states are, however, almost pure $(1f^2_{7/2})$ wave functions. In the calculation for ^{90}Zr the model space for the two valence protons included both the $(1g^2_{9/2})$ and $(2p^2_{1/2})$ configurations.[36] This explains the appearance of two 0^+ states in results for this nucleus.

The theoretical results with core polarization $(G + \delta G)$ are in good agreement with experiment in both cases. The pairing effect is quite evident. The multipole decomposition of the pairing matrix elements appearing in these calculations has been given in Ref. 8 and Ref. 36. Using Eq. (57) we obtain the following results for the pairing energy

$$E_p(j) = \langle (j^2)J = 0|\delta G|(j^2)J = 0\rangle = \sum_j E_p^J(j)$$

$$E_p^J(j) = -\langle k_v\rangle^2 \langle j\|Y_j\|j\rangle^2 \theta_j \quad , \tag{60}$$

where $\langle k_v\rangle$ denotes the radial expectation of $k_v(r)$ and the sum on J runs over even values only. Assuming $\langle k_v\rangle \approx 50$ MeV and comparing Eq. (60) with the matrix elements of Ref. 8 and Ref. 36, we obtain the values of θ_J and C_J listed in Table I. From the table, we see that the core of ^{50}Ti is somewhat softer than that of ^{90}Zr and that J = 2 core excitations give the dominant contribution to the pairing energy in both cases. The values of θ_J decrease steadily with increasing multipolarity; however, the core coupling is by no means negligible even for the highest core multipoles.

With the values of θ_J determined above, it is straightforward to estimate the corresponding effect of core polarization in inelastic proton scattering. One simply constructs the valence radial form factor according to the prescription of Sec. II.A. and adds to it the core correction

$$\delta\bar{F}^{LSJ}(r_p) = -\delta_{LJ}\delta_{SO}\frac{2}{\hat{J}} \langle j\|Y_J\|j\rangle \langle k_v\rangle \theta_J k(r_p) \tag{61}$$

which follows directly from Eq. (59). Cross sections have been calculated for the excitation of the 2^+ and 4^+ levels in ^{50}Ti and the 2^+, 4^+, 6^+ and 8^+ states in ^{90}Zr in this manner. The ^{50}Ti calculations were made for incident proton energies of 17.5 and 40 MeV to allow comparison with the experimental data of Ref. 37 and 38. The ^{90}Zr calculations were made for an incident proton energy of 18.8 MeV for comparison with the experimental data of Rev. 39. The optical parameters used in the calculations are tabulated in Table XII.

The results are compared with the data in Figs. 2 and 3. The quantity ε_p^{LSJ} shown with each cross section is the enhancement factor for core polarization. This is defined by

$$\sigma^{LSJ} = (\varepsilon_p^{LSJ})\sigma_v^{LSJ} \quad , \tag{62}$$

where σ and σ_v are the theoretical integrated cross sections with and without the inclusion of core polarization. The introduction of this enhancement factor is analogous to the use of effective charges in describing electric γ-transitions.

The theoretical results shown in Figs. 2 and 3 are in good qualitative agreement with experiment with the possible exception of the result for the 8^+ excitation in ^{90}Zr. It is suspected that multipole excitation might be important for this transition at this energy.[18] We also note from the values of ε_p that core polarization leads to an increase in the valence cross section by at least an order of magnitude in each case. We conclude that there is a striking consistency in the effect of core polarization on the low lying energy spectra of these nuclei and on the (p,p') cross sections for the excitation of these low lying states.

The above results were previously reported elsewhere,[40] in less detail than given here, by two of the present authors. The parameters for ^{50}Ti from Table I were subsequently used in the calculation of theoretical (p,p') cross sections for low lying excitations in ^{51}V.[38] This nucleus has three valence protons and the dominant configuration for the low lying states is $(1f^3_{7/2})$. The theoretical results were found to be in good agreement with experiment which tends to indicate that the effects of core polarization can be factorized, as lowest order perturbation theory implies, at least when

the number of valence nucleons is small. A more recent (e,e') study of ^{51}V has provided evidence which contradicts this conclusion to some degree.[41]

To improve on first order estimates of δT it is necessary to include the effect of configuration interaction in the excluded space, which requires higher order perturbation theory. Formally these effects can be seen by rewriting Eqs. (39), (43), and (52) in the explicit representation.

$$\bar{G} = G + G \frac{Q}{E-H_0-G} G \tag{63}$$

$$N^2 = 1 + G \frac{Q}{(E-H_0-G)^2} G \tag{64}$$

$$\bar{T} = T + T \frac{Q}{E-H_0-G} G + G \frac{Q}{E-H_0-G} T + G \frac{Q}{E-H_0-G} T \frac{Q}{E-H_0-G} G \quad . \tag{65}$$

These relations are similar in structure to the lowest order perturbative expressions in that the coupling between the model space and the excluded space is given by G interactions alone ($\bar{G}$ interactions appear on the right hand side in Eqs. (39), (43), and (52)); however, the propagators in Eqs. (63) - (65) project onto eigenstates of H in the excluded space instead of eigenstates of H_0 as is true in the case of the lowest order perturbative expressions. The spectrum of H differs from that of H_0 due to the effect of G interactions in the excluded space and this in turn affects the results for $\bar{G}$, N^2, and $\bar{T}$.

Equations (63) - (65) cannot be evaluated exactly because it is impossible to diagonalize H in the excluded space which is still infinite; however, it is possible to evaluate these relations approximately by making

suitable truncations in the excluded space. The effects of configuration interaction in the space of p-h excitations of the core is well established from the T.D.A. and R.P.A. calculations of Gillet and collaborators,[42] i.e. it gives rise to low lying normal parity vibrational states which are nearly iso-scalar in character and pushes the iso-vector core excitations up in energy. Transitions provide many clear examples that these, or related and possibly more complicated, effects are important. For example, it has already been mentioned that experiment indicates that valence neutrons and protons have approximately equal polarization charges. This implies that the dominant coupling occurs with iso-scalar core excitations. Results obtained for inelastic proton scattering and γ-transitions using the hydrodynamical core model[15,43-46] provide another example of this same effect. Here, at least for transitions of low multipolarity, the coupling constants θ_J deduced from fits to inelastic proton scattering cross sections using Eq. (59) are found to be nearly equal to those required to reproduce the effective charge,[15] i.e.

$$e^{Jq}_{eff} = e_q + \theta_J \frac{3Z_c}{4\pi} eR_c^J \langle k_v \rangle / \langle r^J \rangle \tag{66}$$

where $e_q = 1$ or 0 for $q = p$ or n, Z_c is the core charge, R_c its radius, and the radial expectations $\langle\rangle$ are taken with respect to the radial wave functions of the valence nucleons. The θ_J in Eq. (59) and Eq. (66) are only equal in the limit of coupling to iso-scalar core excitations.[35] (Note that our schematic discussion of the relationship between the pairing effect and the enhancement of (p,p') cross sections required no reference to the iso-spin nature of the coupling between the core and the valence protons.) A third

and perhaps even more striking example of the importance of configuration interaction in the excluded space is seen in nuclei around ^{208}Pb where there are clear cut cases of coupling between valence nucleons and low lying vibrational states of the core.[43,17]

Including only the effect of configuration interaction in the core by means of the T.D.A. or R.P.A. approximations seems to provide the best estimate of transition matrix elements insofar as agreement with experiment is concerned.[10] These calculations are equivalent to assuming a particle-vibrational model and preserve the factorizability of core polarization effects. Similar calculations for $\bar{G}$ result in an overestimation of the pairing energy.[9,11] One would like to find a suitable approximation for evaluating Eqs. (63) - (65) which would improve the lowest order estimates of the transition matrix elements and at the same time preserve the lowest order results of Kuo and Brown for the effective interaction. So far this has not been accomplished.[11] In fact, the most complete treatment of the effect of configuration interaction in the excluded space which has been made to date[11] leads to results for $\bar{G}$ which are not much different than those for G and results for $\bar{T}$ which are similar to those obtained using first order perturbation theory.

Harvey has suggested[34] that a possible way of "bootstrapping" the effect on $\bar{T}$ of configuration interaction in the excluded space might be to use Eq. (43) and Eq. (52) approximating $\bar{G}$ by a two-body interaction $\bar{G}'$ which fits the two-body spectra. He points out that this procedure was followed by Horie and Arima[2] in their early calculations. Owing to the uncertainty in the perturbative treatment of these higher order effects[11] and faced with the need of including some estimate of the effect of core correlations, we

have crudely followed this approach for our second estimate of the matrix elements of $\bar{T}$. Specifically, we have repeated the first order calculations using the renormalized core coupling interaction

$$\bar{G}' = G - \sum_{\substack{i<j \\ JM}} \theta_J k_v(r_i) k_v(r_j) Y^*_{JM}(\hat{r}_i) Y_{JM}(\hat{r}_j) P_1^T \quad , \tag{67}$$

where P_1^T projects onto triplet iso-spin states and the θ_J are fixed from the pairing matrix elements of Ref. 8 and Ref. 36 in the manner described above. This interaction is somewhat incomplete in that it does not contain any spin dependence and is missing some small renormalization terms which act in iso-spin singlet states. It does, however, contain the major components required to fit the two-body spectra. In Section IV, it will be seen that the results obtained using this interaction are similar to those obtained using the "bare" G and treating core correlations in the T.D.A. approximation.[10,11]

C. Explicit Expressions for Matrix Elements of $\bar{T}$

In this section we construct the explicit expression for the reduced matrix element of $\bar{T}$ between two model space states. This is obtained directly from the expressions for the amplitudes of the excluded space configurations in the model space configurations and the reduced matrix elements for T between two model space states and between a model space state and an excluded space state. We consider only one body operators which transform like the "spin-angle" tensor defined in Eq. (17) and throughout this section the use of G is intended to imply either G or $\bar{G}'$.

We define the model space states by

$$|\phi_M\rangle = |\alpha_1(n) J_1 M_1\rangle = Z^+_{\alpha_1 J_1 M_1}(n)|C\rangle \quad , \tag{68}$$

where $Z^{+}_{\alpha_1 J_1 M_1}(n)$ creates an np or nh state with quantum numbers α_1, J_1, M_1 by operating on the closed shell state $|C\rangle$. J_1 and M_1 denote the total angular momentum and projection while α_1 represents all other quantum numbers required to completely specify the state.

In first order only (n+1)p-1h [(n+1)h-1p] and np(nh) intermediate states can contribute to the renormalization of T. We include only the former with the remark that the latter are best included in the model space whenever they are important. The (n+1)p-1h [(n+1)h-1p] excluded space states are defined by

$$|\phi_E\rangle = |\alpha_2(n)J_2, (p\bar{h})J_c; J_3M_3\rangle \tag{69}$$

$$= \sum_{M_2M_c} \langle J_2\, J_c M_2 M_c | J_3\, M_3\rangle\, Z^{+}_{\alpha_2 J_2 M_2}(n)\, A^{+}_{J_c M_c}(ph)|C\rangle \quad ,$$

where

$$A^{+}_{J_c M_c}(ph) = \sum_{m_p m_h} \langle j_p\, j_h\, m_p - m_h | J_c M_c\rangle (-1)^{j_h - m_h}\, a^{+}_p\, a_h \tag{70}$$

creates a p-h pair with angular momentum J_c and projection M_c. In writing Eq. (69) it has been assumed that p and h are distinct from any of the particle or hole states contained in $Z^{+}_{\alpha_2 J_2 M_2}(n)$, i.e. we neglect the Pauli principle in intermediate states. The error introduced by making this simplification should not be serious because we consider only cases where n is relatively small.

The amplitude of the excluded space state with energy $\varepsilon_{\alpha_2 J_2 ph}$ in the model space state with energy $\varepsilon_{\alpha_1 J_1}$ is easily found to be

$$a(\alpha_2 J_2,(p\bar{h})J_c;J_3|\alpha_1 J_1) = \delta_{J_1 J_3}(-1)^{J_2 - J_1}\,\hat{j}_p \hat{J}_2 \hat{J}_1^{-1}$$

$$\times \sum_{\substack{j_\alpha j_\gamma \\ q}} S_q^{J_c}(\alpha_2 J_2,\alpha_1 J_1;j_\alpha j_\gamma)\alpha_{qq'}^{J_c}(j_p j_h,j_\alpha j_\gamma)/(\varepsilon_{\alpha_1 J_1} - \varepsilon_{\alpha_2 J_2 ph}) , \tag{71}$$

where

$$S_q^{J_c}(\alpha_2 J_2,\alpha_1 J_1;j_\alpha j_\gamma) = \hat{j}_\alpha \hat{J}_c^{-1} \langle \alpha_2(n)J_2 \| A^+_{J_c}(\alpha\gamma) \| \alpha_1(n)J_1 \rangle \tag{72}$$

is a spectroscopic amplitude which depends only on the structure of the valence configurations, and

$$\alpha_{qq'}^{J_c}(j_p j_h,j_\alpha j_\gamma) = \sum_{J'} (-1)^{j_\alpha + j_h - J'} \frac{\hat{J}_c \hat{J}'^2}{\hat{j}_p \hat{j}_\alpha} \begin{Bmatrix} j_p & j_\alpha & J' \\ j_\gamma & j_h & J_c \end{Bmatrix}$$

$$\times \langle j_p j_\alpha J' | g_{qq'} | j_h j_\gamma J' \rangle_a \tag{73}$$

is the Jth multipole coefficient of the coupling interaction. The indices q and q' which appear in Eq. (72) and (73) specify the charge state of the valence particles $(j_\alpha j_\gamma)$ and the core excitation $(j_p j_h)$, respectively. This in turn determines which component of g is effective in the polarizing process. The subscript a on the two-body matrix element in Eq. (73) indicates that the matrix element is antisymmetrized but not normalized. The values of $S_q^{J_c}$ for

the transitions of interest in this work are given in the Appendix. It is the separation of the amplitude of eq. (66) into a geometrical factor $S_q^{J_c}$ and a dynamical factor $\alpha_{qq'}^{J_c}$, which give rise to the factorizability of core polarization effects in lowest order. Additional factorization of $\alpha_{qq'}^{J_c}$ into valence and core parts is the essential feature built into all phenomenological models for effective operators.[15,35,47,48]

We also note the following symmetry relations for $S_q^{J_c}$ and $\alpha_{qq'}^{J_c}$.

$$S_q^{J_c}(\alpha_1 J_1,\alpha_2 J_2;j_\alpha j_\gamma) = (-1)^{J_1 - J_2 + j_\gamma - j_\alpha}\hat{J}_2\hat{j}_\alpha\hat{J}_1^{-1}\hat{j}_\gamma^{-1}\; S_q^{J_c}(\alpha_2 J_2,\alpha_1 J_1;j_\gamma j_\alpha) \quad (74)$$

$$\alpha_{qq'}^{J_c}(j_p j_h,j_\alpha j_\gamma) = (-1)^{j_\alpha - j_\gamma + j_h - j_p}\;\hat{j}_h\hat{j}_\gamma\hat{j}_\alpha^{-1}\hat{j}_p^{-1}\;\alpha_{qq'}^{J_c}(j_h j_p,j_\gamma j_\alpha) \quad (75)$$

As an example of the usefulness of these relations, we observe that they may be used to show that

$$a(\alpha_2 J_2(p\bar{h})J_c;J_1|\alpha_1 J_1) = (-1)^{J_2 - J_1}\hat{J}_2\hat{J}_1^{-1}\; a(\alpha_1 J_1,(p\bar{h})J_c;J_2|\alpha_2 J_2) \quad (76)$$

in cases when there is only one active orbit in the states $\alpha_1 J_1$ and $\alpha_2 J_2$, i.e. $j_\alpha = j_\gamma = j$.

The reduced matrix element of a one body operator T^{LSJ} taken between a model space and an excluded space state is

$$\langle \phi_E \| T^{LSJ} \| \phi_M \rangle = \delta_{\alpha_1\alpha_2}\delta_{J_1 J_2}\delta_{JJ_c}\;\hat{j}_p\hat{J}^{-1}\langle j_p \| t_q^{LSJ} \| j_h \rangle \quad , \quad (77)$$

where the superscripts LSJ have been added to T since we consider operators which transform like the "spin-angle" tensor of Eq. (17). The subscript q

appearing on t^{LSJ} in this equation is a charge index. It is needed because, in general t^{LSJ} will not be the same for a proton p-h pair and a neutron p-h pair. The main point to notice about the result is that the p-h pair is produced solely by the action of T, with the valence nucleons serving merely as spectators. The result for the reversed matrix element $\langle \phi_M \| T^{LSJ} \| \phi_E \rangle$ will not be given since it easily derived from the following conjugation relation for operators of the "spin-angle" type.

$$\langle J_a \| T^{LSJ} \| J_h \rangle = (-1)^{S + J + J_a - J_b} \hat{J}_b \hat{J}_a^{-1} \langle J_b \| T^{LSJ} \| J_a \rangle \tag{78}$$

The reduced matrix element of T^{LSJ} between two model space states is simply

$$\langle \alpha_2(n) J_2 \| T^{LSJ} \| \alpha_1(n) J_1 \rangle = \sum_{\substack{j_\alpha j_\gamma \\ q}} S_q^J(\alpha_2 J_2, \alpha_1 J_1; j_\alpha j_\gamma) \langle j_\alpha \| t_q^{LSJ} \| j_\gamma \rangle \tag{79}$$

Use of the above results for the matrix elements of T and G and the associated symmetry and conjugation relations in Eq. (56) leads directly to the expression for the reduced matrix element of the renormalized transition operator taken between two model space states. This is the essential relation for the calculations of this work. The result is

$$\begin{aligned} \langle \alpha_f(n) J_f \| \bar{T}^{LSJ} \| \alpha_i(n) J_i \rangle = & \sum_{\substack{j_\alpha j_\gamma \\ q}} S_q^J(\alpha_f J_f, \alpha_i J_i; j_\alpha j_\gamma) \\ & \times \left[\langle j_\alpha \| t_q^{LSJ} \| j_\gamma \rangle + \sum_{\substack{j_p j_h \\ q'}} \left\{ \frac{1}{\varepsilon_{\alpha_i J_i} - \varepsilon_{\alpha_f J_f ph}} + \frac{1}{\varepsilon_{\alpha_f J_f} - \varepsilon_{\alpha_i J_i ph}} P_{ph} \right\} \right. \\ & \left. \times F^J_{qq'}(j_p j_h, j_\alpha j_\gamma) \right] , \end{aligned} \tag{80}$$

where P_{ph} acts to the right and means to interchange j_p and j_h, and

$$F^J_{qq'}(j_p j_h, j_\alpha j_\gamma) = (-1)^{j_p - j_h} \hat{j}_p \hat{j}_h \hat{J}^{-1} \alpha^J_{qq'}(j_p j_h, j_\alpha j_\gamma) \langle j_h \| t^{LSJ}_{q'} \| j_p \rangle . \quad (81)$$

In Eq. (80) the first term on the left is the normal valence contribution and the second term is the core polarization contribution. Using Eq. (75) and Eq. (78) in Eq. (81) we also note that

$$P_{ph} F^J_{qq'}(j_p j_h, j_\alpha j_\gamma) = (-1)^{S + J - j_\alpha - j_\gamma} \hat{j}_\alpha \hat{j}_\gamma^{-1} F^J_{qq'}(j_p j_h, j_\gamma j_\alpha) . \quad (82)$$

D. Enhancement and Retardation of Transition Operators

The expression for the reduced matrix element of $\bar{T}$ given in the preceding section can be reduced further by specializing to the case of a zero-range coupling interaction, i.e.

$$g_{qq'}(1,2) = (g^0_{qq'} + g^1_{qq'} \bar{\sigma}_1 \cdot \bar{\sigma}_2) \, \delta(\bar{r}_1 - \bar{r}_2) . \quad (83)$$

We pursue this here as it allows us to derive a general rule concerning the phase of the contribution from core polarization. Calculations using typical finite-range interactions produce results consistent with this rule.

The derivation requires further specification of the form of the one-body operator of interest. We consider only one-body operators which can be written

$$t^J_q = f^{LSJ}_q T^{LSJ} = \beta^{LSJ}_q h^{LSJ}_q T^{LSJ} \quad (84)$$

where T^{LSJ} is the spin-angle tensor defined in Eq. (17) and f_q^{LSJ} contains the radial dependence of the operator, h_q^{LSJ}, as well as the coupling constant, β_q^{LSJ}, e.g. $h_q^{LSJ} = \delta_{S0}\delta_{LJ}r^L$ and $\beta_q^{LSJ} = e_q$ in the case of an electric γ-transition.

In the case of a zero-range interaction the direct and exchange parts of two-body matrix elements are identical and the multipole coefficient of Eq. (73) can be factorized, i.e.

$$\alpha^J_{qq'}(j_p j_h, j_\alpha j_\gamma) = \frac{2}{\hat{J}} \sum_{LS} g^S_{qq'}(-1)^{S+J} \langle j_p \| T^{LSJ} \| j_h \rangle \times \langle j_\alpha \| T^{LSJ} \| j_\gamma \rangle \; I(\ell_p \ell_h \ell_\alpha \ell_\gamma). \tag{85}$$

The reduced matrix elements in Eq. (85) contain only integrations over spin and angular coordinates and I is a radial overlap integral

$$I(\ell_p \ell_h, \ell_\alpha \ell_\gamma) = \int_0^\infty u_p(r) u_\alpha(r) u_h(r) u_\gamma(r) r^2 dr \quad , \tag{86}$$

where the u(r) denote single particle radial wave functions. The factorization of $\alpha^J_{qq'}$ further implies that

$$P_{ph} F^J_{qq'}(j_p j_h, j_\alpha j_\gamma) = F^J_{qq'}(j_p j_h, j_\alpha j_\gamma) \tag{87}$$

which is easily demonstrated using Eq. (78) and Eq. (85) in Eq. (82). Use of Eq. (84), (85), and (86) in Eq. (80) we obtain the desired result for the matrix element of $\bar{T}$ in the case of a zero-range coupling interaction. This is

$$\langle \alpha_f(n)J_f \| \bar{T}^{LSJ} \| \alpha_i(n)J_i \rangle = \sum_{\substack{j_\alpha j_\gamma \\ q}} S_q^J(\alpha_f J_f, \alpha_i J_i; j_\alpha j_\gamma) \times \left\{ \langle j_\alpha \| T^{LSJ} \| j_\gamma \rangle \langle h_q^{LSJ} \rangle_{\alpha\gamma} \beta_q^{LSJ} + \sum_{L'S'} \langle j_\alpha \| T^{L'S'J} \| j_\alpha \rangle H_{L'S'}^{LSJ}(\alpha,\gamma) \right\} \tag{88}$$

where

$$H_{L'S'}^{LSJ}(\alpha,\gamma) = -\sum_{\substack{j_p j_h \\ q'}} \frac{\varepsilon(ph)}{\varepsilon^2(ph) - Q^2} \frac{4\hat{j}_p^2}{\hat{J}^2} g_{qq'}^{S'} \langle j_p \| T^{LSJ} \| j_h \rangle \times \langle j_p \| T^{L'S'J} \| j_h \rangle I(\ell_p \ell_\alpha \ell_h \ell_\gamma) \langle h_{q'}^{LSJ} \rangle_{ph} \beta_{q'}^{LSJ} \tag{89}$$

and

$$\langle h_{q'}^{LSJ} \rangle_{ph} = \int_0^\infty u_p(r) h_{q'}^{LSJ} u_h(r) r^2 dr \tag{90}$$

$$\varepsilon(ph) = \varepsilon_p - \varepsilon_h \qquad Q = \varepsilon_{\alpha_i J_i} - \varepsilon_{\alpha_f J_f} \tag{91}$$

The phase rule of interest applies only to a single pair of active valence orbitals, i.e. fixed $j_\alpha j_\gamma q$. The phase relation between different terms in the sum over $j_\alpha j_\gamma q$ is a function of the model space configurations and not

of core polarization. Restricting consideration to a fixed set of values for $j_\alpha j_\gamma q$ we have only to consider the sum over L' and S' in Eq. (88). Due to parity and angular momentum selection rules, there are only two allowed sets of values of L'S' for given LSJ. It is sufficient to note that one set is L'S' = LS and the other is L'S' $\neq$ LS.

For the first set, L'S' = LS, we note that the sign of each term in the sum over j_p and j_h in Eq. (89) is given by

$$- \sum_{q'} g^{S}_{qq'} \langle h^{LSJ}_{q'} \rangle_{ph} \; I(\ell_p \ell_\alpha \ell_h \ell_\gamma) \; \beta^{LSJ}_{q'} \quad ,$$

where it has been assumed that $\varepsilon^2(ph) > Q^2$. We then argue that the important terms in the sum over j_p and j_h are those where

$$u_p(r) u_h(r) \approx u_\alpha(r) u_\gamma(r) \quad .$$

This is sufficient to guarantee that for these important terms

$$I(\ell_p \ell_\alpha \ell_h \ell_\gamma) > 0$$

$$\langle h^{LSJ}_{q'} \rangle_{ph} \approx \langle h^{LSJ}_{q} \rangle_{\alpha\gamma} \quad .$$

Considering only the contribution from the term H^{LSJ}_{LS} to the renormalization of the matrix element of T^{LSJ}, we conclude that the relative signs of the valence and core contribution are given by

$$\langle T^{LSJ}_{q'} \rangle_{fi} \sim \beta^{LSJ}_{q}$$
$$\langle \delta T^{LSJ} \rangle_{fi} \sim -\sum_{q'} \beta^{LSJ}_{q'} \; g^{S}_{qq'} \tag{92}$$

Finally we argue that the contribution from the term $H^{LSJ}_{L'S'}$ with $L'S' \neq LS$ can, in fact, be neglected, because the various terms comprising this quantity have random phases.

Using Eq. (92) it is a simple matter to compute the relative sign of the valence contribution and the core polarization contribution for a given one-body operator. For inelastic proton scattering we have $\beta^{LSJ}_{q} = \bar{V}^{S}_{pq}$ from Eq. (14). Using the fact that $\bar{V}^{S}_{pq} \sim g^{S}_{pq}$ and the relationship between the components of g^{S}_{pq} given in Eq. (4), it immediately follows that the valence and core contribution are in phase for S = 0 amplitudes and out of phase for S = 1 amplitudes, i.e. the S = 0 amplitude are enhanced while the S = 1 amplitudes are retarded.

For longitudinal electron scattering and electric γ-transitions S = 0 and $\beta^{LSJ}_{q} = e_q = 0$ or 1, as q = p or n. Since g^{0}_{pq} is attractive, we conclude that the valence and core contributions are in phase for this case. For magnetic γ-transitions S = 1 and $\beta^{LSJ}_{q} = \mu_q$ which is positive or negative as q = p or n. Using Eq. (4) we find that the valence and core contributions are out of phase. These results demonstrate that there is a close correspondence between the effects of core polarization in inelastic proton scattering and in electromagnetic interactions.

It is possible to go one step beyond Eqs. (88) - (91) and write a closed coordinate space expression for δT^{J}. This is

$$\delta T^{LSJ}_{M_J} = \sum_{\substack{i \\ L'S'}} \delta t_q^{L'S'J}(r_i) T^{L'S'J}_{M_J}(i) \ , \tag{93}$$

where the sum on i runs only over the valence nucleons and q = p or n, as i designates a proton or a neutron. The radial factors in Eq. (93) are given by

$$\delta t_q^{L'S'J}(r_i) = -\sum_{\substack{j_p j_h \\ q'}} \frac{\varepsilon(ph)}{\varepsilon^2(ph) - Q^2} \frac{4\hat{j}_p^2}{\hat{J}^2} \langle j_p \| T^{LSJ} \| j_h \rangle$$
$$\times \langle j_p \| T^{L'S'J} \| j_h \rangle \, g^{S'}_{qq'} \, \beta^{LSJ}_{q'} \langle h^{LSJ}_{q'} \rangle_{ph} u_p(r_i) u_h(r_i). \tag{94}$$

An operator of this form has been used to fit the magnetic moments in the Pb region.[48] The force strengths $g^S_{qq'}$ were treated as adjustable parameters in obtaining the fit. This approach could be extended to other one-body operators.

IV. RESULTS

In this section we present the results of our calculations for selected transitions in ^{42}Ca, ^{50}Ti, ^{89}Y, ^{90}Zr, ^{207}Pb, and ^{209}Bi. The nuclides ^{50}Ti and ^{90}Zr have already been discussed in connection with the schematic model in Sec. III.B . They have two valence protons outside of ^{48}Ca and ^{88}Sr cores, respectively. ^{42}Ca has two valence neutrons outside a ^{40}Ca core; ^{89}Y has one valence proton outside a ^{88}Sr core; ^{207}Pb has one valence neutron hole in a ^{208}Pb core; while ^{209}Bi has a single valence proton outside a ^{208}Pb core. The transitions we have considered are summarized in Table II. The initial and final model space wave function assumed in each case are specified in the table.

A. Parameters of the Calculations

For the first order estimates of δT we have used the long range part of the Kallio-Kolltveit (KK) potential[49] for G. This is an S-wave interaction which gives matrix elements which are in rough agreement with those obtained with the more realistic HJ interaction.[5] The S-wave form of the KK force greatly simplifies the calculation of two-body matrix elements. This feature has made this interaction popular in the past[10] and it is also the main reason why it has been chosen here. The differences between the KK and HJ interaction are well within the accuracy of the models being used in this work, so there is no real inconsistency in using the KK force for G in calculating the bound state matrix elements and using the HJ interaction for t^R_{ip} in calculating the (p,p') cross sections.

For ^{50}Ti and ^{90}Zr, in the calculations of δT using the renormalized coupling interaction defined in Eq. (67), we have used the values of $\theta_L^p = 1/C_L^p$ given in Table I. The ^{90}Zr parameters were also used in the calculations for ^{89}Y. For ^{42}Ca we have used $C_0^p = 6020$ MeV, $C_2^p = 355$ MeV, $C_4^p = 578$ MeV, and $C_6^p = 1050$ MeV and in the Pb region we have used $C_0^p = 3790$ MeV, $C_2^p = 1040$ MeV, $C_4^p = 1580$ MeV, $C_6^p = 2450$ MeV, and $C_8^p = 3650$ MeV. These last two sets of values have been determined from matrix elements given in Ref. 8 in the same manner that was used to determine the values given in Table I. It is interesting to note the large increase in the stiffness of the core in passing from the Ca region to the Pb region.

We do not actually evaluate the radial integrals $\langle k_v \rangle$ which arise in the calculation of the matrix elements of $\bar{G}'$. Instead we assume that

$$\langle k_v \rangle_{13} \langle k_v \rangle_{24} = 2500\ f(n_1 n_3; n_2 n_4)\ \mathrm{MeV}^2$$

where $n(=1, 2, \ldots, \infty)$ denotes the principle quantum number which characterizes the shape of the radial wave functions. The factor

$$f(n_1 n_3; n_2 n_4) = (-1)^{|n_1-n_3| + |n_2-n_4|}\ (0.75)^{n_1+n_2+n_3+n_4-4}$$

has the value unity when $n_1=n_2=n_3=n_4=1$, i.e., when all of the radial wave functions have good overlap with $k_v(r)$, and is appropriately smaller and properly phased when there are shape differences between the radial wave functions and $k_v(r)$.

Harmonic oscillator radial wave functions have been used throughout in the calculations. The oscillator well parameter $\alpha = (M\omega/\hbar)^{1/2} F^{-1}$ has been

fixed according to[31]

$$\hbar\omega = 41\ A^{-1/3}\ \text{MeV} \quad .$$

The energy denominators used in the calculations were taken for the most part from the zero deformation axis of the Nilsson scheme.[50] In some cases they were taken from experiment. The Nilsson energies for the first 40 single particle states are given in Table III as a function of $\hbar\omega$. In the table each single particle state has been assigned an identification number as a matter of convenience.

The range of intermediate states used in estimating δT for the various transitions being considered is summarized in Table IV. All possible (n+1)p-1h [(n+1)h-1p] states which can be obtained by raising a core nucleon from one of the single particle states designated as a hole level to one of the single particle states designated as a particle level have been included in the calculations of δT. Inspection of the table will show that we have "approximately" followed the rule of including all (n+1)p-1h [(n+1)h-1p] intermediate states with energies up to $2\hbar\omega$ for positive parity transitions and $1\hbar\omega$ for negative parity transitions.

Experimental single particle energies have been used for the $1\hbar\omega$ positive parity core excitations which enter the calculations of δT for transitions in ^{50}Ti and ^{90}Zr. The energies of these particular core excitations are relatively small and the Nilsson scheme cannot be expected to be reliable in these cases. Specifically, we use experimental energy splittings for the $2p_{3/2} - 1f_{7/2}^{-1}$, $2p_{1/2} - 1f_{7/2}^{-1}$, and $1f_{5/2} - 1f_{7/2}^{-1}$ neutron excitations in ^{50}Ti, the $2p_{1/2} - 2p_{3/2}^{-1}$, $2p_{1/2} - 1f_{5/2}^{-1}$, and $2p_{1/2} - 1f_{7/2}^{-1}$ proton excitations in ^{90}Zr, and the $2d_{5/2} - 1g_{9/2}^{-1}$, $3s_{1/2} - 1g_{9/2}^{-1}$, $2d_{3/2} - 1g_{9/2}^{-1}$

and $1g_{7/2} - 1g_{9/2}^{-1}$ neutron excitations in ^{90}Zr. The experimental energy splittings are, respectively, 4.80, 6.82, and 8.75 MeV[8], 3.5, 4.0, and 5.5 MeV[51,52], and 4.50, 5.53, 6.50, and 7.17 MeV[51,52] which are typically larger than the values which would be deduced from Table III. For the calculations in the Pb region we chose to use experimental energy values in all cases where they were available, namely proton levels #11-22 and 24 and neutron levels #16-29 and 32.[53] The Nilsson energies were used for the other levels with some slight modifications. These were to increase the Nilsson energies for proton orbitals #23, 25 and above by 2.41 MeV, so that level #23 would not fall below level #24, and to make the neutron levels #30 and 31 degenerate with level #32 instead of below it as the Nilsson scheme suggests.

B. Wave Functions

It is useful to examine the most important core admixtures in the various model space configurations being treated. Due to space limitations we consider only two typical examples here. More complete information can be obtained from the authors by request.

Tables V and VI contain the amplitudes of the most important $|(j^2)J,(p\bar{h})J;0\rangle$ core admixtures in the $|(j^2)0^+\rangle$ model space configurations for ^{50}Ti$(j = 1f_{7/2})$ and ^{90}Zr$(J = 1g_{9/2})$. These tables contain all the information needed to describe the $|(j^2)0^+\rangle \rightarrow |(j^2)J^+\rangle$ transitions in these nuclei, since the amplitudes of the $|(j^2)0,(p\bar{h})J;J\rangle$ core admixtures in the $|(j^2)J^+\rangle$ are easily obtained from the given amplitudes by means of Eq. (76).

It is apparent from the tables that the number of core admixtures that make important contributions are not large in comparison to the total number of allowed admixtures. There are two factors which limit the number of configurations which make important contributions. The first is the requirement of good overlap between the radial wave functions for the p-h pair and the active valence particles, e.g. see the discussion in Sec. III.D. The second is that $|(j^2)J,(p\bar{h})J;0\rangle$ admixtures where the p and h orbits are co-planar are heavily favored. This condition, which may be stated

$$|\ell_p \pm \ell_h| = J \quad ,$$

is a property of the reduced matrix elements $\langle j_p \| T^{JOJ} \| j_h \rangle$ which enter in the calculation of the Jth multipole coefficient of the coupling interaction, e.g. see Eq. (85) for the multipole coefficient in the zero range limit. The same $|(j^2)J,(p\bar{h})J,0\rangle$ admixtures which mix strongly with the $|(j^2)0^+\rangle$

configurations also produce the largest matrix elements of T because the latter, Eq. (77), are also proportional to $\langle j_p \| T^{JOJ} \| j_h \rangle$. These points are summarized explicitly in the zero-range expression for the matrix elements of T, Eqs. (88)-(91), where it is seen that dominant terms are proportional to

$$\langle j_p \| T^{JOJ} \| j_h \rangle^2 \; I(\ell_p \ell_\alpha \ell_h \ell_\gamma) \quad .$$

We also note that the amplitudes for some of the positive parity $1\hbar\omega$ excitations are quite large, particularly in the calculations where $\bar{G}'$ has been used. Our estimate of these large admixtures is undoubtedly unreliable and it would appear necessary to include the second order terms in estimating δT to improve this situation. Additional indications that the second order terms may be important in some cases will be seen in the next section.

Agassi and Schaeffer[16] have previously reported the results of a first order estimate of the effect of core polarization in the excitation of 2^+ states in various nuclei. The $0^+ \rightarrow 2^+$ transition in ^{90}Zr is the only point of overlap between the calculations of Ref. 16 and the present work. Agassi and Schaeffer obtained a particularly small core polarization effect in this case while we obtain a large effect as will be seen in the next section. From their published amplitudes we find that the core coupling interaction they have used is quite similar to the KK force used in the present work, however, we note that they have used a much smaller excluded space than we have (all $2\hbar\omega$ excitations) and thus they have missed several important core admixtures.

C. Radial Transition Densities and Radial Form Factors

Before examining the (e,e') form factors and (p,p') differential cross sections which are the final results of this paper, it is useful to discuss the radial transition densities and radial form factors which provide the link between the wave functions described in the preceding section and these final results. The radial transition densities and the radial form factors were defined in Sec. II. These functions are the matrix elements of the one body operators for which we are calculating the renormalization due to core polarization.

The LSJ = 202 trantition densities for $0^+ \rightarrow 2^+$ transitions in ^{50}Ti and ^{90}Zr, the $1h_{9/2} \rightarrow 2f_{7/2}$ transition in ^{209}Bi, and the $3p_{1/2} \rightarrow 2f_{5/2}$ transition in ^{207}Pb are shown in fig. 4. The valence transition densities as well as the complete proton and neutron transition densities [D+C(p) and D+C(n)] obtained with core polarization included are shown in each case. We have shown the results obtained using the renormalized core coupling interaction, although for our purposes here the first order results would have served equally well. For the first three transitions the valence transition densities have shapes which are very similar to the complete proton and neutron transition densities. This is a typical feature of the transition densities obtained for most of the transitions considered in this work. It was anticipated in the overlap argument used in the discussion of the enhancement and retardation effects due to core polarization given in Sec. III. D. The results for the $3p_{1/2} \rightarrow 2f_{5/2}$ transition in ^{207}Pb is a case where the differences in shape between the valence transition densities and the complete proton and neutron transition densities are the largest. Even here the differences are not too great in the important surface region.

The radial form factors obtained by averaging the real part of $\bar{V}$ over the transition densities of Fig. 4 are shown in Fig. 5. The distributions in Fig. 5 are quite similar to those shown in Fig. 4, except that the neutron functions are increased in size relative to the proton functions. This occurs because $\bar{V}^0_{pn} \approx 3\bar{V}^0_{pp}$. The main point is that the projectile-target interaction acts much like an overall scaling factor for the transition densities. Because of the finite range of this interaction the averaging does tend to smear out the transition densities slightly. This has the effect of reducing, to some degree, the importance of any shape differences between the various transition density functions.

The above discussion suggests that the results for the (e,e') and (p,p') reactions can be qualitatively understood by comparing the relative magnitudes of a single moment of the various transition density functions, most logically the lowest moment, and by introducing appropriate scaling factors which are characteristic of these reactions. For (p,p') the scaling factors are the relative strengths of the various components of the projectile-target interaction and for (e,e') the scaling factors are the nucleon charges, i.e. $e_p = 1$ and $e_n = 0$. A comparison of this type is useful, because it allows the general features of the results to be displayed in a transparent and compact form. The (p,p') differential cross sections and (e,e') form factors do show some sensitivity to higher moments of the transition densities,[14] so any fine details in the results can only be seen by calculating these quantities as prescribed in Sec. II. These final results will be shown in the next section, after we make this rough comparison.

To make this comparison in cases where there are valence protons, we divide the complete proton transition density into valence and core parts and introduce the parameters

$$\lambda_p^{LSJ} = \frac{\int_0^\infty F_{p_c}^{LSJ}(r)\ r^{L+2} dr}{\int_0^\infty F_{p_v}^{LSJ}(r)\ r^{L+2} dr} \tag{95}$$

$$\lambda_n^{LSJ} = \frac{\int_0^\infty F_n^{LSJ}(r)\ r^{L+2} dr}{\int_0^\infty F_{p_v}^{LSJ}(r)\ r^{L+2} dr} \tag{96}$$

which measure the contribution to the nuclear transition densities from core polarization relative to the valence transition density. We then assume that the effect of core polarization on the (p,p') cross sections can be adequately characterized by the enhancement factor which was introduced in Eq. (62). In terms of λ_p^{LSJ} and λ_n^{LSJ} this factor is approximately given by

$$\varepsilon_p^{LSJ}(p) = 1 + \lambda_p^{LSJ} + \alpha_S \lambda_n^{LSJ} \quad , \tag{97}$$

where $\alpha_S = V_{pn}^S / V_{pp}^S$. In a similar fashion we introduce the effective charge

$$e_{eff}^{Jp} = 1 + \lambda_p^{JOJ} \tag{98}$$

to characterize the effect of core polarization on the (e,e') form factors. The effective charge has precise meaning for inelastic electron scattering in the low q limit, corresponding to γ-decay, because only the lowest moment of the proton transition densities come into consideration here. This was pointed

out at the end of Sec. II-B. In cases where there are valence neutrons the definitions of λ_p^{LSJ} and λ_n^{LSJ} are modified

$$\lambda_p^{LSJ} = \frac{\int_0^\infty F_p^{LSJ}(r) r^{L+2} dr}{\int_0^\infty F_{n_v}^{LSJ}(r) r^{L+2} dr} \tag{99}$$

$$\lambda_n^{LSJ} = \frac{\int_0^\infty F_{n_c}^{LSJ}(r) r^{L+2} dr}{\int_0^\infty F_{n_v}^{LSJ}(r) r^{L+2} dr} \tag{100}$$

and

$$\varepsilon_p^{LSJ}(n) = 1 + \alpha_S^{-1} \lambda_p^{LSJ} + \lambda_n^{LSJ} \tag{101}$$

$$e_{eff}^{Jn} = \lambda_p^{JOJ} \quad . \tag{102}$$

As it is sometimes convenient to talk in terms of the iso-scalar and iso-vector contributions to $\varepsilon_p^{LSJ}(q)$ and e_{eff}^{Jq}, it is also useful to give Eqs. (97), (98), (101) and (102) in terms of these quantities. These expressions are

$$\varepsilon_p^{LSJ}(q) = 1 + \alpha_S^0(q)\lambda_0^{LSJ} + \alpha_S^1(q)\lambda_1^{LSJ} \tag{103}$$

$$e_{eff}^{Jq} = e_q + \frac{1}{2}(\lambda_0^{JOJ} + \lambda_1^{JOJ}) \quad , \tag{104}$$

where

$$\lambda_0^{LSJ} = \lambda_p^{LSJ} + \lambda_n^{LSJ} \qquad \lambda_1^{LSJ} = \lambda_p^{LSJ} - \lambda_n^{LSJ} \tag{105}$$

$$\alpha_S^0(q) = \frac{1}{2}(V_{pp}^S + V_{pn}^S)/V_{pq}^S \qquad \alpha_S^1(q) = \frac{1}{2}(V_{pp}^S - V_{pn}^S)/V_{pq}^S \quad . \tag{106}$$

Equations analagous to those just given have previously been used by Atkinson and Madsen[22] to compute enhancement factors for normal parity transitions in (p,p') scattering from known effective charges. They assumed iso-scalar coupling and so took $\lambda_p^{JOJ} = \lambda_n^{JOJ}$. Using these relations in this manner is quite similar to the application of the schematic model made by Love and Satchler.[15] These relations might also be used as the basis for a phenomenological study of the available experimental data. Schaeffer[23] has used scaling factors, similar to the λ_q^{LSJ} introduced here, in a study of some experimental (p,p') and γ-decay data for collective excitations in various nuclei. The purpose of this study was to gain information about the relationship between the proton and neutron transition densities for transition of this type. In the present work we obtain λ_p^{LSJ} and λ_n^{LSJ} directly from the calculations and this scheme is only being used to summarize our results.

Table VII contains the results we have obtained using first order perturbation theory for all of the allowed S = 0 transition densities which occur in the cases being considered. The parameters, λ_p^{JOJ}, λ_n^{JOJ}, λ_0^{JOJ}, and λ_1^{JOJ} are shown in each case with the corresponding values of ε_p^{JOJ} and e_{eff}^J computed according to Eqs. (97), (98), (101), and (102) or the equivalent relations Eqs. (103)-(106). In these computations we have used

$\alpha_0 = 2.75$ which is satisfactory for our choice of $\bar{V}$ as was discussed in Sec. II.A.2. Corresponding to this value for α_0, we have $\alpha_0^0(p) = 1.88$, $\alpha_0^1(p) = -0.88$, $\alpha_0^0(n) = 0.68$, and $\alpha_0^1(n) = -0.32$ in the iso-spin notation.

Also shown in Table VII are values of ε_p^{J0J} and e_{eff}^J which have been estimated from the available experimental data. The experimental values of ε_p^{J0J} have been obtained by taking the square roots of the ratios of the experimental and theoretical valence integrated cross sections. Only the real part of $\bar{V}$ has been used in calculating the theoretical valence cross sections as we wish to keep separate the effect of the imaginary part of $\bar{V}$ which will be discussed later. The experimental data was taken from the references indicated in the table and the experimental integrated cross sections have been determined by normalizing the results of DWBA collective model calculations[69] to the experimental differential cross sections. For transitions where data is available at more than one incident proton energy, the experimental ε_p^{J0J} shown are average values. In all but a few instances the experimental ε_p^{J0J} were found to be nearly energy independent. The optical model parameters used in calculating the collective model cross sections and the theoretical valence cross sections have been taken from the same references where the experimental data was found. Most of these parameter sets have been included in Table XII. For $2p_{1/2} \rightarrow 1g_{9/2}$ transition in ^{89}Y and the $1h_{9/2} \rightarrow 2f_{7/2}$ transition in ^{209}Bi it was not possible to determine the experimental ε_p^{J0J} because more than one LSJ-transfer is observed to contribute to the experimental cross section in these cases.

The references containing the data which was used to determine the experimental values of e^J_{eff} are also shown in Table VII. Generally there was more than one piece of data available for each determination. For transitions where electron scattering data was available two methods were used to extract the experimental effective charge. One of these methods was to determine e^J_{eff} from the values of B(EJ↑) obtained from transition densities which were fitted to the experimental form factors. The second method was to normalize the peak value of theoretical valence form factors to the peak value of the experimental form factors. It has been suggested[70] that the second method is somewhat more reliable than the first. The sensitivity of the experimental effective charges to the theoretical radial wave functions was also checked. In most cases the changes in the effective charge due to reasonable changes in the radial wave functions were well within the variations noted in the experimental data itself. An exception to this is the $1h_{9/2} \rightarrow 2f_{7/2}$ transition in ^{209}Bi where harmonic oscillator radial wave functions and finite well wave functions[71] produced values for e^2_{eff} which differed by nearly a factor of two. The experimental values for e^J_{eff} shown in Table VII are averages of the values determined from the various sets of experimental data according to the methods described above. The uncertainties shown are average deviations which are mainly due to fluctuations in the experimental data.

Table VIII contains a summary of the results we have obtained for the S = 0 transition densities in the calculations using the renormalized core coupling interaction of Eq. (67). The format of this table is identical to that of Table VII.

The results obtained for the S = 1 transition densities using first order perturbation theory are shown in Table IX. In calculating the theoretical values of ε_p^{LIJ}, it was assumed that $\alpha_1 = -0.20$ which corresponds to $\alpha_1^0(p) = 0.40$, $\alpha_1^1(p) = 0.60$, $\alpha_1^0(n) = -2.00$, and $\alpha_1^1(n) = -3.00$. These are again satisfactory for our choice of $\bar{V}$. No experimental values for ε_p^{L1J} are shown because S = 1 amplitudes were not found to be dominant in any of the transitions which we have considered. The results for the S = 1 transition densities obtained using $\bar{G}'$ for the core coupling interaction do not differ greatly from the first order results; therefore, they have not been shown. The differences are small because we have assumed that $\bar{G}'$-G is spin-independent. Even if the appropriate spin dependence had been included in $\bar{G}'$-G, the results would not have been effect greatly. The main thing to notice in Table IX is the retardation of the S = 1 amplitudes compared to the enhancement of the S = 0 amplitudes apparent from Tables VII and VIII.

From Table VII we see that the first order calculations predict important core polarization corrections for the S = 0 amplitudes, even for the highest multipoles considered. In all cases, however, the correction fall somewhat short of experiment. The most notable feature of these calculations is that they predict a large iso-vector component in the S = 0 transition densities. This is not born out experimentally for the transition where both electromagnetic and proton scattering data are available. This may be seen by comparing the theoretical and experimental results for the polarization charge ($\delta e_{eff}^J = \lambda_p^{JOJ}$) and the corresponding factor for proton scattering ($\delta\varepsilon_p^{JOJ} = \varepsilon_p^{JOJ} - 1$). For the cases where there are valence protons the first order calculations give a better estimate of $\delta\varepsilon_p^{JOJ}$ than they do of δe_{eff}^J while the reverse is true for the transition involving valence neutrons.

From Table VIII we see that the main effect of interactions in the excluded space, as determined by our calculations using $\bar{G}'$ as the core coupling interaction, is to increase the iso-scalar components of the S = 0 transition densities relative to the iso-vector components which in turn brings improved agreement with experiment. The magnitude of this effect decreases with increasing multipolarity. In Table X we compare the results of our first order calculations and our calculation using $\bar{G}'$ with the first order and TDA results of Siegal and Zamick[10] for LSJ = 202 and the $1f_{7/2} \rightarrow 1f_{7/2}$ neutron transition assuming a ^{40}Ca core. We conclude that our result obtained using G' is consistent with the estimate of excluded space interactions using the TDA. It was not possible to make a similar comparison for any of the higher mulitpoles we have considered; however, the decrease in the importance of excluded space interactions with increasing multipolarity, predicted by our calculations with $\bar{G}'$, is consistent with the results of TDA and RPA calculations[42] for closed shell cores which indicate that the collectivity of core excitations decrease with increasing multipolarity.

Although the results obtained with $\bar{G}'$ are a definite improvement over the first order results for δT, some important discrepancies still appear in Table XI. One is that the theoretical values of ε_p^{JOJ} fall off somewhat faster with increasing multipole than do the experimental values. In the next section it will be seen that this discrepancy is removed when the imaginary part of $\bar{V}$ is introduced.

Another discrepancy is the relatively poor values obtained for the effective charge in the case of the $0^+ \rightarrow 2^+$ transitions in ^{42}Ca and ^{90}Zr while the theoretical e^2_{eff} for the $0^+ \rightarrow 2^+$ transition in ^{50}Ti appears to be adequate. The B(E2) for the $6^+ \rightarrow 4^+$ transitions in ^{42}Ca and ^{50}Ti and the

$8^+ \rightarrow 6^+$ transition in ^{90}Zr have been determined experimentally.[59,72] The experimental values of e^2_{eff} for these transitions are compared with the theoretical results we have obtained using G and $\bar{G}'$ in Table XI. We note that our model for core polarization predicts that e^2_{eff} for the transitions between the two upper states of a (j^2) configuration should be the same as for the $0^+ \rightarrow 2^+$ transition. This is born out by the data only in the case of ^{50}Ti. For ^{42}Ca our theoretical result for e^2_{eff} is in quite good agreement with the experimental value for the $6^+ \rightarrow 4^+$ transition which is only about half the value required for the $0^+ \rightarrow 2^+$ transition. Experimentally the situation is about the same for ^{90}Zr. We conclude that it is necessary to include second order terms in estimating δT in order to resolve these discrepancies. This is consistent with the suggestion of others[73,74] that 4p-2h admixtures are important in ^{42}Ca and ^{90}Zr

The final discrepancy we note is that the calculations fail to reproduce the large values of e^3_{eff} and ε_p^{303} required to explain the $1h_{9/2} \rightarrow 1i_{3/2}$ transition in ^{209}Bi. It is well known[47] that there are important contributions to this transition from admixtures of low-lying particle-vibration states in the single particle states, i.e. $|1h_{9/2} \times 3^-;13/2\rangle$ and $|1i_{13/2} \times 3^-;9/2\rangle$ where 3^- is the first excited state of the ^{208}Pb core. It would be possible to reproduce this effect by introducing a spin-independent J = 3 component in $\bar{G}'$; however, since we have no independent way of fixing the strength of this component a more reasonable approach would be to introduce these admixtures explicitly. This has been done elsewhere[17] and a reasonable description of the (p,p') cross sections for this transition has been obtained. In these calculations it was necessary to include both the contribution from these low-lying particle-vibration admixtures and the contribution due to admixtures of states formed from

higher lying 3^- core excitations. The results shown in Tables VII and VIII for the $1h_{9/2} \rightarrow 1i_{13/2}$ transition are representative of the latter contribution only.

A previous estimate of the (p,p') cross section for the $1h_{9/2} \rightarrow 2f_{7/2}$ transition in ^{209}Bi has also been made.[17] The first order wave functions of this work were used in this calculation. The calculations predicted important contributions to the cross section from all allowed JOJ amplitudes. This result was found to be consistent with the experimental data. An estimate of the modification of the first order results due to the addition of contributions from low-lying particle-vibration admixtures was also made. Specifically, contributions from the particle-vibration states formed from the first 2^+, 4^+, 6^+ and 8^+ excitations of the ^{208}Pb core were introduced. With these contributions, the first order ε_p^{JOJ} were increased to $\varepsilon_p^{202} = 6.94$, $\varepsilon_p^{404} = 6.56$, $\varepsilon_p^{606} = 5.17$, and $\varepsilon_p^{808} = 4.03$. These values are in good agreement with the results we have obtained using $\bar{G}'$ as the core coupling interaction. This is another indication that the effect of core correlations can be reproduced by using a rather simple effective interaction in calculating $\bar{T}$.

E2 effective charges are known[64] for several transitions in the Pb region where there is no inelastic scattering data available. As an additional check on the consistency of our calculations we have calculated these effective charges. The results have been included in Table XI. The agreement between theory and experiment is quite good, with the possible exception of the result for the $1h_{9/2} \rightarrow 1h_{9/2}$ proton transition.

D. Cross Sections and Form Factors

In this section we compare our theoretical (p,p') cross sections and (e,e') form factors directly with experiment. The discussion will be brief since many of the important points have already been covered above. The optical model parameters used in the DWA calculations are summarized in Table XII. The ground state proton density parameters used in estimating the imaginary part of $\bar{V}$ are summarized in Table XIII.

1. ^{42}Ca

The theoretical (p,p') cross sections for the excitation of the first 2^+ and 4^+ states in ^{42}Ca are compared with the 22.9 MeV experimental data of Ref. 56 in Fig. 6. The dotted curves D(HJ) are the results obtained using only the real part of $\bar{V}$ and the valence wave functions of Table II. The solid [D + C(HJ)] and dashed [D + C(HJ + Im] curves are the results obtained with the transition densities of Table VIII using only the real part of $\bar{V}$ and both the real and imaginary parts of $\bar{V}$, respectively. We do not show the results obtained with the transition densities of Table VII, because the differences between the calculations using G and $\bar{G}'$ have been adequately discussed in the preceding section. The values of ε_p shown in the figure are the square roots of the ratios of the D + C(HJ) and D(HJ) integrated cross sections. They differ somewhat from the values based on Eq. (101) and Eq. (103) which were given in Table VIII as expected.

The value of ε_I provides a measure of the importance of the imaginary part of $\bar{V}$, i.e. ε_I^2 is the ratio of the D + C(HJ + IM) and D + C(HJ) integrated cross sections.

The agreement between experiment and the theoretical results with core polarization included is quite reasonable. We see clearly that the effect of core polarization decreases only slowly with increasing multipole. The theoretical cross sections obtained with the imaginary component of $\bar{V}$ included in the calculations have slightly sharper structure than the cross sections obtained using only the real part of $\bar{V}$. The shape of the experimental differential cross sections favor the former. We also note that the effect of the imaginary part of $\bar{V}$ increases with increasing multipole.

The theoretical (e,e') form factor for the excitation of the first 2^+ state in ^{42}Ca is compared with the data of Ref. 65 in Fig. 7. In the calculation we have used the transition density of Table VIII. There is no valence form factor in this case, because the assumed model space consists only of neutron configurations. The theoretical result falls short of the data by about a factor of three as was pointed out previously. This deficiency in the theoretical wave functions does not show up in (p,p') results because neutron excitations are dominant there.

2. ^{50}Ti

The theoretical (p,p') cross sections for the excitation of the first

2^+ and 4^+ states in ^{50}Ti are compared with the 17.5 and 40.0 MeV data of Refs. 37 and 38 in Fig. 8. The format of the figure is the same as that of Fig. 6. With the exception of the values of ε_p, the results for ^{50}Ti have the same general characteristics as the results for ^{42}Ca. The increase in the values of ε_p for ^{50}Ti, compared to ^{42}Ca, is not due to an increase in the strength of core polarization in ^{50}Ti. It only reflects that the valence cross section D(HJ) for ^{50}Ti are smaller, because the model space includes only proton configurations in this case.

The theoretical (e,e') form factors for the excitation of the first 2^+ and 4^+ states in ^{50}Ti are compared with the data of Refs. 54 and 58 in Fig. 9. Here we have shown the results obtained using the wave function of Table II (D) and the transition densities of Table VIII (D + C). The results here show rather clearly the importance of E4 polarization.

3. ^{90}Zr

The theoretical (p,p') cross sections for the excitation of the first 2^+, 4^+, 6^+, 8^+, and 5^- states in ^{90}Zr are compared with the 18.8 and 61.2 MeV data of Refs. 39 and 43 in Figs. 10, 11, and 12. The LSJ = 515 contribution to the 5^- cross section was found to be negligible and has not been shown. Results for the excitation of these same levels by 40 MeV protons have previously been presented elsewhere.[18]

Again the overall agreement between experiment and the theoretical results with core polarization included is reasonable. Relative to the results for the 2^+, 4^+, and 6^+ excitations, the cross sections for the 8^+ and

5^- levels appear to be underestimated at 18.8 MeV. The situation is somewhat improved at 61.2 MeV. This improvement is also evident in the 40 MeV results. Collective model calculations[18,39,43] for the 8^+ and 5^- excitations yield considerably larger values of β_L at 18.8 MeV than at 40 and 61.2 MeV. This is simply an indication that multiple excitation is important for these levels at the lower energies.

The imaginary part of $\bar{V}$ is essential in reproducing the forward peaks of the 61.2 MeV cross sections for all of the excitations except the 2^+ level. It is also important in giving the correct multipole dependence for the theoretical cross sections. These same observations were made with respect to the 40 MeV results for these same excitations.[18] These effects do not show up so clearly at 18.8 MeV partly because of the difficulty in reproducing the 8^+ and 5^- cross sections at this energy and partly because the shapes of the angular distributions are not so distinctive at the lower energies. The latter remark applies equally well to the 22.9 MeV results for ^{42}Ca and the 17.5 MeV results for ^{50}Ti. The effect of the imaginary part of $\bar{V}$ is starting to show up in the results for ^{50}Ti at 40 MeV; however, the picture is not complete because of the limited range of multipoles which are available in this case.

The increasing importance of the imaginary part of $\bar{V}$ with increasing multipole is a result of the zero-range form of t^I_{ip} in contrast to the finite-range form of t^R_{ip}. The results we have obtained do not undeniably establish that the phenomenological treatment[20] of the imaginary part of $\bar{V}$ is correct. We can conclude, however, that the multipole dependence obtained in the calculations using only the real part of $\bar{V}$ is inadequate and it is interesting

that the simple prescription for including the imaginary part of $\bar{V}$ gives reasonable results.

Even with the imaginary part of $\bar{V}$ included there are still some deficiencies in the 61.2 MeV results. These occur mainly at back angles where the D + C(HJ+Im) results have more structure than the data for the 2^+, 4^+, 6^+, and 5^- excitations. In addition, the D + C(HJ+Im) results for the 8^+ state appears to underestimate the back angle cross section. It has been shown[27,43] that the inclusion of a spin-orbit component in $\bar{V}$ can improve these results. In addition, the presence of contributions from this interaction component does provide some direct evidence of the decreasing importance of core correlations with increasing multipolarity[18].

The theoretical (e,e') form factors for the excitation of the first 2^+ and 4^+ states in ^{90}Zr are compared with the experimental data of Refs. 58, 60, and 61 in Fig. 13. The format of the figure is the same as Fig. 9. Here again we have an example of important E4 polarization.

4. ^{89}Y

The theoretical (p,p') cross sections for the first $9/2^+$ excitation in ^{89}Y are compared with the 18.9, 24.5, and 61.2 MeV experimental cross sections of Refs. 76, 77, and 46 in Fig. 14. There are four allowed LSJ-amplitudes for this transition. These are LSJ = 314, 514, 505, and 515. The contributions from the 514 and 515-amplitudes were found to be negligible. The 505-amplitude was found to be dominant, but the contribution from the 314-amplitude is appreciable, particularly at forward angles. This is consistnet with the fact that the $9/2^+$ level in ^{89}Y is known to decay by M4 γ-emission.[81]

In Fig. 14 we have shown the LSJ = 314 and 505 cross sections obtained using the real part of $\bar{V}$ and the transition densities of Table VIII and IX. We have also shown the sum of these two cross sections. As before these curves are labeled D + C(HJ). The valence results, D(HJ), have not been shown. The fourth curve shown D + C(HJ+Im) is the sum of the LSJ = 314 and 505 cross sections obtained using both the real and imaginary parts of V. For the LSJ = 505 cross section at 24.5 MeV, $\varepsilon_p = 3.16$ and $\varepsilon_I = 1.37$. At 18.9 and 61.2 MeV ε_p and ε_I for the LSJ = 505 cross section have the same values that were given in Fig. 12 for the excitation of the 5^- state in ^{90}Zr at these energies. (It is shown in the Appendix that the LSJ = 505 form factors for the $1/2^- \rightarrow 9/2^+$ transition in ^{89}Y and the $0^+ \rightarrow 5^-$ transition in ^{90}Zr are essentially the same in our model.) For the LSJ = 314 cross sections, $\varepsilon_p = 0.51$, 0.52, and 0.50 at 18.9, 24.5, and 61.2 MeV. For this cross section, $\varepsilon_I = 1.0$ at all energies, because we have taken the imaginary part of $\bar{V}$ to be spin independent.

From Fig. 14 we see that the theoretical calculations do not reproduce the energy dependence of the experimental cross sections exactly. The theoretical results are in good agreement with the data at the lower energies, but a bit too high at 61.2 MeV. A similar discrepancy was noted in the results for the 5^- level in ^{90}Zr, except that the theoretical results were a little low at 18.8 MeV and in fairly good agreement with the data at 61.2 MeV. There is a noticable difference in shape, at forward angles, between the 61.2 MeV experimental cross sections for the $9/2^+$ excitation in ^{89}Y and the 5^- excitation in ^{90}Zr. This is consistent with the presence of the LSJ = 314

contribution to the former. It appears that the LSJ = 505 contribution to the ^{89}Y cross section is slightly overestimated in our calculation, so this effect does not show up quite so clearly in our theoretical results. We conclude that the LSJ = 505 contribution to the cross section for the $9/2^+$ state in ^{89}Y is somewhat smaller than the corresponding contribution to the cross section for the 5^- state in ^{90}Zr, a feature which cannot be reproduced with the simple model for core polarization that we are using.

5. ^{207}Pb

The theoretical (p,p') cross sections for the excitation of the first four single particle states in ^{207}Pb are compared with the 20.2 MeV experimental data of Ref. 65 in Fig. 15. Results for the excitation of these same levels at 39.5 MeV have previously been presented elsewhere.[46] Contributions from S=1 amplitudes were found to be negligible in all cases and only S=0 contributions to the cross sections are shown in the figure. There are two interesting aspects to the results. One is that ε_p for the $7/2^-$ excitation which goes by LSJ = 404 transfer is comparable to ε_p for the $5/2^-$ and $3/2^-$ excitations which proceed with LSJ = 202 transfer. Other evidence for large L=4 core polarization in the Pb region was seen previously in the cross section for the excitation of the $2f_{7/2}$ single particle state in ^{209}Bi by 61.2 MeV protons.[17] The other interesting feature is that there is a shape difference between the cross section for the $3/2^-$ level and $5/2^-$ level both of which are excited by LSJ = 202 transfer. Although the theoretical results do not give a completely accurate reproduction of the experimental data, they do show this shape difference rather nicely. The difference in

shapes is due to the differences in the radial wave functions for the valence neutrons in the two final states. Similar effects are not seen in the lighter nuclei, because the radial wave functions tend to be more similar there, at least for the cases we have considered.

6. ^{209}Bi

Theoretical (p,p') cross sections for states in ^{209}Bi obtained using the wave functions of this work have been discussed in detail elsewhere[17] and will not be discussed here.

V. CONCLUSIONS

We have shown that a fair sized sampling of experimental inelastic electron and proton scattering data for nuclei near closed shells can be understood, at least qualitatively, in calculations which assume to a first approximation that the interaction between two bound nucleons and between a bound and a continuum nucleon are given by G matrix interactions derived from free two-nucleon potentials. In the calculations, the (e,e') reaction was treated using a modified Born approximation. The (p,p') reaction was treated using the distorted wave approximation and the G matrix interaction was modified to account for "knock-on" exchange and excluded reaction channels. Core polarization was treated in lowest order and with the G matrix interaction renormalized to roughly account for the effect of long range core correlations. The results clearly show that core polarization effects are large and persist as the multipolarity of the transitions increase. They also show that the motions of target protons and neutrons are strongly correlated although there may be some weakening in the correlation for transitions where the L-transfer exceeds 5.

Although our results indicate a strong correlation between proton and neutron motions in the excitation of the levels considered, in detail there are small differences between proton and neutron motions even for the L = 2 transitions. Brown and Madsen[82] have recently discussed some of the expected differences and it would surely be interesting to examine our results more carefully in this regard. This can in principle be done on the basis of the data we have considered[14], but it requires considerably greater care in the calculations than we have expended and thus must be postponed until a later date. Forthcoming data[83] for the excitation of nuclear levels by π^+ and π^-

inelastic scattering should provide additional information concerning these differences.

Finally we note that the use of an "effective" core coupling interaction in a first order treatment of the renormalization of one body operators was found to give reasonable results in the sense that it does seem to account for some of the effects attributable to collective correlations in the core. It would be interesting to pursue this further taking care to include the second order terms that we have ignored. Other interaction choices might also be investigated, for example the recent "effective" interaction of Schiffer and True.[84]

Acknowledgments

One of us (F.P.) would like to thank the staff of the Michigan State University Cyclotron for their hospitality during extended visits in which various parts of this work were performed, the staff of the Physics Department of The Florida State University where the final manuscript was prepared, and Wanda Smith and Teri Tanasovich of Lawrence Berkeley Laboratory for typing the manuscript.

APPENDIX

In this appendix we give the values of the spectroscopic amplitudes S_q^J for the specific transitions we are considering. S_q^J is defined in Eq. (71)

1. Single Particle Transitions

For a transition between two single particle states,

$$|\alpha_i(n)J_iM_i\rangle \equiv |n_i\ell_ij_im_i\rangle = a_i^+|C\rangle \tag{B.1}$$

$$|\alpha_f(n)J_fM_f\rangle \equiv |n_f\ell_fj_fm_f\rangle = a_f^+|C\rangle \tag{B.2}$$

Eq. (74) gives

$$S_q^J(n_f\ell_fj_f,n_i\ell_ij_i;j_\alpha j_\gamma) = \delta_{j_ij_\gamma}\,\delta_{j_fj_\alpha} \quad . \tag{B.3}$$

Inserting this result in Eq. (80) we obtain

$$\langle n_f\ell_fj_f\|\bar{T}^{LSJ}\|n_i\ell_ij_i\rangle = \langle j_f\|t_q^{LSJ}\|j_i\rangle \tag{B.4}$$

$$+\sum_{\substack{j_pj_h\\q'}}\left\{\frac{1}{Q-\varepsilon(ph)}+\frac{1}{-Q-\varepsilon(ph)}P_{ph}\right\}F^J_{qq'}(j_pj_h,j_fj_i) \quad ,$$

where Q and $\varepsilon(ph)$ have been defined in Eq. (91).

2. Single Hole Transition

For a transition between two single hole states,

$$|\alpha_i(n)J_iM_i\rangle \equiv |n_i\ell_ij_i^{-1},-m_i\rangle = (-1)^{j_i-m_i}\,a_i|C\rangle \tag{B.5}$$

$$|\alpha_f(n)J_fM_f\rangle \equiv |n_f\ell_f j_f^{-1},-m_f\rangle = (-1)^{j_f-m_f}\, a_f|C\rangle \quad , \tag{B.6}$$

Eq. (74) gives

$$S_q^J(n_f\ell_f j_f^{-1},n_i\ell_i j_i^{-1};j_\alpha j_\gamma) = (-1)^{j_i+j_f-J}\, \hat{j}_i\, \hat{j}_f^{-1}\, \delta_{j_i j_\alpha}\delta_{j_f j_\gamma} \quad . \tag{B.7}$$

Inserting this result in Eq. (80) and then making use of the conjugation relation Eq. (78) and the permutation property of $F^J_{qq'}$ given in Eq. (82), we find

$$\langle n_f\ell_f j_f^{-1}\|\bar{T}^{LSJ}\|n_i\ell_i j_i^{-1}\rangle = -(-1)^S\Bigg[\langle j_f\|t_q^{LSJ}\|j_i\rangle + \sum_{\substack{j_p j_h\\ q'}}\left\{\frac{1}{Q-\varepsilon(ph)}P_{ph} + \frac{1}{-Q-\varepsilon(ph)}\right\}F^J_{qq'}(j_pj_h,j_fj_i)\Bigg] \quad . \tag{B.8}$$

The matrix elements for a single hole transition differ from the matrix elements for a single particle transition by an overall phase which depends on the particular operator being considered. This is of no consequence in this work because we are only interested in the square of these matrix elements. Another difference is that the position of P_{ph} has been shifted from the second to the first term inside the brackets. This has nearly a negligible effect because $\varepsilon(ph)$ is typically much greater than Q and the effect of P_{ph} on $F^J_{qq'}$ is weak as may be seen from Eq. (87) which is valid for the case of a zero range coupling interaction. We conclude that single particle transitions and single hole transitions are equivalent for all practical purposes.

3. Transitions Between Two Particle States

For a transition between two particle states,

$$|\alpha_i(n)J_iM_i\rangle \equiv |(jj_1)J_iM_i\rangle = \sum_{mm_1} \langle jj_1\, mm_1|J_iM_i\rangle\; a^+a_1^+|C\rangle \tag{B.9}$$

$$|\alpha_f(n)J_fM_f\rangle \equiv |(jj_2)J_fM_f\rangle = \sum_{mm_2} \langle jj_2 mm_2|J_fM_f\rangle\; a^+a_2^+|C\rangle \quad , \tag{B.10}$$

the spectroscopic amplitude is given by

$$S_q^J((jj_2)J_f,(jj_1)J_i;j_\alpha j_\gamma) = (1+\delta_{jj_1})^{-1/2}(1+\delta_{jj_2})^{-1/2}(-1)^{j+j_1+J}\hat{J}_i$$

$$\times \left[(1+(-1)^{J_i}\delta_{jj_1}+(-1)^{J_f}\delta_{jj_2})\delta_{j_\alpha j_2}\delta_{j_\gamma j_1}(-1)^{J_f}\hat{j}_2 \begin{Bmatrix} j & j_1 & J_i \\ J & J_f & j_2 \end{Bmatrix}\right.$$

$$\left. + \delta_{j_1j_2}\delta_{j_2j}\delta_{j_\gamma j}(-1)^{J_i}\hat{j} \begin{Bmatrix} j_1 & j & J_i \\ J & J_f & j \end{Bmatrix}\right] \tag{B.11}$$

In the special case $j_1 = j_2 = j$, J_i and J_f must be even and Eq. (B.11) reduces to

$$S_q^J((j^2)J_f,(j^2)J_i,j_\alpha j_\gamma) = -\delta_{j_\alpha j}\;\delta_{j_\gamma j}\;(-1)^J\, 2\hat{J}_i\hat{j} \begin{Bmatrix} j & j & J_i \\ J & J_f & j \end{Bmatrix} \quad . \tag{B.12}$$

For this case we find

$$\langle (j^2)J_f \| \bar{T}^{LSJ} \| (j^2)J_i \rangle = -(-1)^J 2\hat{J}_i \hat{j} \begin{Bmatrix} j & j & J_i \\ J & J_f & j \end{Bmatrix} \tag{B.13}$$

$$\times \left[\langle j \| t_q^{LSJ} \| \hat{j} \rangle + \sum_{\substack{j_p j_n \\ q'}} \left\{ -\frac{1}{\varepsilon(ph)} (1 + (-1)^{S+J}) \right\} F_{qq}^J (j_p j_h, jj) \right] ,$$

where we have again used Eq. (82). It is interesting to note that when $J_i = 0$, then $J = J_f$ is even, and the second term on the right hand side of Eq. (B.13) vanishes when $S = 1$. The valence contribution given by the first term on the right of Eq. (B.13) vanishes in this case also; so, core polarization does not break the valence selection rule. When $J_i = 0$ and $S = 0$, the factor in parenthesis in the square brackets becomes 2 and core polarization is effective.

Another case of particular interest here is the transition between the states

$$|\alpha_i(n)J_iM_i\rangle = a|(j_1{}^2)J_i{=}0\ M_i{=}0\rangle + b|(j_2{}^2)J_i{=}0\ M_i{=}0\rangle \tag{B.14}$$

$$|\alpha_f(n)J_fM_f\rangle = |(j_2j_1)J_fM_f\rangle \quad . \tag{B.15}$$

This corresponds to the description of the 0^+ to 5^- transition in ^{90}Zr given in Table II. In this case we find

$$S_q^J(\alpha_f J_f, \alpha_i J_i; j_\alpha j_\gamma) = \sqrt{2}\, \hat{J}_f^{-1} \left\{ a\, \hat{j}_2 \hat{j}_1^{-1}\, \delta_{j_\alpha j_2} \delta_{j_\gamma j_1} - (-1)^{j_1+j_2-J_f}\, b\, \hat{j}_1 \hat{j}_2^{-1}\, \delta_{j_\alpha j_1} \delta_{j_\gamma j_2} \right\}. \tag{B.16}$$

Inserting this expression into Eq. (80) and again making use of Eq. (78) and Eq. (82), we obtain

$$\langle \alpha_f J_f \| \bar{T}^{LSJ} \| \alpha_i J_i \rangle = \sqrt{2}\, \hat{J}_f^{-1} \left\{ a \hat{j}_2 \hat{j}_1^{-1} + (-1)^S b \right\} \times \left[\langle j_2 \| t_q^{LSJ} \| j_1 \rangle \right.$$

$$\left. + \sum_{\substack{j_p j_h \\ q'}} \left\{ \frac{1}{\varepsilon(12) - \varepsilon(ph)} + \frac{1}{\varepsilon(21) - \varepsilon(ph)} \right\} P_{ph}\, F^J_{qq'}(j_p j_h, j_2 j_1) \right] \quad \text{(B.17)}$$

These expressions differ from those for the single particle transition $j_1 \to j_2$ only by an overall constant. With $j_1 = 2p_{1/2}$, $j_2 = 1g_{9/2}$, $a = 0.8$, $b = 0.6$, $J_f = 5$, and $S = 0$, this constant has the value 1.02. With $S = 1$ the constant is 0.507. We conclude that the important LSJ = 505 amplitude for the $0^+ \to 5^-$ transition in ^{90}Zr is nearly identical to the corresponding amplitude for the $2p_{1/2} \to 1g_{9/2}$ transition in ^{89}Y. The LSJ = 515 amplitude for the ^{90}Zr transition is reduced in magnitude in comparison to corresponding amplitude for the ^{89}Y transition.

REFERENCES

1. L. L. Foldy and J. T. Milford, Phys. Rev. 80, 751 (1950); A. Bohr and B. Mottelson, Kgl. Danske Videnskab. Selskab, Mat.-Fys. Medd 27, 16 (1953); A. Kerman, Phys. Rev. 92, 1176 (1953); K. W. Ford and C. A. Levinson, Phys. Rev. 100, 1 (1955); R. D. Amado, Phys. Rev. 108, 1462 (1957).

2. R. J. Blin-Stoyle, Proc. Phys. Soc. A66, 1158 (1953); R. J. Blin-Stoyle and M. A. Perks, Proc. Phys. Soc. A67, 885 (1954); A. Arima and H. Horie, Progr. Theoret. Phys. 11, 509 (1954); 12, 623 (1954); H. Horie and A. Arima, Phys. Rev. 99, 778 (1955); A. de-Shalit, Phys. Rev. 113, 547 (1959).

3. G. F. Bertsch, Nucl. Phys. 74, 234 (1965).

4. T. T. S. Kuo and G. E. Brown, Nucl. Phys. 85, 40 (1966).

5. G. E. Brown, Unified Theory of Nuclear Models and Nucleon-Nucleon Forces, (North-Holland Publishing Company, Amsterdam, The Netherlands, 1967), 2nd edition.

6. M. H. MacFarlane, in Rendicotti S. I. F. Course XL, 1967 (Academic Press, New York, 1969) p. 457.

7. Other works cited in Refs. 3 - 6.

8. T. T. S. Kuo, Nucl. Phys. A90, 199 (1967); A103, 71 (1967); G. E. Brown and T. T. S. Kuo, Nucl. Phys. A92, 481 (1967); T. T. S. Kuo and G. E. Brown, Nucl. Phys. A114, 241 (1968); T. T. S. Kuo and G. Herling, Nucl. Phys. A181, 113 (1972).

9. B. R. Barrett and M. W. Kirson, Phys. Letters 27B, 544 (1968); 30B, 8 (1969); Nucl. Phys. A148, 145 (1970); M. W. Kirson, Ann. Phys 66, 624 (1971).

10. J. Blomqvist, N. Freed, H. O. Zetterstrom, Phys. Letters 18, 47 (1965); H. A. Mavromatis, L. Zamick, Nucl. Phys. A104, 17 (1967); J. D. Vergados, Phys. Letters 36B, 12 (1971); A. Arima and L. J. Huang-Lin, Phys. Letters 41B, 429, 435; P. Federman and L. Zamick, Phys. Rev. 177, 1534 (1969); S. Siegal and L. Zamick, Phys. Letters 28B, 450, 453, (1969); Nucl. Phys. A145, 89 (1970).

11. B. R. Barrett and M. W. Kirson, to be published.

12. F. Petrovich, H. McManus, V. Madsen, and J. Atkinson, Phys. Rev. Letters 22, 895 (1969); K. H. Bray et al., Nucl. Phys. A189, 35 (1972); D. Slanina and H. McManus, Nucl. Phys. A116, 271 (1968).

13. G. R. Satchler, Comm. Nucl. Particle Phys. 5, 39 (1972) and references contained therein.

14. G. R. Hammerstein, R. H. Howell, and F. Petrovich, Nucl.Phys. A213, 45 (1973).

15. W. G. Love and G. R. Satchler, Nucl. Phys. A101, 424 (1967).

16. D. Agassi and R. Schaeffer, Nucl. Phys. A145, 401 (1970).

17. W. Benenson, S. M. Austin, P. J. Locard, F. Petrovich, J. Borysowicz, and H. McManus, Phys. Rev. Letters 24, 901 (1970); A. Scott, M. Owais, and F. Petrovich, Nucl. Phys. A226, 109 (1974).

18. R. A. Hinrichs, D. Larson, B. M. Preedom, W. G. Love, and F. Petrovich, Phys. Rev. C7, 1981 (1973).

19. N. Vinh-Mau, in Theory of Nuclear Structure (Trieste lectures, 1969), I.A.E.A., Vienna, 1970.

20. G. R. Satchler, Phys. Letters 35B, 279 (1971).

21. R. H. Howell and G. R. Hammerstein, Nucl. Phys. A192, 651 (1972).

22. K. A. Amos, V. A. Madsen, and I. E. McCarthy, Nucl. Phys. A94, 103 (1967); J. Atkinson and V. A. Madsen, Phys. Letters 21, 295 (1968); Phys. Rev. C1, 1377 (1970).

23. D. Agassi and R. Schaeffer, Phys. Letters 26B, 703 (1968); R. Schaeffer, Nucl. Phys. A132, 186 (1969): Orsay thesis 1969 (unpublished).

24. W. G. Love, Part. and Nuclei 3, 318 (1972).

25. T. Hamada and I. D. Johnston, Nucl. Phys. 34, 382 (1962).

26. J. Raynal, Symposium sur les Mechanismes de Réactions Nucléaires et phénomenes de Polarisation, Université Laval, Quebec (1969); 27. W. G. Love, Phys. Letters 35B, 371 (1971); Nucl. Phys. A192, 49 (1972); W. G. Love, and L. J. Parish, Nucl. Phys. A157, 625 (1970).

28. N. K. Glendenning, in Rednicotti S. I. F. Course XL, 1967 (Academic Press, New York, 1969) p. 332.

29. N. K. Glendenning and M. Veneroni, Phys. Rev. 144, 839 (1966); G. R. Satchler, Nucl. Phys. 77, 481 (1966); V. A. Madsen, Nucl. Phys. 80, 177 (1966).

30. D. M. Brink and G. R. Satchler, Angular Momentum (Oxford University Press, Oxford, 1962).

31. T. deForest, Jr. and J. D. Walecka, Adv. in Phys. 15, 1 (1966).

32. T. Janssens, J. Hofstadter, E. B. Hughes, and M. R. Yearian, Phys. Rev. 124, B922 (1966).

33. G. R. Satchler, J. Math. Phys. 13, 1118 (1972).

34. M. Harvey, Chalk River Report (unpublished).

35. G. R. Satchler and W. G. Love, Nucl. Phys. A172, 449 (1971).

36. T. T. S. Kuo, unpublished.

37. H. O. Funsten, N. R. Roberson, and E. Rost, Phys. Rev. 134, 117B (1964).

38. B. M. Preedom, C. R. Gruhn, T. Y. T. Kuo, and C. J. Maggiore, Phys. Rev. C2, 166 (1970).

39. W. S. Gray, R. A. Kenefick, J. J. Kraushaar, and B. W. Ridley, Phys. Rev. 142, 735 (1966).

40. F. Petrovich and H. McManus, Bull. Am. Phys. Soc. 13, 631 (1968).

41. G. A. Peterson, K. Hosoyama, M. Nagao, A. Nakado, and Y. Torizuka, Phys. Rev. C7, 1028 (1973).

42. See, for example, V. Gillet and N. Vinh Mau, Nucl. Phys. 54, 321 (1964).

43. M. L. Whiten, A. Scott, and G. R. Satchler, Nucl Phys A181, 417 (1972).

44. A. Scott, M. Owais, and W. G. Love, submitted to Nucl. Phys.

45. M. Owais, A. Scott, and W. G. Love, to be published.

46. W. T. Wagner, G. R. Hammerstein, G. M. Crawley, J. Borysowicz, and F. Petrovich, Lawrence Berkeley Laboratory Report (LBL-1938); Phys. Rev. C7, 1981 (1973).

47. B. R. Mottleson, J. Phys. Soc. Japan 24, Suppl., 96 (1968); I. Hamamoto, Nucl. Phys. A126, 545 (1969); N. Auerbach and N. Stein, Phys. Letters 28B, 628 (1969); R. Broglia, J. Damgaard, M. Molinari, Nucl Phys A127, 429 (1969).

48. F. Petrovich, Nucl. Phys. A203, 65 (1972).

49. A. Kallio and K. Kolltveit, Nucl. Phys. 53, 87 (1964).

50. S. G. Nilsson, Mat. Fys. Medd. Dan. Vid. Selsk 29, 16 (1955).

51. J. H. E. Mattauch, W. Thiele, and A. H. Wapstra, Nucl. Phys. 67, 1 (1965).

52. R. H. Trilling, private communication.

53. D. A. Bromley and J. Weneser, Comments Nucl. Particle Physics 11, 121 (1968).

54. J. Heisenberg, J. S. McCarthy, and I. Sick, Nucl. Phys. A164, 353 (1971).

55. A. M. Bernstein, E. P. Lippincott, G. T. Sample, and C. B. Thorn, Nucl. Phys. A115, 79 (1968).

56. J. C. Bane, J. J. Kraushaar, B. W. Ridley, and M. M. Stautberg, Nucl. Phys. A116, 580 (1968)

57. H. J. Eramuspe, Nucl. Phys. A101, 138 (1967).

58. Phan-Xuan-Ho, J. Bellicard, Ph. Leconte, and I. Sick, Nucl. Phys. A210, 189 (1973).

59. J. Vervier, Phys. Letters 13, 47 (1964).

60. J. Bellicard, Ph. Leconte, T. H. Curtiss, R. A. Eisenstein, D. W. Madsen, and C. Bockleman, Nucl. Phys. A143, 213 (1970).

61. M. Mills, MIT Thesis, 1972 (unpublished).

62. R. T. Wagner, E. R. Schunk, and R. B. Day, Phys. Rev. 130, 1962 (1962)

63. Landolt-Bernstein, Energy Levels in Nuclei, ed. by A. M. Hellwege and K. H. Hellwege (Springer-Verlag, Berlin, 1961).

64. G. Astner, J. Bergström, J. Blomqvist, B. Fant, and K. Wikström, Nucl. Phys. A182, 219 (1972)

65. C. Glashausser, B. G. Harvey, D. L. Hendrie, J. Mahoney, E. A. McClatchie, and J. Saudinos, Phys. Rev. Letters 21, 918 (1968)

66. J. W. Hertel, D. G. Fleming, J. P. Schiffer, and H. E. Gove, Phys. Rev. Letters 23, 448 (1969).

67. R. A. Broglia, J. S. Lilley, R. Perazzo, and W. R. Phillips, Phys. Rev. C1, 1508 (1970)

68. J. F. Ziegler and G. A. Peterson, Phys. Rev. 165, 1337 (1968).

69. R. H. Bassel, G. R. Satchler, R. M. Drisko, and E. Rost, Phys. Rev. 128 2293 (1962).

70. G. R. Hammerstein, D. Larson, and B. H. Wildenthal, to be published.

71. J. Blomqvist and S. Wahlborn, Arkiv. f. Fys. 16, 545 (1960).

72. T. Nomura, C. Gil, H. Saito, and T. Yamazaki, Phys. Rev. Letters 25, 1342 (1970).

73. B. H. Flowers and L. D. Skouras, Nucl. Phys. A116, 529 (1968).

74. W. J. Courtney and H. T. Fortune, Phys. Letters 41B, 4 (1972).

75. R. J. Peterson, Annals of Phys. 53, 40 (1969)

76. M. M. Stautberg, J. J. Kraushaar, and B. W. Ridley, Phys. Rev. 157, 977 (1967).

77. W. Benenson, S. M. Austin, R. A. Paddock, and W. G. Love, Phys. Rev. 176, 1268 (1968).

78. C. B. Fulmer, J. B. Ball, A. Scott, and M. L. Whiten, Phys. Rev. 181, 1565 (1969).

79. R. H. Helm, Phys. Rev. 104, 1466 (1956); G. A. Peterson and J. Alster, Phys. Rev. 166, 1136 (1967).

80. J. F. Ziegler and G. A. Peterson, Phys. Rev. 165, 1337 (1968).

81. M. Goldhaber and A. W. Sunyar, Phys. Rev. 83, 906 (1951).

82. V. R. Brown and V. A. Madsen, Phys. Rev. C11, 1298 (1975).

83. B. J. Lieb, W. F. Lankford, H. S. Plendl, C. E. Stronach, H. O. Funsten, W. J. Kossla, V. G. Lind, and A. J. Buffa, to be published.

84. J. P. Schiffer and W. W. True, to be published.

Table I. Core Coupling Constants Determined from Bound State Pairing Matrix Elements.

Nuclide	J	J	$^{a}E_{p}^{J}(j)$ (MeV)	θ_J (MeV^{-1})	C_J (MeV)
^{50}Ti	$1f_{7/2}$	0	-0.033	1.78×10^{-4}	5610
	$1f_{7/2}$	2	-0.753	3.18×10^{-3}	314
	$1f_{7/2}$	4	-0.460	2.20×10^{-3}	455
	$1f_{7/2}$	6	-0.233	1.55×10^{-3}	645
^{90}Zr	$1g_{9/2}$	0	-0.020	1.01×10^{-4}	9920
	$1g_{9/2}$	2	-0.578	2.38×10^{-3}	420
	$1g_{9/2}$	4	-0.359	1.58×10^{-3}	633
	$1g_{9/2}$	6	-0.218	1.14×10^{-3}	877
	$1g_{9/2}$	8	-0.122	9.00×10^{-4}	1110
	$2p_{1/2}$	0	-0.210	1.22×10^{-3}	820

[a]Values for ^{50}Ti are from Ref. 8 and values for ^{90}Zr are from Ref. 36.

Table II. Summary of transitions considered in this work. Initial and final model space wave functions are given in each case.

[a]Target	J_i^π	$\lvert\phi_M^i\rangle$	J_f^π	$\lvert\phi_M^f\rangle$	[b]Q (MeV)
			2^+	$\lvert(1f_{7/2}{}^2)2\rangle$	-1.52
^{42}Ca(2n)	0^+	$\lvert(1f_{7/2}{}^2)0\rangle$	4^+	$\lvert(1f_{7/2}{}^2)4\rangle$	-2.76
			6^+	$\lvert(1f_{7/2}{}^2)6\rangle$	-3.19
			2^+	$\lvert(1f_{7/2}{}^2)2\rangle$	-1.56
^{50}Ti(2p)	0^+	$\lvert(1f_{7/2}{}^2)0\rangle$	4^+	$\lvert(1f_{7/2}{}^2)4\rangle$	-2.68
			6^+	$\lvert(1f_{7/2}{}^2)6\rangle$	-3.20
^{89}Y(1p)	$1/2^-$	$\lvert 2p_{1/2}\rangle$	$9/2^+$	$\lvert 1g_{9/2}\rangle$	-0.91
			2^+	$\lvert(1g_{9/2}{}^2)2\rangle$	-2.18
			4^+	$\lvert(1g_{9/2}{}^2)4\rangle$	-3.08
^{90}Zr(2p)	0^+	$0.8\lvert(2p_{1/2}{}^2)0\rangle$ $+0.6\lvert(1g_{9/2}{}^2)0\rangle$	6^+	$\lvert(1g_{9/2}{}^2)6\rangle$	-3.45
			8^+	$\lvert(1g_{9/2}{}^2)8\rangle$	-3.60
			5^-	$\lvert(1g_{9/2}\ 2p_{1/2})5\rangle$	-2.32
			$5/2^-$	$\lvert 2f_{5/2}{}^{-1}\rangle$	-0.57
			$3/2^-$	$\lvert 3p_{3/2}{}^{-1}\rangle$	-0.89
^{207}Pb($1n^{-1}$)	$1/2^-$	$\lvert 3p_{1/2}{}^{-1}\rangle$	$13/2^+$	$\lvert 1i_{13/2}{}^{-1}\rangle$	-1.63
			$7/2^-$	$\lvert 2f_{7/2}{}^{-1}\rangle$	-2.33
^{209}Bi(1p)	$9/2^+$	$\lvert 1h_{9/2}\rangle$	$7/2^-$	$\lvert 2f_{7/2}\rangle$	-0.90
			$13/2^+$	$\lvert 1i_{13/2}\rangle$	-1.61

[a]The number and type of valence nucleons is indicated in parenthesis.
[b]This column lists experimental Q-value which is not to be confused with theoretical Q-value defined in Eq. (91).

Table III. Single Particle Energies for Spherical Potential as Determined by Nilsson.

#	N^a	$n\ell j^\pi$	$E_{n\ell j}/\hbar\omega^b$	#	N^a	$n\ell j^\pi$	$E_{n\ell j}/\hbar\omega^b$
1	0	$1s_{1/2}^+$	1.50	21	5	$2f_{5/2}^-$	6.43
2	1	$1p_{3/2}^-$	2.45	22	5	$3p_{1/2}^-$	6.56
3	1	$1p_{1/2}^-$	2.60	23	6	$2g_{9/2}^+$	6.85
4	2	$1d_{5/2}^+$	3.40	24	6	$1i_{11/2}^+$	6.91
5	2	$2s_{1/2}^+$	3.50	25	7	$1j_{15/2}^-$	7.03
6	2	$1d_{3/2}^+$	3.65	26	6	$3d_{5/2}^+$	7.27
7	3	$1f_{7/2}^-$	4.14	27	6	$2g_{7/2}^+$	7.30
8	3	$2p_{3/2}^-$	4.42	28	6	$4s_{1/2}^+$	7.50
9	3	$1f_{5/2}^-$	4.49	29	6	$3d_{3/2}^+$	7.52
10	3	$2p_{1/2}^-$	4.57	30	7	$2h_{11/2}^-$	7.65
11	4	$1g_{9/2}^+$	4.85	31	8	$1k_{17/2}^+$	7.66
12	4	$2d_{5/2}^+$	5.27	32	7	$1j_{13/2}^-$	7.78
13	4	$1g_{7/2}^+$	5.30	33	7	$3f_{7/2}^-$	8.11
14	4	$3s_{1/2}^+$	5.50	34	7	$2h_{9/2}^-$	8.20
15	4	$2d_{3/2}^+$	5.52	35	9	$1\ell_{19/2}^-$	8.25
16	5	$1h_{11/2}^-$	5.58	36	8	$2i_{13/2}^+$	8.36
17	5	$2f_{7/2}^-$	6.08	37	7	$4p_{3/2}^-$	8.44
18	5	$1h_{9/2}^-$	6.13	38	7	$3f_{5/2}^-$	8.46
19	6	$1i_{13/2}^+$	6.26	39	8	$1k_{15/2}^+$	8.56
20	5	$3p_{3/2}^-$	6.41	40	7	$4p_{1/2}^-$	8.59

(continued)

Table III. (cont.)

[a] $N = 2(n-1) + \ell$ is the major shell quantum number.

[b] $E_{n\ell j}/\hbar\omega = N - 0.05\ j(j+1) + 0.05\ (1-\mu)\ \ell(\ell+1) + 1.5375$ where $\hbar\omega$ determines the major shell separation and:

$\mu = 0.00$	$N = 0,1,2$
$\mu = 0.35$	$N = 3$
$\mu = 0.45$	$N = 4,5,6$
$\mu = 0.40$	$N = 7$

Table IV. Particle and hole levels used to form intermediate states in the perturbative calculations of δT.

Target	Transitions (J_f^π)	Hole Levels		Particle Levels	
		Protons	Neutrons	Protons	Neutrons
^{42}Ca	$2^+,4^+,6^+$	# 2-6	# 2-6	# 7-15	# 7-15
^{50}Ti	$2^+,4^+,6^+$	# 2-6	# 2-7	# 7-15	# 8-15
^{89}Y	$9/2^+$	# 7-9	# 7-11	#10-23	#12-23
^{90}Zr	$2^+,4^+,6^+,8^+$	# 4-9	# 4-11	#10-23	#12-23
^{90}Zr	5^-	# 7-9	# 7-11	#10-23	#12-23
^{207}Pb	$3/2^-,5/2^-,7/2^-$	# 7-16	#11-22	#17-35	#23-35
^{207}Pb	$13/2^+$	#11-16	#16-22	#17-30	#23-34
^{209}Bi	$7/2^-$	# 7-16	#11-22	#17-35	#23-35
^{209}Bi	$13/2^+$	#11-16	#16-22	#17-30	#23-34

Table V. Core admixtures in ground state of ^{50}Ti.

$p\bar{h}$	ε(ph) (MeV)	$a((1f_{7/2}^{2})J, (p\bar{h})J; 0\|(1f_{7/2}^{2})0)$[a] protons J=2	protons J=4	protons J=6	neutrons J=2	neutrons J=4	neutrons J=6
$1g_{9/2}-1d_{5/2}^{-1}$	15.5	-.06 -.22	-.02 -.08	-.01 -.03	-.19 -.26	-.10 -.13	-.05 -.06
$1g_{7/2}-1d_{3/2}^{-1}$	17.7	-.05 -.17	-.03 -.07		-.14 -.19	-.07 -.09	
$1f_{5/2}-1p_{1/2}^{-1}$	20.9	-.04 -.08					
$2p_{3/2}-1f_{7/2}^{-1}$	4.8				.30 .38	.15 .15	
$1f_{5/2}-1f_{7/2}^{-1}$	8.8				-.11 -.16	-.14 -.17	-.16 -.16
$1g_{9/2}-2s_{1/2}^{-1}$	14.3		-.03 -.07			-.10 -.11	
$1g_{7/2}-2s_{1/2}^{-1}$	19.3		.02 .04			.06 .07	
$1g_{9/2}-1d_{3/2}^{-1}$	12.7		-.04 -.09	-.04 -.09		-.07 -.09	-.09 -.12
$1g_{7/2}-1d_{5/2}^{-1}$	20.5	.01 .04	.02 .05	.02 .05	.04 .06	.05 .07	.06 .08
$1f_{5/2}-1p_{3/2}^{-1}$	22.5	.02 .03	.03 .04		.05 .06	.07 .08	
$2p_{1/2}-1f_{7/2}^{-1}$	6.8					-.12 -.14	
$1f_{7/2}-1p_{3/2}^{-1}$	18.0	-.04 -.11	-.01 -.01				
$1f_{7/2}-1p_{1/2}^{-1}$	16.4		-.03 -.06				

[a]The first entry for a given $p\bar{h}$ and J is the amplitude obtained using first order perturbation theory and the second entry is the amplitude obtained using the renormalized coupling interaction.

Table VI. Core admixtures in $(1g_{9/2}^2)$ configuration in ^{90}Zr.

$p\bar{h}$	ε(ph) (MeV)	$a((1g_{9/2}^2)J, (p\bar{h})J; 0 \mid (1g_{9/2}^2)0)^a$ protons J=2	J=4	J=6	J=8	neutrons J=2	J=4	J=6	J=8
$1h_{11/2}-1f_{7/2}^{-1}$	12.5	-.06 -.22	-.02 -.08	-.01 -.04	-.00 -.00	-.17 -.25	-.10 -.13	-.06 -.08	-.03 -.04
$1h_{9/2}-1f_{5/2}^{-1}$	14.5	-.05 -.17	-.03 -.08	-.02 -.04		-.13 -.19	-.07 -.10	-.04 -.05	
$1g_{7/2}-1d_{3/2}^{-1}$	15.0	-.05 -.12	-.03 -.05			-.12 -.15	-.06 -.07		
$2f_{7/2}-2p_{3/2}^{-1}$	15.0	-.01 -.11	-.01 -.04			-.04 -.09	-.02 -.04		
$1i_{13/2}-1g_{9/2}^{-1}$	13.0					-.16 -.24	-.10 -.11	-.06 -.05	-.04 -.01
$2d_{5/2}-1g_{9/2}^{-1}$	4.5					.21 .31	.12 .13	.07 .05	
$1h_{11/2}-1f_{5/2}^{-1}$	9.5		-.04 -.08	-.04 -.07	-.03 -.07		-.06 -.07	-.07 -.09	-.08 -.10
$1h_{11/2}-2p_{3/2}^{-1}$	10.5		-.04 -.08	-.01 -.03			-.11 -.13	-.05 -.06	
$1g_{7/2}-1d_{5/2}^{-1}$	17.0	.01 .02	.02 .03	.02 .01		.03 .04	.04 .05	.06 .07	
$1g_{7/2}-2s_{1/2}^{-1}$	16.0		.02 .03				.06 .07		
$1i_{13/2}-1d_{5/2}^{-1}$	26.0		.02 .04	.01 .00	.00 -.01		.04 .06	.02 .02	.01 .00
$1h_{9/2}-2p_{1/2}^{-1}$	14.0						-.06 -.08		
$1g_{7/2}-1g_{9/2}^{-1}$	7.2					-.07 -.12	-.10 -.13	-.10 -.12	-.12 -.12
$1h_{9/2}-1f_{7/2}^{-1}$	17.5	.00 .03	.02 .04	.02 .04	.02 .04	.03 .04	.04 .05	.04 .05	.04 .06

(continued)

Table VI. (continued)

$p\bar{h}$	ε(ph) (MeV)	$a((1g_{9/2}^2)J, (p\bar{h})J; 0 \mid (1g_{9/2}^2)0)$[a] protons J=2	J=4	J=6	J=8	neutrons J=2	J=4	J=6	J=8
$1h_{9/2}-2p_{3/2}^{-1}$	15.5		.01 .03	.02 .04			.03 .04	.05 .06	
$1i_{13/2}-2s_{1/2}^{-1}$	25.0			.01 .01				.03 .03	
$1h_{11/2}-2p_{1/2}^{-1}$	9.0							-.08 -.09	
$2d_{3/2}-1g_{9/2}^{-1}$	6.5						-.05 -.07	-.08 -.09	
$1i_{13/2}-1d_{3/2}^{-1}$	24.0			.01 .02	.01 .01			.02 .02	.02 .02
$2p_{1/2}-2p_{3/2}^{-1}$	3.5	-.10 -.37							
$2p_{1/2}-1f_{5/2}^{-1}$	4.0	.10 .24							
$1g_{9/2}-1d_{5/2}^{-1}$	13.5	-.04 -.14	-.01 -.02	-.01 .02					
$2p_{1/2}-1f_{7/2}$	5.5		-.06 -.12						
$1g_{9/2}-2s_{1/2}^{-1}$	12.5		-.03 -.04						
$1g_{9/2}-1d_{3/2}^{-1}$	11.5		-.03 -.06	-.03 -.05					

[a]The first entry for a given $p\bar{h}$ and J is the amplitude obtained using first order perturbation theory and the second entry is the amplitude obtained using the renormalized coupling interaction.

Table VII. Parameters for S = 0 transition densities obtained from first order calculations.

Target	Transition J_f^π (JOJ)	λ_p^{JOJ}	λ_n^{JOJ}	λ_0^{JOJ}	λ_1^{JOJ}	Theory[a] e_{eff}^J	Theory[a] ε_p^{JOJ}	Experiment[a] e_{eff}^J	Experiment[a] ε_p^{JOJ}
^{42}Ca	2^+ (202)	0.68	0.23	0.91	0.45	0.68	1.47	1.7±.1[b]	2.03[c]
	4^+ (404)	0.48	0.17	0.65	0.31	0.48	1.34	—	2.12[c]
	6^+ (606)	0.22	0.08	0.30	0.14	0.22	1.16	—	—
^{50}Ti	2^+ (202)	0.22	0.88	1.10	-0.66	1.22	3.65	1.7±.2[d]	5.34[e]
	4^+ (404)	0.16	0.70	0.86	-0.54	1.16	3.09	1.4±.1[f]	4.86[e]
	6^+ (606)	0.07	0.43	0.50	-0.36	1.07	2.25	—	—
^{89}Y	$9/2^+$ (505)	0.28	0.74	1.02	-0.46	1.28	3.32	—	—
^{90}Zr	2^+ (202)	0.31	1.22	1.53	-0.91	1.31	4.92	2.8±.4[g]	6.45[h]
	4^+ (404)	0.23	0.97	1.20	-0.74	1.23	3.90	2.1±.3[i]	5.39[h]
	6^+ (606)	0.12	0.74	0.86	-0.62	1.12	3.16	—	4.94[h]
	8^+ (808)	0.08	0.45	0.53	-0.37	1.08	2.54	—	6.35[h]
	5^- (505)	0.28	0.74	1.02	-0.46	1.28	3.32	1.4±.1[j]	4.55[h]
^{207}Pb	$5/2^-$ (202)	0.62	0.38	1.00	0.24	0.62	1.60	.93±.01[k]	2.50[ℓ]
	$3/2^-$ (202)	0.58	0.36	0.94	0.22	0.58	1.57	.75±.02[k]	1.91[ℓ]
	$13/2^+$ (707)	0.39	0.32	0.71	0.07	0.39	1.46	—	3.07[ℓ]
	$7/2^-$ (404)	0.61	0.39	1.00	0.22	0.61	1.61	—	2.63[ℓ]

(continued)

Table VII. (continued)

Target	Transition J_f^π (JOJ)	λ_p^{JOJ}	λ_n^{JOJ}	λ_0^{JOJ}	λ_1^{JOJ}	Theory[a] e_{eff}^J	Theory[a] ε_p^{JOJ}	Experiment[a] e_{eff}^J	Experiment[a] ε_p^{JOJ}
^{209}Bi	$7/2^-$ (202)	0.38	1.25	1.63	-0.87	1.38	4.82	2.3±.6[m]	—
	(404)	0.33	1.22	1.55	-0.89	1.33	4.68	—	—
	(606)	0.26	1.16	1.42	-0.90	1.26	4.44	—	—
	(808)	0.18	1.00	1.18	-0.82	1.18	3.93	—	—
	$13/2^+$ (303)	0.38	1.32	1.70	-0.94	1.38	5.01	5.3±.7[n]	24.0[o]
	(505)	0.24	1.10	1.34	-0.86	1.24	4.27	—	—
	(707)	0.14	0.81	0.95	-0.67	1.14	3.38	—	—
	(909)	0.08	0.53	0.61	-0.45	1.08	2.54	—	—
	(11011)	0.01	0.37	0.38	-0.36	1.01	2.03	—	—

[a]See text for comments on the manner in which the numbers listed in these columns have been obtained.

[b]Ref. 54 and 55. [c]Ref. 56. [d]Ref. 54 and 57-59. [e]Ref. 44 and 45. [f]Ref. 54 and 58.

[g]Ref. 58-61. [h]Ref. 18, 39, and 46. [i]Ref. 58. [j]Ref. 62 and 63. [k]Ref. 64.

[ℓ]Ref. 42 and 65. [m]Ref. 66 and 67. [n]Ref. 66-68. [o]Ref. 17.

Table VIII. Parameters for S = 0 transition densities obtained using renormalized coupling interaction.

Target	Transition J_f^π (JOJ)	λ_p^{JOJ}	λ_n^{JOJ}	λ_0^{JOJ}	λ_1^{JOJ}	Theory[a] e_{eff}^J	Theory[a] ε_p^{JOJ}	Experiment[a] e_{eff}^J	Experiment[a] ε_p^{JOJ}
^{42}Ca	2^+ (202)	0.98	0.83	1.81	0.15	0.98	2.18	1.7±.1	2.03
	4^+ (404)	0.61	0.41	1.02	0.20	0.61	1.62	—	2.12
	6^+ (606)	0.25	0.14	0.39	0.11	0.25	1.23	—	—
^{50}Ti	2^+ (202)	0.81	1.36	2.17	-0.55	1.81	5.61	1.7±.2	5.34
	4^+ (404)	0.40	0.90	1.30	-0.50	1.40	3.95	1.4±.1	4.86
	6^+ (606)	0.18	0.49	0.67	-0.31	1.18	2.53	—	—
^{89}Y	$9/2^+$ (505)	0.35	0.79	1.14	-0.44	1.35	3.52	—	—
^{90}Zr	2^+ (202)	1.30	2.07	3.37	-0.77	2.30	7.95	2.8±.4	6.45
	4^+ (404)	0.66	1.37	2.06	-0.71	1.69	5.43	2.1±.3	5.39
	6^+ (606)	0.33	0.89	1.25	-0.56	1.33	3.78	—	4.94
	8^+ (808)	0.16	0.49	0.76	-0.33	1.16	2.51	—	6.35
	5^- (505)	0.35	0.79	1.14	-0.44	1.35	3.52	1.4±.1	4.55
^{207}Pb	$5/2^-$ (202)	0.85	1.10	1.95	-0.25	0.85	2.41	.93±.01	2.50
	$3/2^-$ (202)	0.87	1.20	2.07	-0.33	0.87	2.51	.75±.02	1.91
	$13/2^+$ (707)	0.41	0.59	1.00	-0.18	0.41	1.74	—	3.07
	$7/2^-$ (404)	0.78	0.82	1.60	-0.04	0.78	2.10	—	2.63

(continued)

Table VIII. (continued)

Target	Transition J_f^π	(JOJ)	λ_p^{JOJ}	λ_n^{JOJ}	λ_0^{JOJ}	λ_1^{JOJ}	Theory[a] e_{eff}^J	Theory[a] ε_p^{JOJ}	Experiment[a] e_{eff}^J	Experiment[a] ε_p^{JOJ}
^{209}Bi	$7/2^-$	(202)	0.87	1.63	2.50	-0.76	1.87	6.35	2.3±.6	—
		(404)	0.80	1.65	2.45	-0.85	1.80	6.34	—	—
		(606)	0.60	1.39	1.99	-0.79	1.60	5.42	—	—
		(808)	0.36	1.06	1.42	-0.70	1.36	4.28	—	—
	$13/2^+$	(303)	0.14	1.42	1.56	-1.28	1.14	5.05	5.3±.7	24.0
		(505)	0.14	1.05	1.19	-0.91	1.14	4.03	—	—
		(707)	0.12	0.68	0.80	-0.56	1.12	2.99	—	—
		(909)	0.05	0.49	0.54	-0.44	1.05	2.39	—	—
		(11011)	0.02	0.35	0.37	-0.33	1.02	1.98	—	—

[a]See text for comments on the manner in which the numbers listed in these columns have been obtained. References for experimental values have been given in Table VII.

Table IX. Parameters for S = 1 transition densities obtained from first order calculations.

Target	Transition J_f^π	(LIJ)	λ_p^{LIJ}	λ_n^{LIJ}	λ_0^{LIJ}	λ_1^{LIJ}	ε_p^{LIJ}
^{89}Y	$9/2^+$	(314)	-0.45	0.08	-0.37	-0.53	0.53
		(514)	-0.28	0.05	-0.23	-0.33	0.71
		(515)	-0.25	0.05	-0.20	-0.30	0.74
^{90}Zr	5^-	(515)	-0.25	0.05	-0.20	-0.30	0.74
^{207}Pb	$5/2^-$	(212)	0.05	-0.41	0.36	0.46	0.34
		(213)	0.03	-0.32	0.29	0.35	0.53
		(413)	0.04	-0.27	0.23	0.31	0.53
	$3/2^-$	(011)	0.05	-0.20	0.15	0.25	0.55
		(211)	0.09	-0.44	0.35	0.53	0.11
		(212)	0.06	-0.39	0.33	0.45	0.31
	$13/2^+$	(516)	0.05	-0.45	0.40	0.50	0.30
		(716)	0.02	-0.11	0.09	0.13	0.79
		(717)	0.03	-0.29	0.26	0.32	0.56
	$7/2^-$	(213)	0.06	-0.42	0.36	0.48	0.28
		(413)	0.08	-0.34	0.26	0.42	0.26
		(414)	0.06	-0.38	0.32	0.44	0.32
^{209}Bi	$7/2^-$	(011)[a]	—	—	—	—	—
		(211)	-0.28	0.06	-0.22	-0.34	0.71
		(212)	-0.38	0.09	-0.29	-0.47	0.61
		(213)	-0.40	0.11	-0.29	-0.51	0.58
		(413)	-0.23	0.09	-0.14	-0.32	0.76
		(414)	-0.32	0.10	-0.22	-0.42	0.66
		(415)	-0.38	0.11	-0.27	-0.49	0.60
		(615)	-0.16	0.09	-0.07	-0.25	0.82
		(616)	-0.25	0.09	-0.16	-0.34	0.73

(continued)

Table IX. (continued)

Target	Transition J_f^π (LIJ)	λ_p^{LIJ}	λ_n^{LIJ}	λ_0^{LIJ}	λ_1^{LIJ}	ε_p^{LIJ}
	(617)	-0.33	0.11	-0.22	-0.44	0.65
	(817)	-0.09	0.08	-0.01	-0.17	0.90
	(818)	-0.17	0.09	-0.08	-0.26	0.84
	$13/2^+$ (112)	-0.33	0.10	-0.23	-0.43	0.65
	(312)	-0.22	0.09	-0.13	-0.31	0.77
	(313)	-0.30	0.11	-0.19	-0.41	0.68
	(314)	-0.29	0.11	-0.18	-0.40	0.69
	(514)	-0.21	0.09	-0.22	-0.30	0.88
	(515)	-0.22	0.10	-0.12	-0.32	0.77
	(516)	-0.23	0.09	-0.14	-0.32	0.75
	(716)	-0.13	0.08	-0.05	-0.21	0.86
	(717)	-0.13	0.08	-0.05	-0.21	0.86
	(718)	-0.16	0.06	-0.10	-0.22	0.83
	(918)	-0.04	0.06	0.02	-0.01	0.94
	(919)	-0.07	0.05	-0.02	-0.12	0.92
	(9110)	-0.13	0.03	-0.10	-0.16	0.87
	(11110)	0.00	0.04	0.04	-0.04	0.99
	(11111)	-0.04	0.03	-0.01	-0.07	0.95

[a]The valence transition is strictly forbidden in this case so λ^{011} cannot be defined. Core polarization does not break this selection rule to any great extent.

Table X. Comparison of the results of this work (PW) for some quadrupole transitions with results obtained previously by Siegal and Zamick.

Core	Transition	PW(G_{KK})[a]		SZ(G_{KK})[b]		PW($\bar{G}'$)[a]		SZ(TDA)[b]	
		λ_0^{202}	λ_1^{202}	λ_0^{202}	λ_1^{202}	λ_0^{202}	λ_1^{202}	λ_0^{202}	λ_1^{202}
^{40}Ca	$1f_{7/2} \rightarrow 1f_{7/2}$	0.91	-0.45	0.80	-0.38	1.81	-0.15	1.86	-0.30

[a]PW denotes present work. G_{KK} refers to first order calculations and $\bar{G}'$ refers to calculations with renormalized coupling interaction.

[b]SZ denotes Siegal and Zamick.[10] TDA refers to the treatment of excluded space interactions in the TDA approximation.

Table XI. Effective charges for some quadrupole transitions not considered in Tables II, XII, and VIII.

Nuclide	Transition	Theory e^2_{eff} (G_{KK})	Theory e^2_{eff} $(\bar{G}')$	Experiment e^2_{eff}
^{42}Ca	$6^+ \rightarrow 4^+$	0.68	0.98	0.8±.1[a]
^{50}Ti	$6^+ \rightarrow 4^+$	1.22	1.81	1.8±.3[a]
^{90}Zr	$8^+ \rightarrow 6^+$	1.31	2.30	2.1±.1[b]
$^{208}Pb + p$	$1h_{9/2} \rightarrow 1h_{9/2}$	1.35	2.27	1.5±.1[c]
$^{208}Pb + n$	$3d_{5/2} \rightarrow 2s_{1/2}$	0.37	0.55	(0.42±.01)[c]
	$2g_{9/2} \rightarrow 2g_{9/2}$	0.36	1.04	(0.84±.07)[c]
$^{208}Pb + n^{-1}$	$1i_{13/2} \rightarrow 1i_{13/2}$	0.81	1.22	(0.96±.04)[c]

[a]Ref. 72. [b]Ref. 59. [c]Ref. 64.

Table XII. Optical parameters used in the present calculations.

System[a]	E (MeV)	V (MeV)	r_o (F)	a (F)	W (MeV)	W_o (MeV)	r_o' (F)	a' (F)	V_s (MeV)	r_s (F)	a_s (F)
$^{42}Ca + p$[b]	22.9	46.9	1.18	.700	1.30	6.80	1.30	.600	6.00	1.05	.700
$^{50}Ti + p$[c]	17.5	48.3	1.24	.600	0.00	10.68	1.26	.520	10.00	1.24	.600
$^{50}Ti + p$[d]	40.0	44.9	1.16	.750	7.82	1.14	1.37	.630	6.04	1.06	.738
$^{89}Y + p$[e]	18.9	52.6	1.20	.700	0.00	9.80	1.25	.650	5.70	1.20	.700
$^{89}Y + p$[f]	24.5	46.6	1.23	.627	0.00	10.9	1.28	.536	7.00	1.23	.627
$^{89}Y + p$[g]	61.2	39.5	1.20	.693	5.12	2.54	1.40	.534	6.92	1.00	.861
$^{90}Zr + p$[h]	18.8	52.0	1.20	.700	0.00	9.25	1.25	.650	6.20	1.20	.700
$^{90}Zr + p$[g]	61.2	39.5	1.20	.693	5.12	2.54	1.40	.534	6.92	1.00	.861
$^{207}Pb + p$[i]	20.2	53.0	1.25	.650	0.00	10.0	1.25	.760	6.00	1.20	.470

[a]We write the optical potential

$$U = -V(1 + e^{x})^{-1} - iW(1 + e^{x'})^{-1} + 4iW_D \frac{d}{dx'}(1 + e^{x'})^{-1} + (\hbar/m_\pi c)^2 V_s \frac{1}{r}\frac{d}{dr}(1 + e^{x_s})^{-1} ,$$

where

$$x = \frac{r - r_o A^{1/3}}{a} , \quad x' = \frac{r - r_o' A^{1/3}}{a'} , \quad x_s = \frac{r - r_s A^{1/3}}{a_s} ,$$

and to which is added the Coulomb potential of a uniformly charged sphere of radius $1.25A^{1/3}$.

[b]Ref. 56. [c]Ref. 75. [d]Ref. 45. [e]Ref. 76. [f]Ref. 77. [g]Ref. 78. [h]Ref. 46. [i]Ref. 65.

Table XIII. Parameters for ground state proton distributions.

Nuclide[a]	ρ_o (F^{-3})	c (F)	a (F)
^{42}Ca[b]	.069	3.83	.595
^{50}Ti[b]	.073	3.92	.553
^{89}Y[c]	.073	4.80	.568
^{90}Zr[c]	.074	4.85	.568
^{207}Pb[d]	.063	6.63	.527

[a]It is assumed that the density distribution is given by

$$\rho_p(r) = \rho_o[1 + \exp(\frac{r - c}{a})]^{-1} \quad .$$

[b]Ref. 54. [c]Ref. 79. [d]Ref. 80.

Figure Captions

Fig. 1. Spectra of ^{50}Ti and ^{90}Zr showing pairing effect due to core polarization.

Fig. 2. Theoretical (p,p') differential cross section obtained with schematic model for the first 2^+ and 4^+ states in ^{50}Ti with E_p = 17.5 and 40.0 MeV. Results with (D) and without (D+C) core polarization are shown.

Fig. 3. Theoretical (p,p') differential cross sections obtained with schematic model for first 2^+, 4^+, 6^+, and 8^+ states in ^{90}Zr with E_p = 18.8 MeV.

Fig. 4. Transition densities for L=2 transitions in ^{50}Ti, ^{90}Zr, ^{207}Pb, and ^{209}Bi.

Fig. 5. Form factors obtained from transition densities of Fig. 4.

Fig. 6. Theoretical (p,p') cross sections for first 2^+ and 4^+ excitations in ^{42}Ca with E_p = 22.9 MeV.

Fig. 7. Theoretical (e,e') form factor for first 2^+ state in ^{42}Ca.

Fig. 8. Theoretical (p,p') cross sections for first 2^+ and 4^+ states in ^{50}Ti with E_p = 17.5 and 40.0 MeV.

Fig. 9. Theoretical (e,e') form factors for first 2^+ and 4^+ states in ^{50}Ti.

Fig. 10. Theoretical (p,p') cross sections for first 2^+, 4^+, 6^+, and 8^+ excitations in ^{90}Zr with E_p = 18.8 MeV.

Fig. 11. Same as Fig. 10 with E_p = 61.2 MeV.

Fig. 12. Theoretical (p,p') cross sections for excitation of first 5^- level in ^{90}Zr at E_p = 18.8 and 61.2 MeV.

Fig. 13. Theoretical (e,e') form factors for first 2^+ and 4^+ excitations in ^{90}Zr.

Fig. 14. Theoretical (p,p') cross sections for $2p_{1/2} \rightarrow 1g_{9/2}$ single proton transition in ^{89}Y with E_p = 18.9, 24.5, and 61.2 MeV.

Fig. 15. Theoretical (p,p') cross sections for neutron hole transitions in ^{207}Pb with E_p = 20.2 MeV.

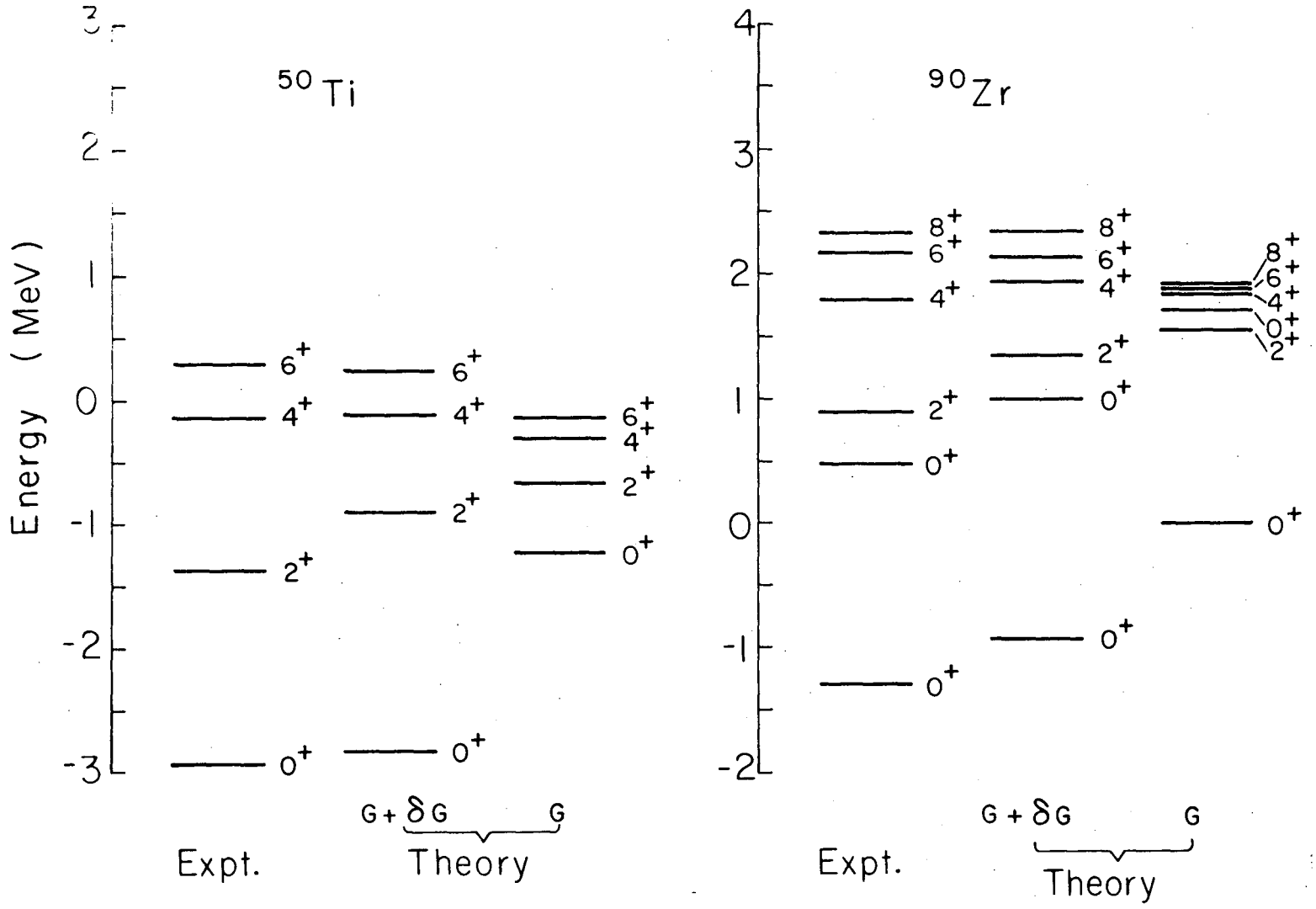

XBL758-3826

Fig. 1

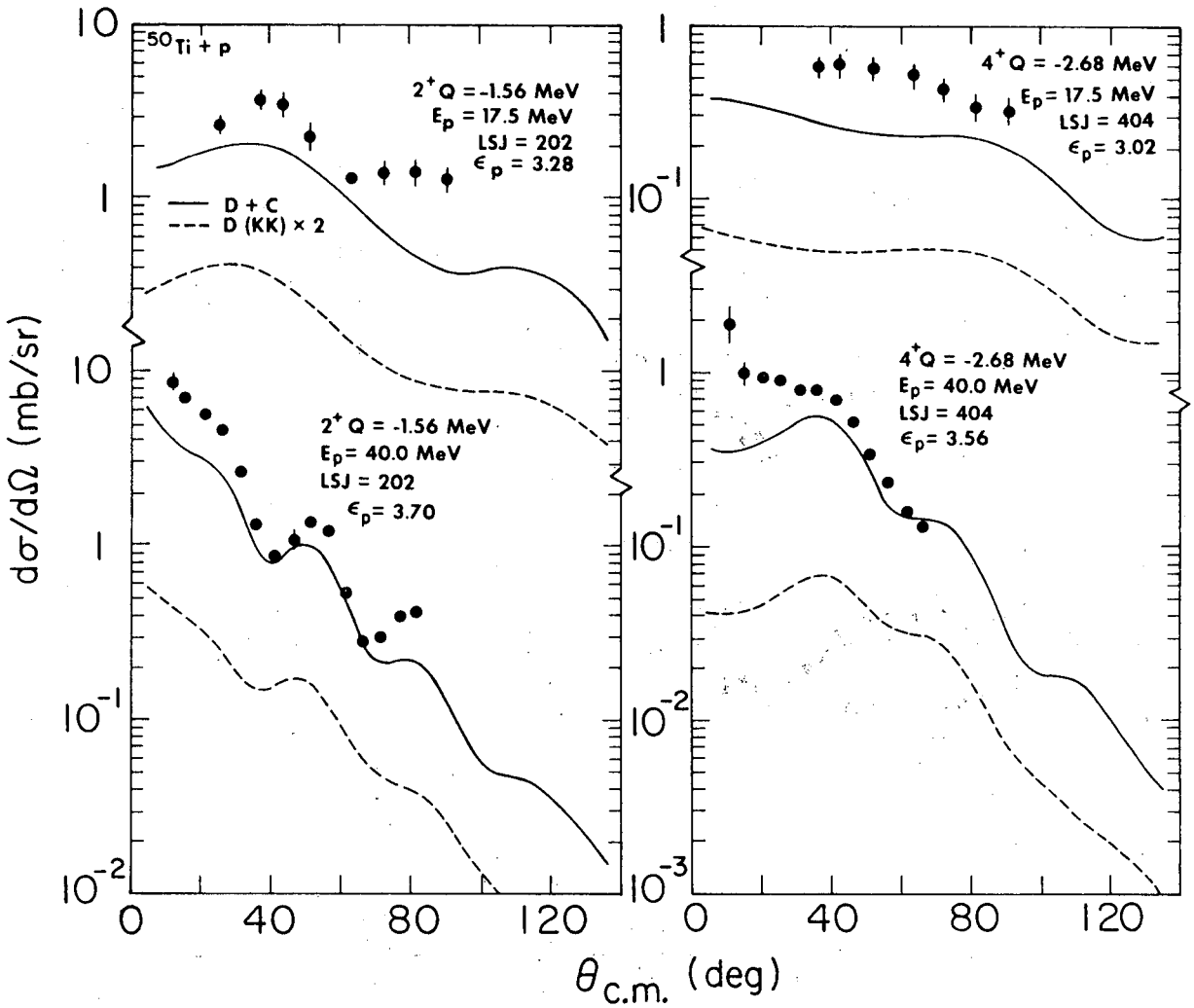
^{50}Ti + p
2^+ Q = -1.56 MeV
E_p = 17.5 MeV
LSJ = 202
ϵ_p = 3.28
D + C
D (KK) × 2
2^+ Q = -1.56 MeV
E_p= 40.0 MeV
LSJ = 202
ϵ_p= 3.70
4^+ Q = -2.68 MeV
E_p= 17.5 MeV
LSJ = 404
ϵ_p= 3.02
4^+ Q = -2.68 MeV
E_p= 40.0 MeV
LSJ = 404
ϵ_p= 3.56
$d\sigma/d\Omega$ (mb/sr)
$\theta_{c.m.}$ (deg)
XBL758-3827

Fig. 2

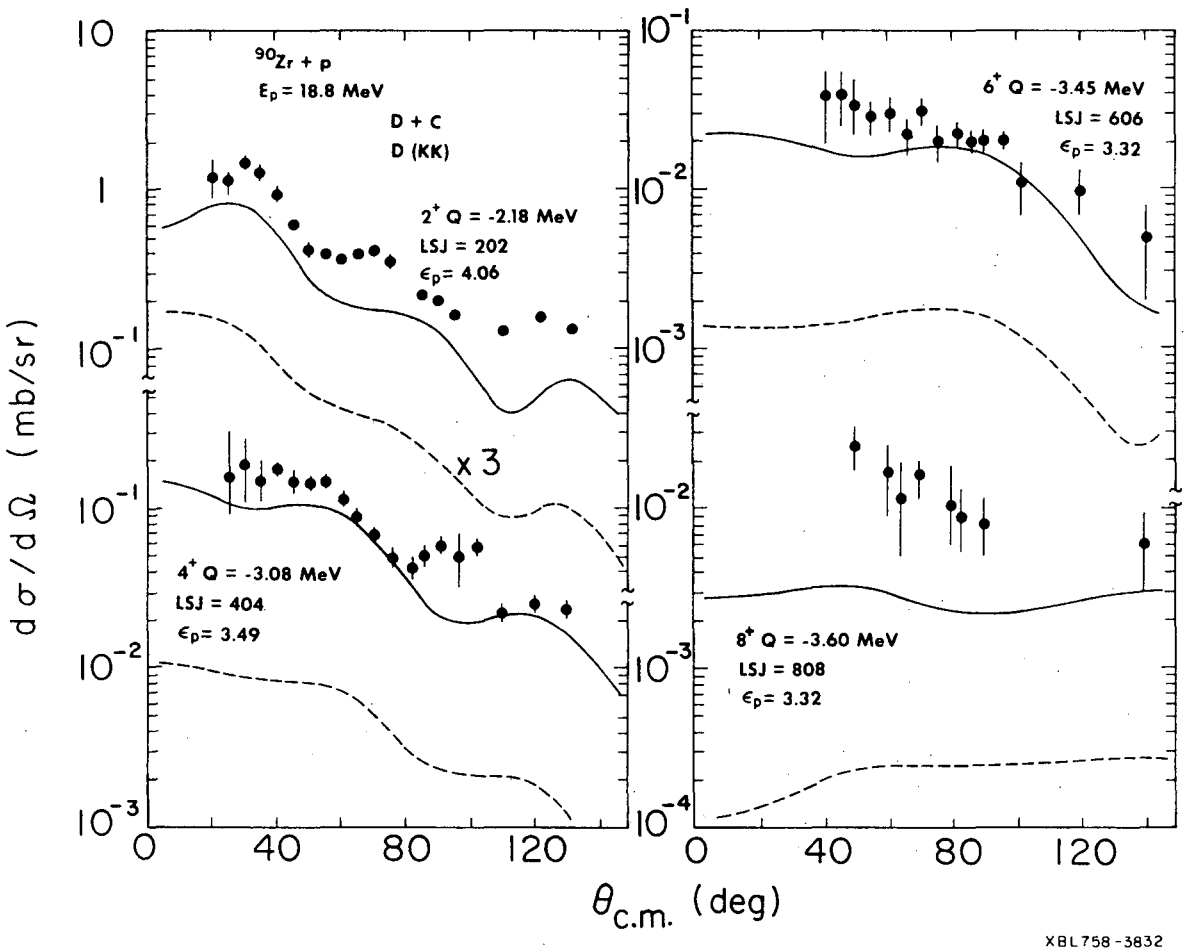
^{90}Zr + p
E_p = 18.8 MeV
D + C
D (KK)
2$^+$ Q = -2.18 MeV
LSJ = 202
ϵ_p = 4.06
x 3
4$^+$ Q = -3.08 MeV
LSJ = 404
ϵ_p = 3.49
6$^+$ Q = -3.45 MeV
LSJ = 606
ϵ_p = 3.32
8$^+$ Q = -3.60 MeV
LSJ = 808
ϵ_p = 3.32
d σ / d Ω (mb/sr)
$\theta_{c.m.}$ (deg)
XBL758-3832

Fig. 3

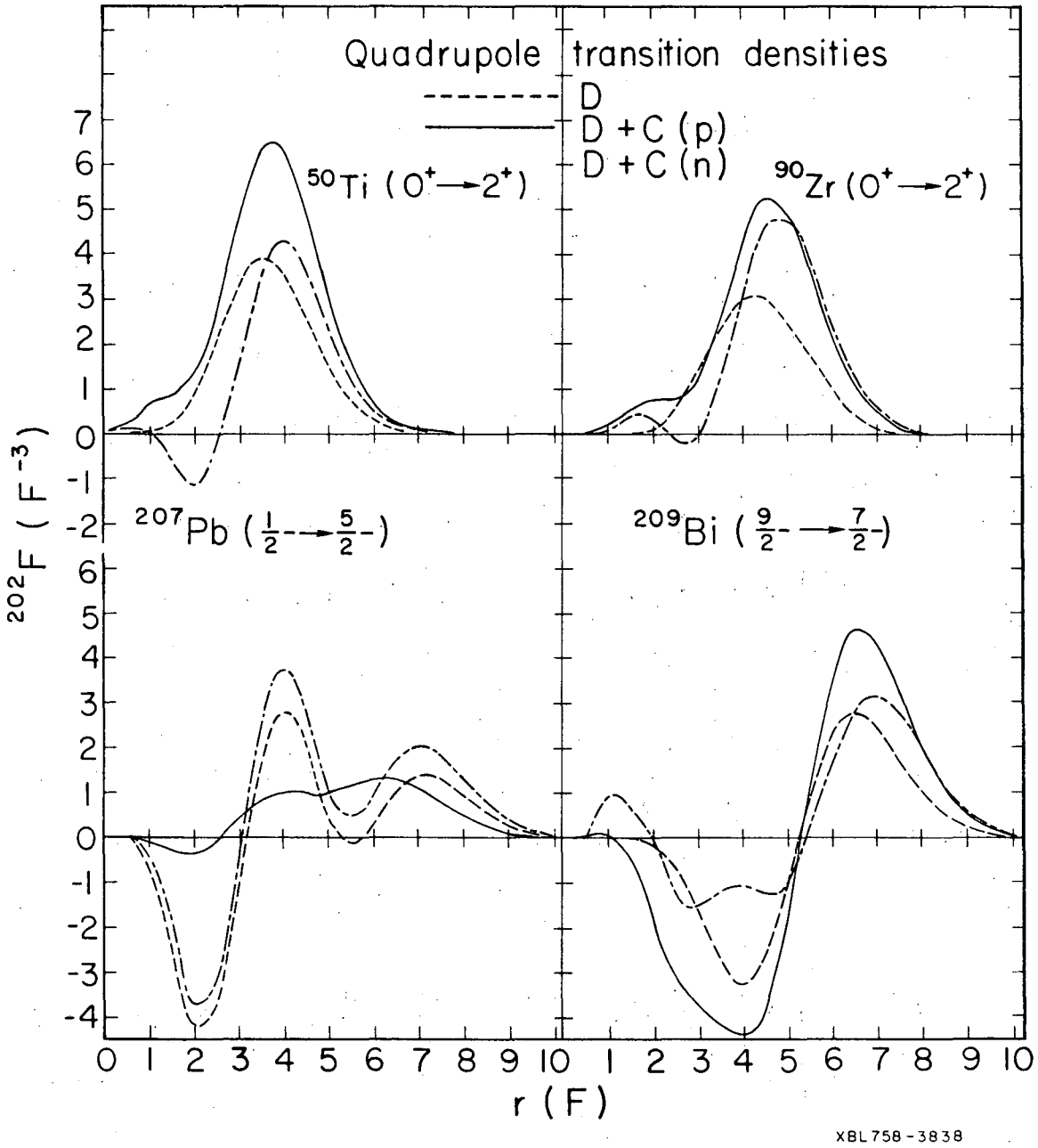
Quadrupole transition densities
D
D + C (p)
D + C (n)
50Ti (0+→2+)
90Zr (0+→2+)
207Pb (1/2-→5/2-)
209Bi (9/2-→7/2-)
202F (F-3)
r (F)
XBL758-3838

Fig. 4

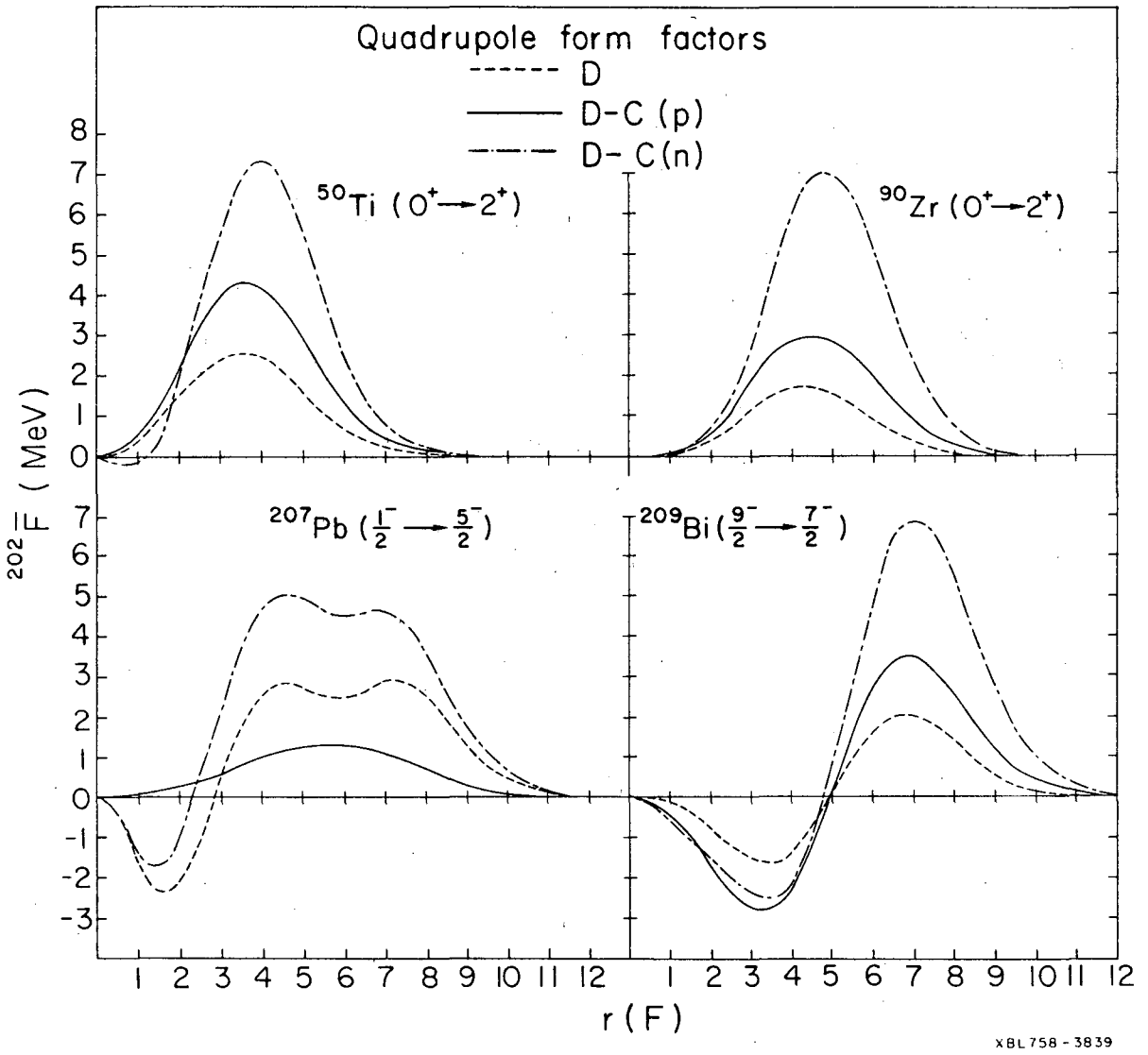
Quadrupole form factors
D
D-C (p)
D- C(n)
50Ti (0+→2+)
90Zr (0+→2+)
207Pb (1/2− → 5/2−)
209Bi (9/2− → 7/2−)
202F (MeV)
r (F)
XBL758-3839

Fig. 5

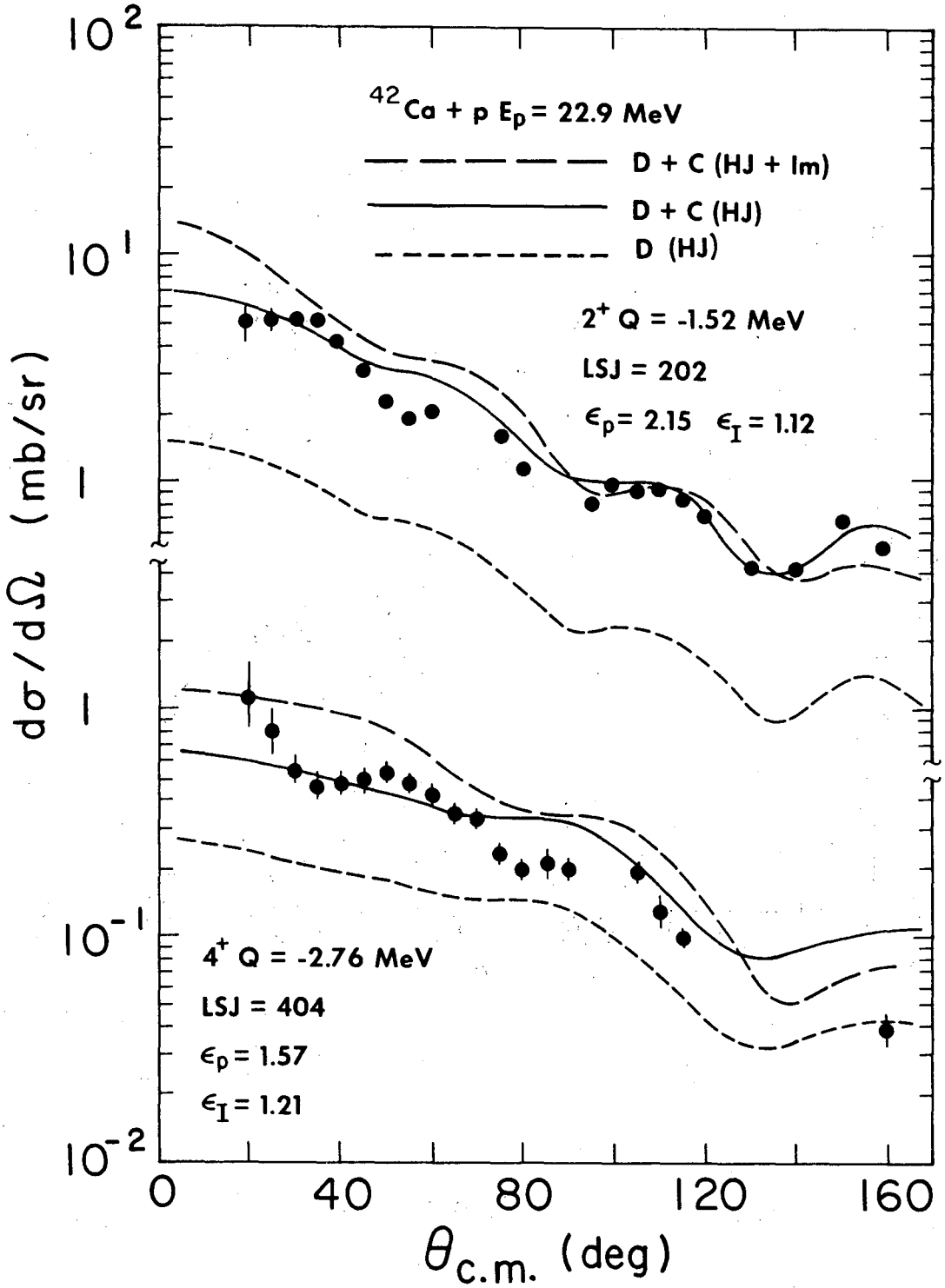

XBL758-3830

Fig. 6

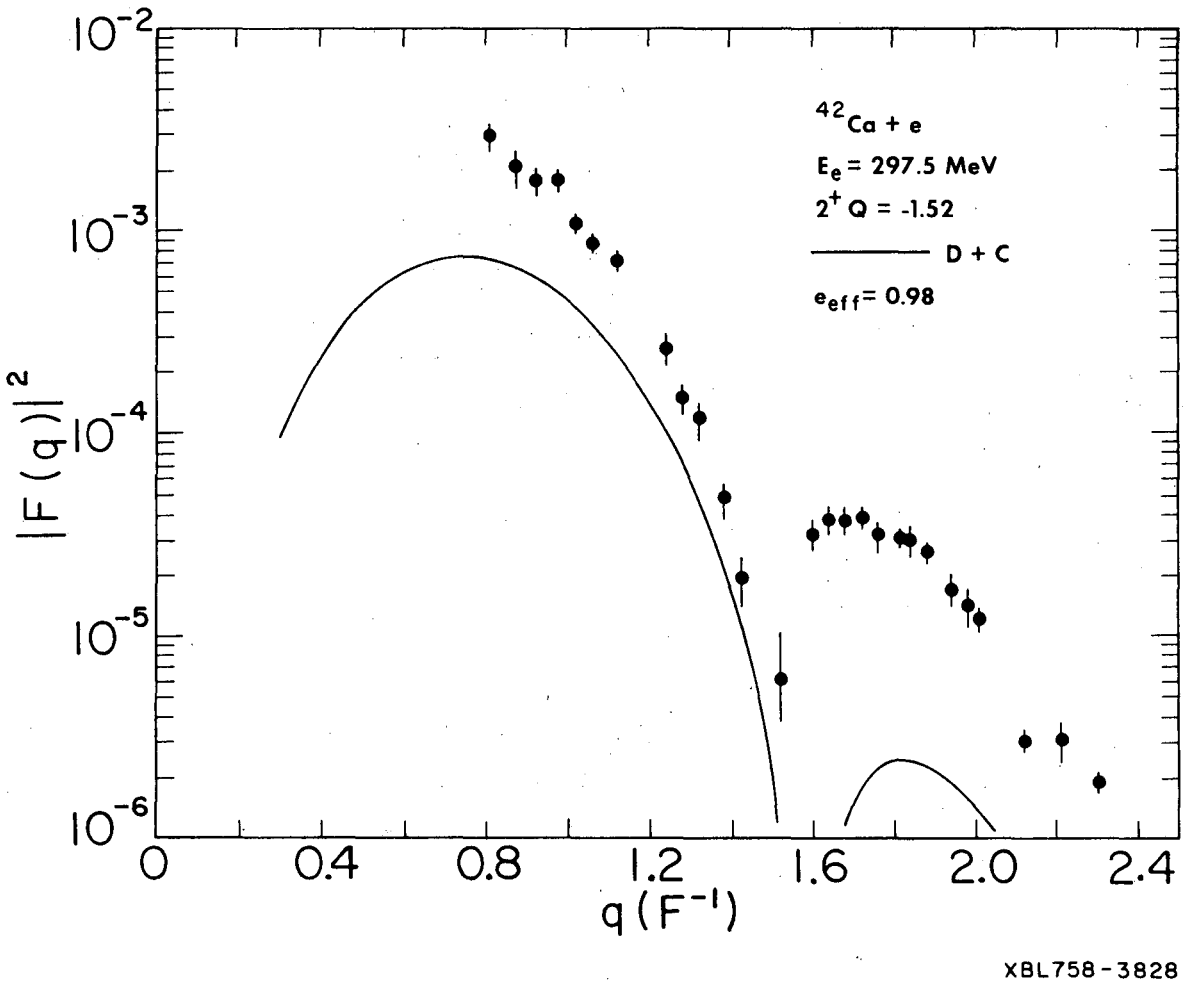
^{42}Ca + e
E_e = 297.5 MeV
2^+ Q = -1.52
D + C
e_{eff} = 0.98
$|F(q)|^2$
10^{-2}
10^{-3}
10^{-4}
10^{-5}
10^{-6}
0
0.4
0.8
1.2
1.6
2.0
2.4
q (F^{-1})
XBL758-3828

Fig. 7

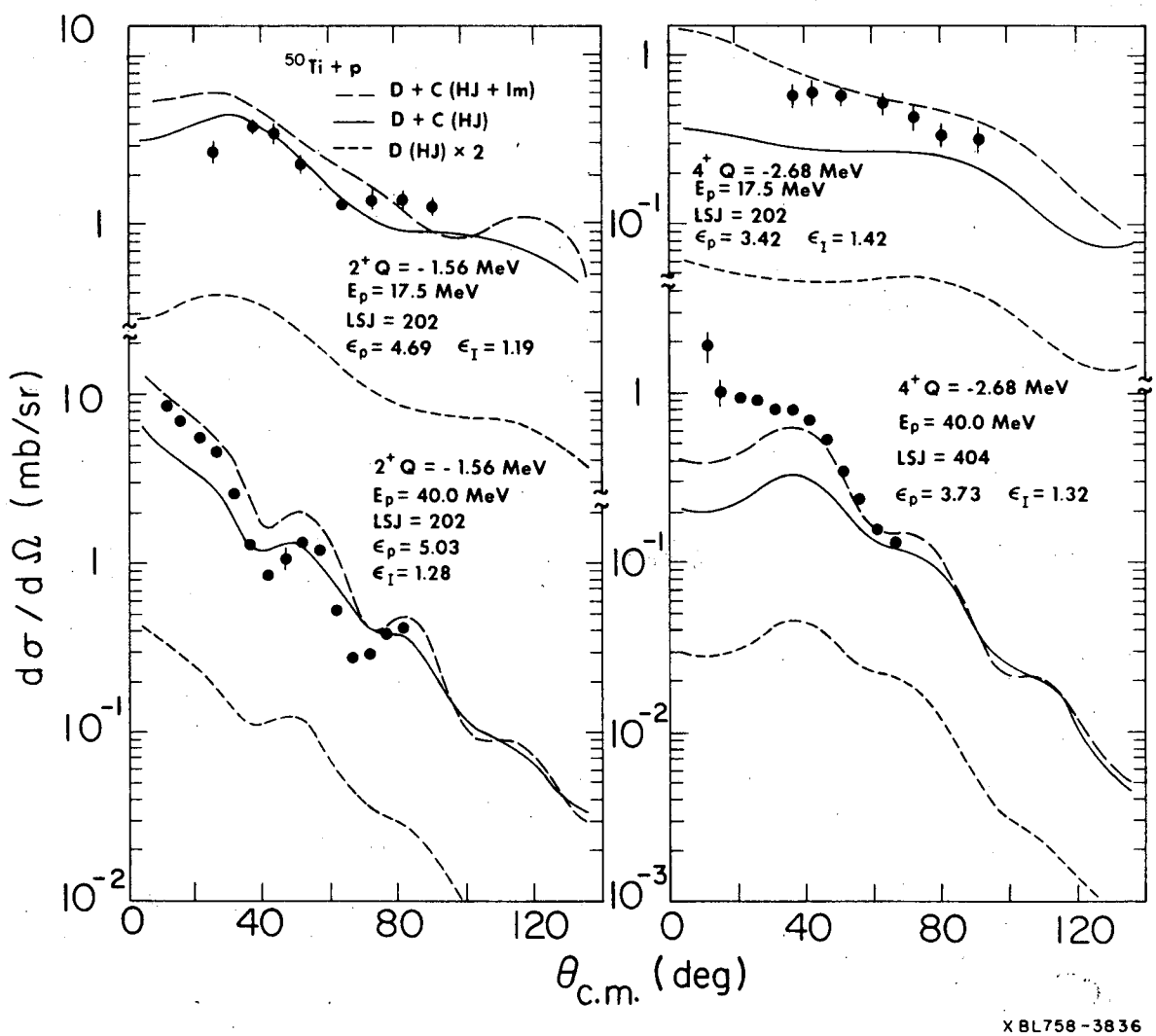
^{50}Ti + p
D + C (HJ + Im)
D + C (HJ)
D (HJ) × 2
2$^+$ Q = - 1.56 MeV
E$_p$ = 17.5 MeV
LSJ = 202
ϵ_p = 4.69 ϵ_I = 1.19
2$^+$ Q = - 1.56 MeV
E$_p$ = 40.0 MeV
LSJ = 202
ϵ_p = 5.03
ϵ_I = 1.28
4$^+$ Q = -2.68 MeV
E$_p$ = 17.5 MeV
LSJ = 202
ϵ_p = 3.42 ϵ_I = 1.42
4$^+$ Q = -2.68 MeV
E$_p$ = 40.0 MeV
LSJ = 404
ϵ_p = 3.73 ϵ_I = 1.32
dσ / dΩ (mb/sr)
θ$_{c.m.}$ (deg)
X BL758-3836

Fig. 8

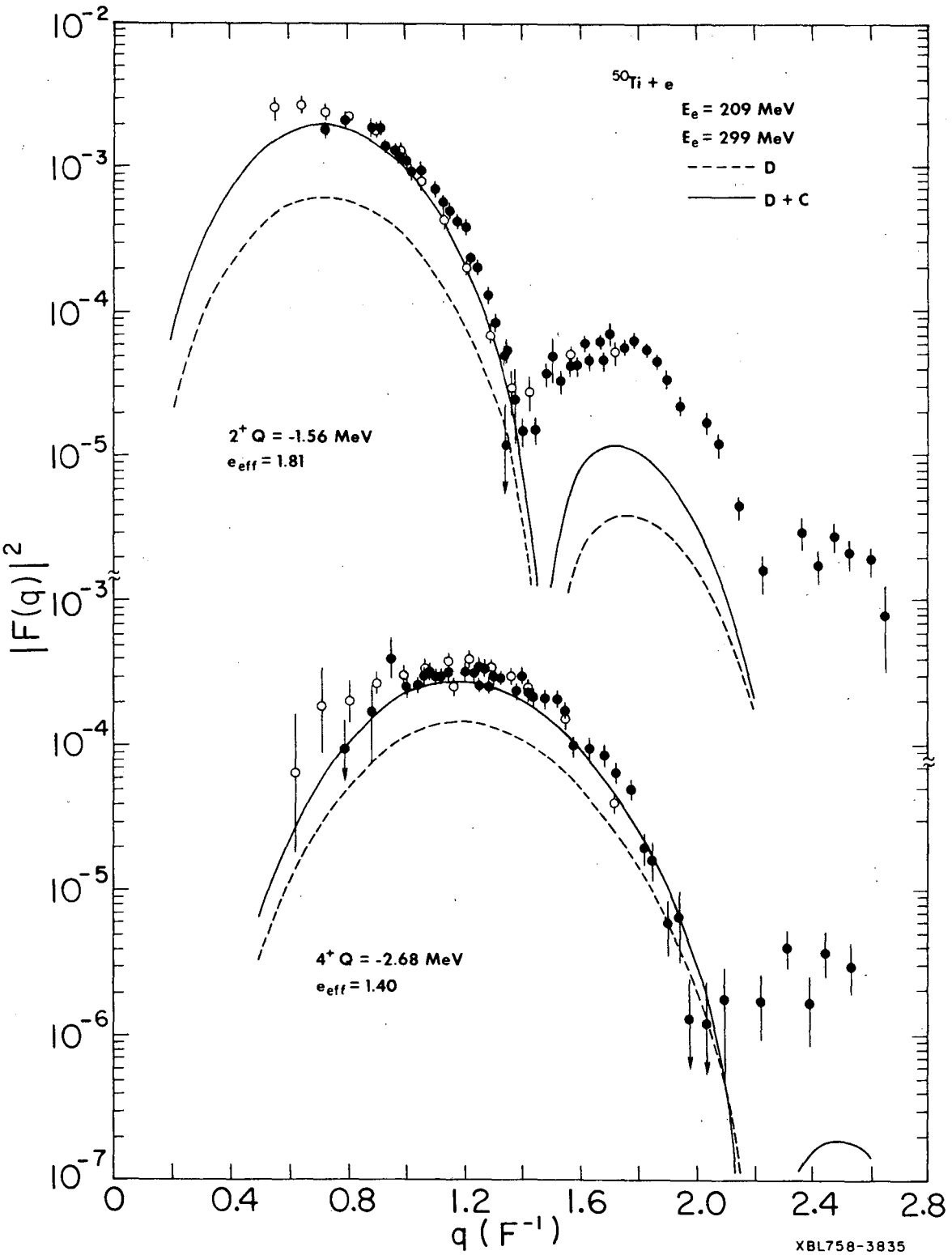
^{50}Ti + e
E_e = 209 MeV
E_e = 299 MeV
D
D + C
2^+ Q = -1.56 MeV
e_{eff} = 1.81
4^+ Q = -2.68 MeV
e_{eff} = 1.40
$|F(q)|^2$
q (F^{-1})
XBL758-3835

Fig. 9

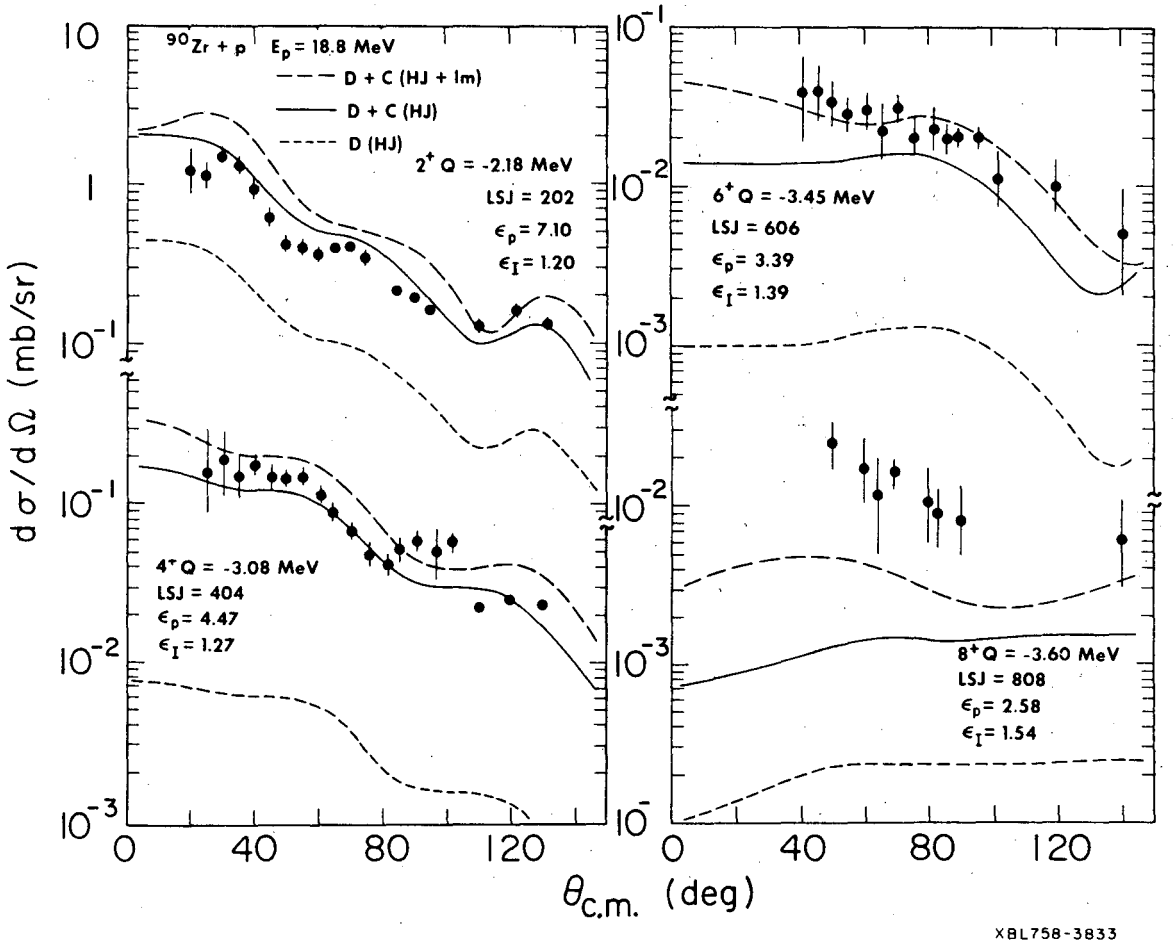
^{90}Zr + p
E_p = 18.8 MeV
D + C (HJ + Im)
D + C (HJ)
D (HJ)
2$^+$ Q = -2.18 MeV
LSJ = 202
ϵ_p = 7.10
ϵ_I = 1.20
4$^+$ Q = -3.08 MeV
LSJ = 404
ϵ_p = 4.47
ϵ_I = 1.27
6$^+$ Q = -3.45 MeV
LSJ = 606
ϵ_p = 3.39
ϵ_I = 1.39
8$^+$ Q = -3.60 MeV
LSJ = 808
ϵ_p = 2.58
ϵ_I = 1.54
d σ / d Ω (mb/sr)
$\theta_{c.m.}$ (deg)
XBL758-3833

Fig. 10

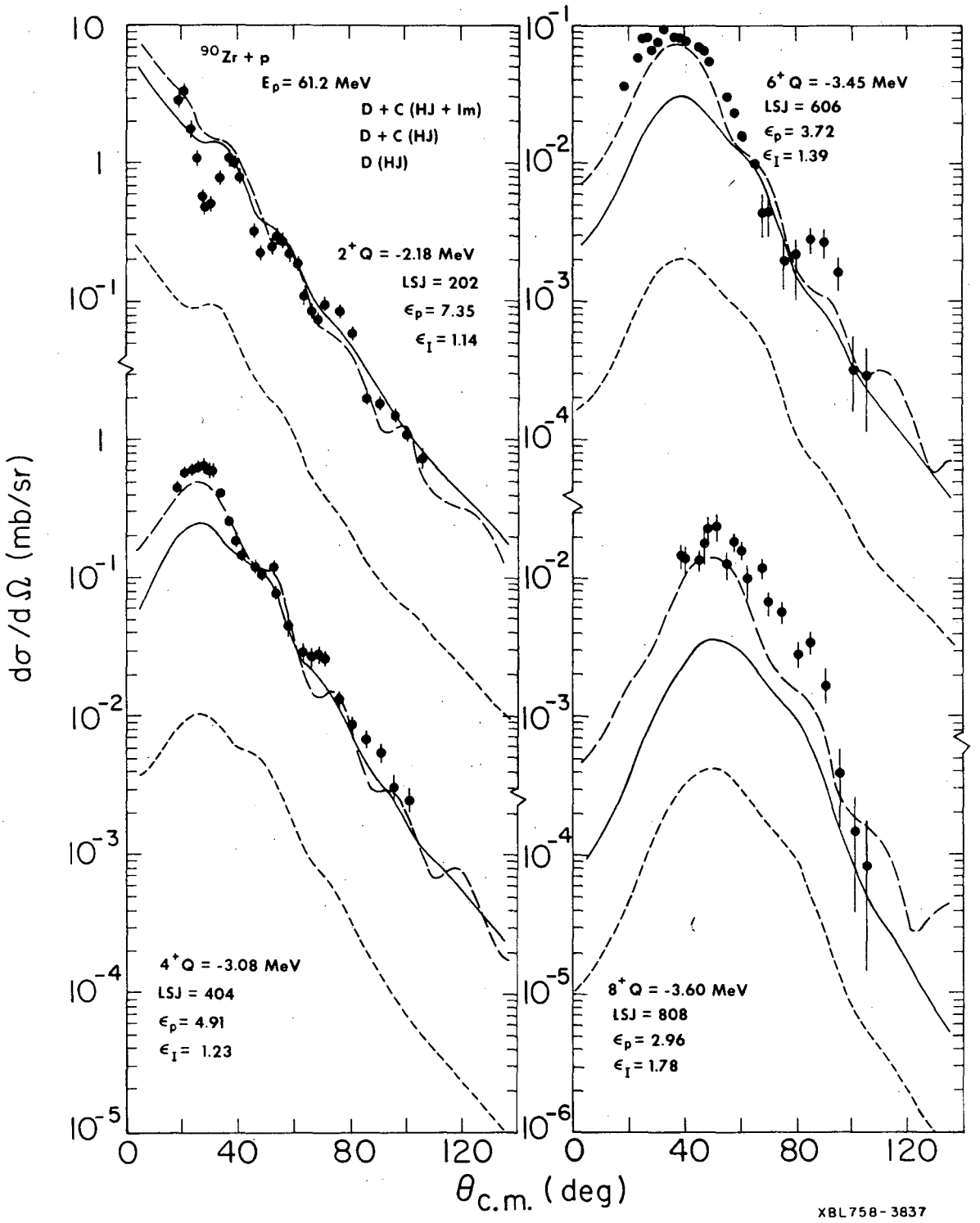
^{90}Zr + p
E_p = 61.2 MeV
D + C (HJ + Im)
D + C (HJ)
D (HJ)
2$^+$ Q = -2.18 MeV
LSJ = 202
ϵ_p = 7.35
ϵ_I = 1.14
4$^+$ Q = -3.08 MeV
LSJ = 404
ϵ_p = 4.91
ϵ_I = 1.23
6$^+$ Q = -3.45 MeV
LSJ = 606
ϵ_p = 3.72
ϵ_I = 1.39
8$^+$ Q = -3.60 MeV
LSJ = 808
ϵ_p = 2.96
ϵ_I = 1.78
dσ/dΩ (mb/sr)
$\theta_{c.m.}$ (deg)
XBL758-3837

Fig. 11

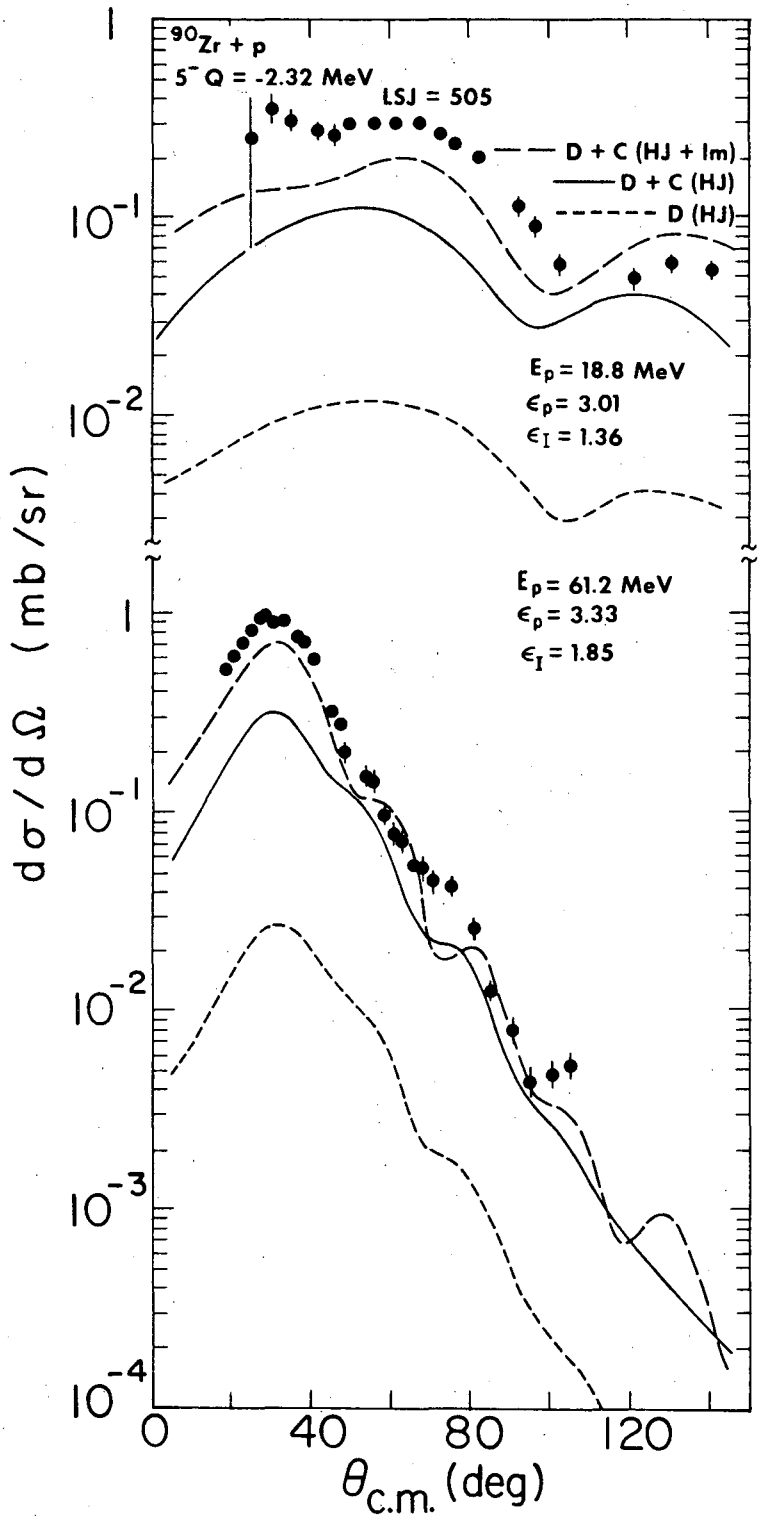
^{90}Zr + p
5$^-$ Q = -2.32 MeV
LSJ = 505
D + C (HJ + Im)
D + C (HJ)
D (HJ)
E_p = 18.8 MeV
ϵ_p = 3.01
ϵ_I = 1.36
E_p = 61.2 MeV
ϵ_p = 3.33
ϵ_I = 1.85
$d\sigma/d\Omega$ (mb/sr)
$\theta_{c.m.}$ (deg)
XBL758-3834

Fig. 12

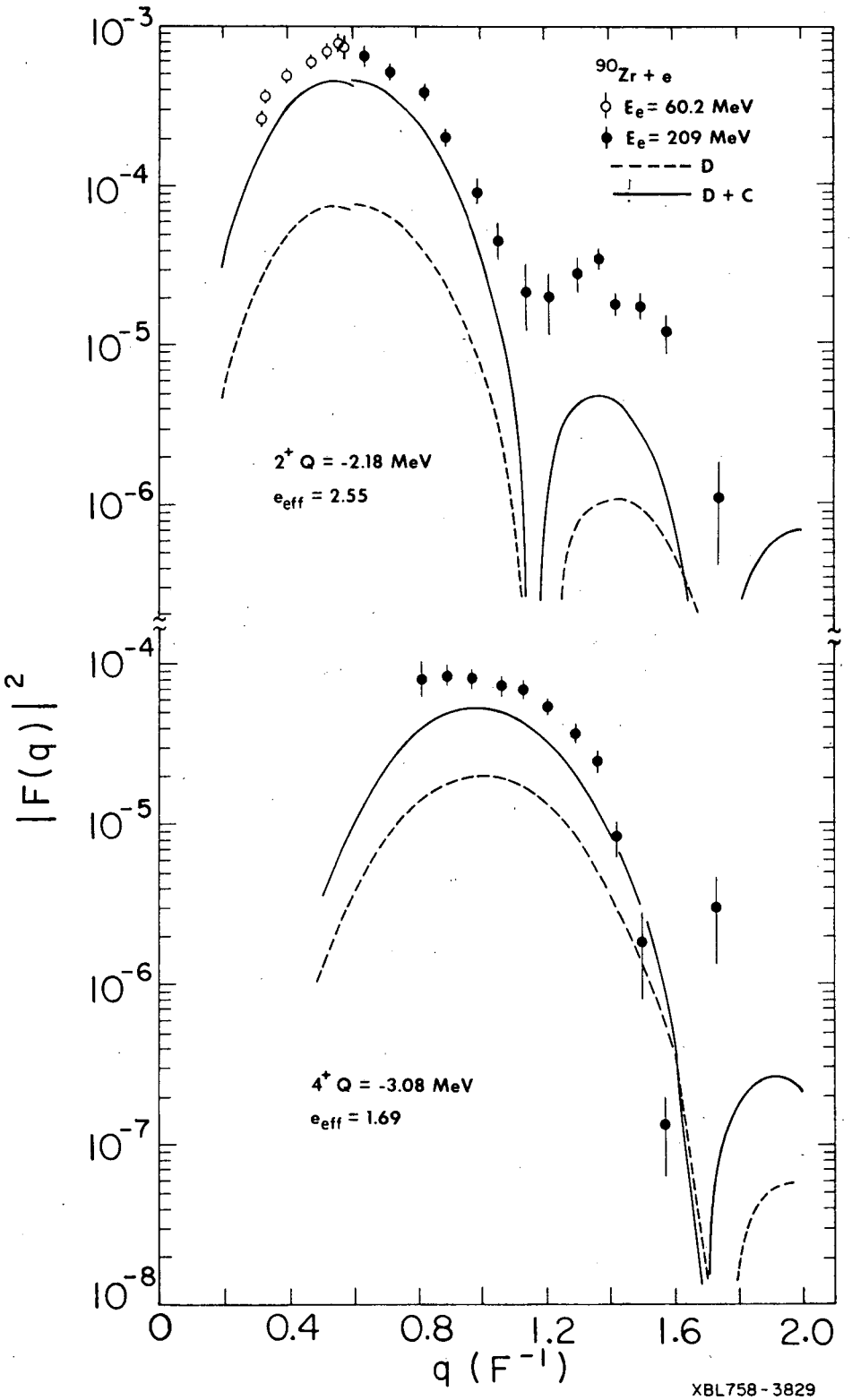
^{90}Zr + e
E_e = 60.2 MeV
E_e = 209 MeV
D
D + C
2^+ Q = -2.18 MeV
e_{eff} = 2.55
4^+ Q = -3.08 MeV
e_{eff} = 1.69
$|F(q)|^2$
q (F^{-1})
XBL758-3829

Fig. 13

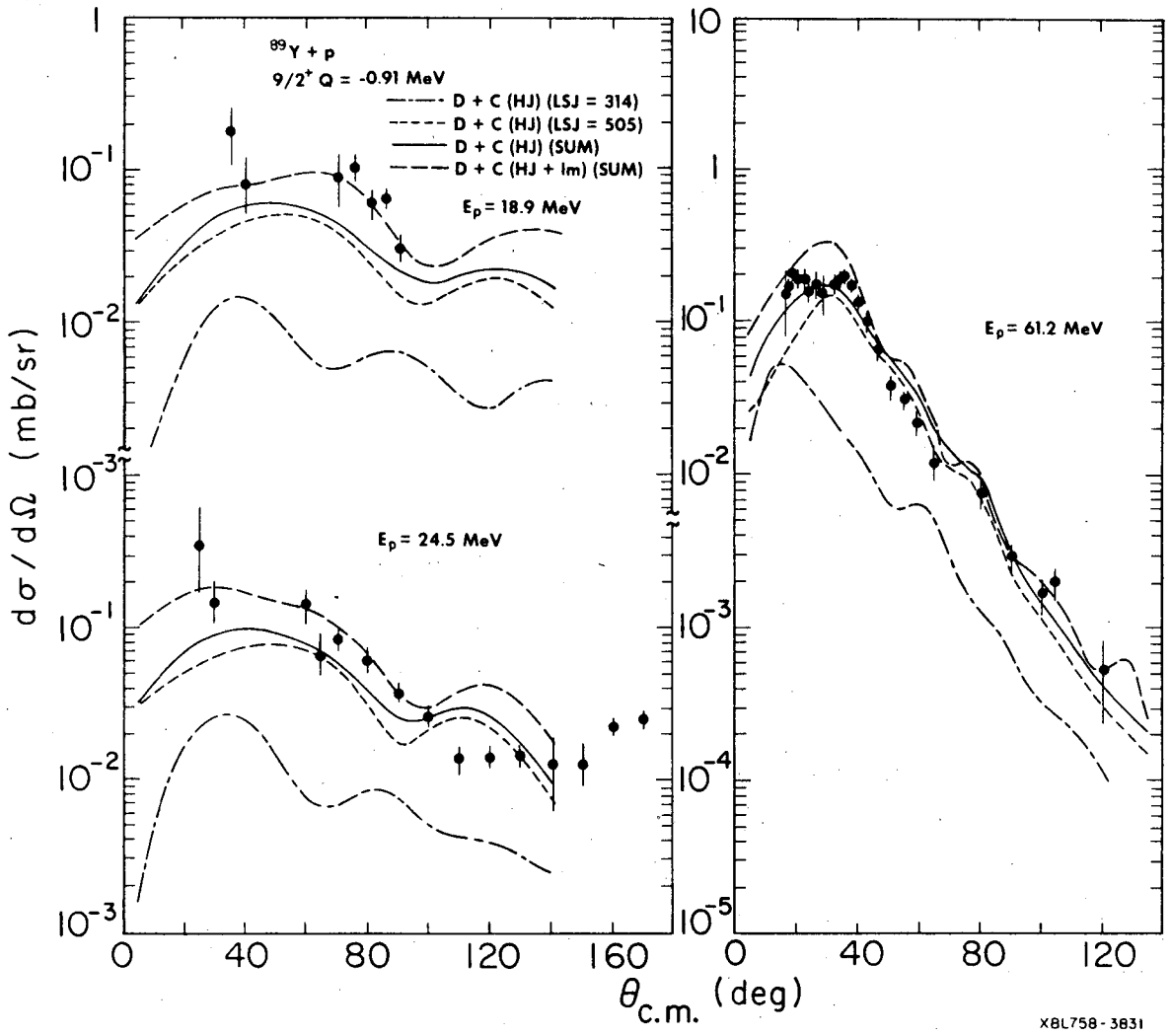
^{89}Y + p
9/2$^+$ Q = -0.91 MeV
D + C (HJ) (LSJ = 314)
D + C (HJ) (LSJ = 505)
D + C (HJ) (SUM)
D + C (HJ + Im) (SUM)
E_p = 18.9 MeV
E_p = 24.5 MeV
E_p = 61.2 MeV
dσ / dΩ (mb/sr)
$\theta_{c.m.}$ (deg)
XBL758-3831

Fig. 14

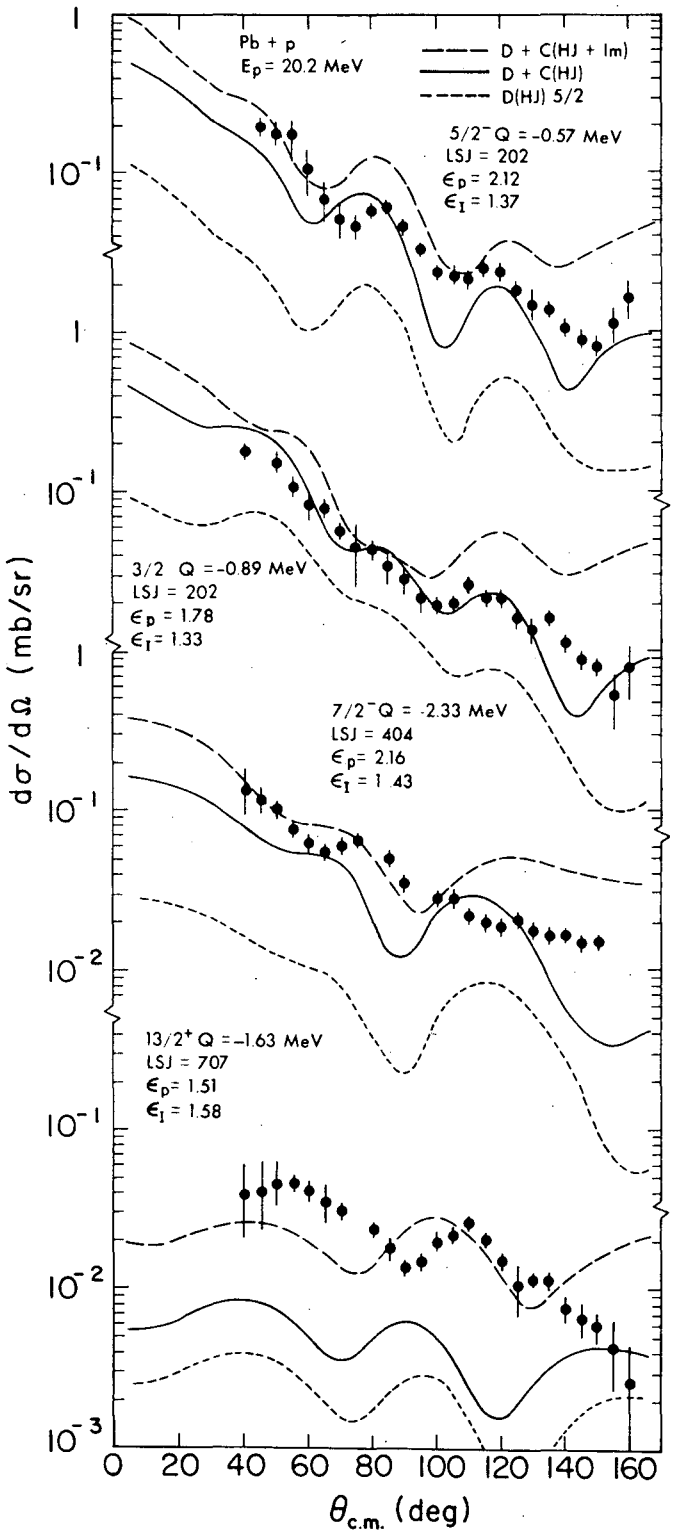
Pb + p
Ep = 20.2 MeV
D + C(HJ + Im)
D + C(HJ)
D(HJ) 5/2
5/2⁻ Q = -0.57 MeV
LSJ = 202
εp = 2.12
εI = 1.37
3/2 Q = -0.89 MeV
LSJ = 202
εp = 1.78
εI = 1.33
7/2⁻ Q = -2.33 MeV
LSJ = 404
εp = 2.16
εI = 1.43
13/2⁺ Q = -1.63 MeV
LSJ = 707
εp = 1.51
εI = 1.58
dσ/dΩ (mb/sr)
θc.m. (deg)
XBL758-3840

Fig. 15

This report was done with support from the United States Energy Research and Development Administration. Any conclusions or opinions expressed in this report represent solely those of the author(s) and not necessarily those of The Regents of the University of California, the Lawrence Berkeley Laboratory or the United States Energy Research and Development Administration.

TECHNICAL INFORMATION DIVISION
LAWRENCE BERKELEY LABORATORY
UNIVERSITY OF CALIFORNIA
BERKELEY, CALIFORNIA 94720